



POLITECNICO DI MILANO  
DEPARTMENT OF AEROSPACE ENGINEERING  
DOCTORAL PROGRAMME IN ROTARY WING AIRCRAFT

---

# WIND TURBINE SYSTEM IDENTIFICATION AND STABILITY ANALYSIS

Doctoral Dissertation of:  
**Stefano Cacciola**

Supervisor:  
**Prof. Carlo L. Bottasso**

Tutor:  
**Prof. Luca Di Landro**

The Chair of the Doctoral Program:  
**Prof. Luigi Vigevano**

Year 2012 – XXV



---

---

## Acknowledgements

---

My sincere gratitude goes to all the components of the Poliwind Research Group and to all the research and industrial subjects, which have contributed supporting the completion of this work in this three year.

In particular a special acknowledgement goes to Professor Carlo Luigi Bottasso for his perseverance and competence in supervising my research, and to Professor Alessandro Croce for his willingness and proficiency.

The Department of Electronic Systems Automation & Control of the University of Aalborg, Denmark, and in particular Professors Rafael Wisniewski, the National Renewable Energy Laboratory (NREL) and in particular Dr. Alan D. Wright, Tozzi Nord S.r.l. and CRIEL S.r.l. are gratefully acknowledged.

I wish to thank also the other colleagues, Carlo, Filippo and Federico, for having shared with me the joy and the hassle of the research with enthusiasm and friendship and all the master's thesis students, for having contributed to the development of this work.

A sincere thank goes to my family, especially to my wife Chiara, that unfliningly and daily helps me to become more and more deeply a man. In life and in faith.



---

# Contents

---

<b>Introduction</b>	<b>3</b>
<b>I Identification of properties of wind turbine models</b>	<b>9</b>
<b>1 Introduction</b>	<b>11</b>
<b>2 The estimation problem</b>	<b>15</b>
2.1 Formulation . . . . .	15
2.1.1 Maximum Likelihood Estimation . . . . .	15
2.2 Identifiability and singular values decomposition . . . . .	17
<b>3 Identification of blade beam models</b>	<b>21</b>
3.1 Model Updating of Blade Beam Models . . . . .	24
3.1.1 Updating Including Modal and Static Response Data .	24
3.1.2 Updating by Constrained Optimization . . . . .	25
3.1.3 Definition of Model Parameters . . . . .	27
3.2 Preliminary results using simulated data . . . . .	29
3.3 Model Update of “Blade A” . . . . .	31
3.3.1 Description of experimental plant . . . . .	32
3.3.2 Estimation of beam properties . . . . .	37
3.4 Model update of “Blade B” . . . . .	39
3.4.1 Description of experiments . . . . .	39
3.4.2 Estimation process . . . . .	45

<b>4</b>	<b>Identification of aerodynamic properties of blades</b>	<b>49</b>
4.1	Estimation process . . . . .	51
4.1.1	Identification using power, thrust and blade loads . . . . .	51
4.1.2	Identification with direct approach . . . . .	54
4.1.3	Identification with the SVD-based approach . . . . .	55
4.2	Results from wind tunnel test data . . . . .	60
4.2.1	Description of experiments . . . . .	60
4.2.2	Direct approach . . . . .	63
4.2.3	SVD-based approach . . . . .	66
<b>5</b>	<b>Conclusions</b>	<b>79</b>
5.1	Identification of beam models . . . . .	79
5.2	Identification of aerodynamic properties . . . . .	81
<b>II</b>	<b>Stability and identification of periodic wind turbine models</b>	<b>83</b>
<b>6</b>	<b>Introduction and motivation</b>	<b>85</b>
6.1	Periodicity . . . . .	86
6.2	Model independence . . . . .	89
6.3	Organization of this part . . . . .	90
<b>7</b>	<b>Stability analysis of LTP systems</b>	<b>93</b>
7.1	Continuous time . . . . .	93
7.2	Discrete time . . . . .	99
7.3	Illustration by a model problem . . . . .	101
<b>8</b>	<b>System identification of LTP systems from input-output data</b>	<b>109</b>
8.1	Identification using the prediction error method (PEM) . . . . .	110
8.1.1	Equation-error identification of LTP systems . . . . .	111
8.1.2	Output-error identification of LTP systems . . . . .	113
8.1.3	Identification of PARMAX model . . . . .	114
8.2	Realization of the PARMAX sequence in state-space form . . . . .	115
<b>9</b>	<b>Results and conclusions</b>	<b>117</b>
9.1	Rotor edgewise response . . . . .	118
9.2	Tower side-side response . . . . .	120
9.3	Tower fore-aft and in-plane whirling response . . . . .	124
9.4	The periodic Campbell diagram . . . . .	124
9.5	Real wind turbines: the effect of turbulence . . . . .	126
9.5.1	First blade edgewise mode . . . . .	126
9.6	Conclusions . . . . .	128

**Conclusions and outlook** 133

**Bibliography** 137





---

# Introduction



---

## Why system identification of wind turbines?

---

**W**IND turbine system identification is one of the most important ways to go in order to address the current and future needs in the field of wind turbine modeling and analysis. This is the basic idea which have encouraged the beginning and motivated the development of this thesis.

First of all, a consideration is right and proper: wind turbines are extremely complex systems, whose dynamics depends on several factors such that complex aerodynamics, complicated structural and mechanical properties, dynamics of foundations, control systems, interactions between tower and blades, turbulent wind conditions, . . . . The modeling and the analysis of such these systems, in the course of time, have required mathematical models increasingly sophisticated and computational power more and more elevated. The design of future large and very large wind turbines will surely increase the importance of having adequate mathematical models, which can correctly capture their relevant physics. Currently, multibody models represent the best compromise between ability in describing the behavior of wind turbines and low computational cost.

In this scenario, we can formulate two main questions:

1. In order to obtain high fidelity models of wind turbines we need not only adequate mathematical models but also the correct tuning of their parameters (e.g. structural and aerodynamic properties), therefore how we can obtain the estimates of such parameters in order to en-

sure the best possible fidelity to the reality?

2. Since research fortunately is continuing to provide improved simulation codes, is it possible to use such these high fidelity models of arbitrary complexity directly to perform important analysis as those related to the stability?

The goal of the research described in this thesis is to explore the possibility of using system identification to answer both the previous questions. Some problems of interest related to the estimation of blades structural and aerodynamic properties and to the stability analysis of a large wind turbines will be solved by means of system identification techniques. As a consequence of that, the truthfulness of the assumption made at the beginning of the introduction, that the system identification can be used to address the current and future need of wind turbine modeling and analysis, will be demonstrated.

## Organization of the thesis and innovative contents

---

The discipline of system identification was largely developed in the course of the years. It is based on a rigorous statistic theory and on a small number of leading principles, but actually it is very difficult to make a survey of this art, as emphasize by the excellent lecture of L. Ljung made in 2008, [1].

Even if there exist many approaches and many fields, in which this discipline can be successfully applied, system identification for wind turbines is still in its infancy and much need to be done before the estimation techniques can be used routinely and efficiency by industry. The main innovative aspect of this research concerns this lack. Some identification procedures are developed and tested using real and virtual experimentation data in order to provide mature and effective *best practices* to follow in the field of wind turbine, and in general of rotary wing system, modeling and analysis.

The work is divided into two parts entitled “Identification of properties of wind turbine models” and “Stability analysis and identification of periodic wind turbine models”.

The first part concerns the estimation of the blades structural and aerodynamic properties from experimental data.

In the five chapters of this part, the problem of obtaining comprehensive validated models of wind turbine will be considered. A brief review of theory of the system identification is presented in Chapter 2 together with several statistical metrics used to evaluate the goodness of the estimates.

In the Chapters 3 the maximum likelihood estimator is performed in order to identify the structural (flapwise and edgewise stiffness and torsional rigidity) and inertial (mass distribution) properties of two real wind turbine blades of 6.2 and 7.5 meters length from experimental data. The estimation procedures is based on a unified approach, in which multiple sources of measurements (e.g. modal and static experiments) as well as suitable constraints (e.g. total mass and center of gravity position) can be used together in a constrained optimization. This new introduced possibility first improves the quality of the estimates with respect to approaches which use only, as example, modal measures, [2–5] and second allows the estimation of the mass distribution together with the other parameters in a non-destructive way.

The Chapter 4 considers the identification of the aerodynamic properties of wind turbine rotors. In particular the lift and drag coefficients of the blade airfoils are estimated from measurements proper to characterize the aerodynamic performances (e.g. thrust and power). Although in literature great attention is deserved on the extraction of lift and drag curves from CFD simulations, [6–10], very few examples of identification from experimental data are proposed, [11]. The proposed estimation procedure, based again on the maximum likelihood formulation, is performed in order to identify the aerodynamic properties of the blade of a wind turbine scaled model using as measures the thrust and power coefficients obtained from wind tunnel experimentations. The solution of this problem appears to be hard, especially if compared with the structural identification, since the accuracy of the estimates results very low. To overcome this drawback, which was also reported (without finding an alternative solution) in [11], a new formulation of the problem, based on the singular values decomposition, are proposed. This new innovative and original method are able to give estimates with higher level of confidence and aerodynamic models better correlated with the experimental measures.

The second part of the thesis is related to the development of a model-independent stability analysis of wind turbines. In literature, most published methods to estimate the frequencies and the damping factors of the modes of interest are based on the linear time invariant system theory, [12], which is not suitable for a rotating system characterized by periodic coefficients, or use the multi-blade coordinate (MBC) transformation of Coleman and Feingold [13–15], which of course is only an approximation of the rigorous Floquet-Lyapunov transformation used in a periodic analysis. It is also important to emphasize the fact that any stability analysis based on the multi-blade coordinates transformation is model dependent, difficult to

implement and maintain

According to the proposed approach, the stability analysis is made by two steps: first a periodic input-output model is estimated from suitable measurements of input and output. Second the stability analysis according to the Floquet theory is performed on the identified model, leading in turn to the computation of all the modes which characterize the response of the system. Consequently such this analysis results to be model-independent, since it operates on the basis of input-output series, which can be obtained from simulations or possibly from real wind turbine responses, and compliant with the periodic nature of the system.

In Chapter 7 the stability analysis and the interpretation of the frequency response of a linear time periodic (LTP) system is presented. Chapter 8 concerns to the estimation of three kind of periodic input-output models, the equation-error, the output-error and the Periodic Auto-Regressive Moving Average with eXogenous input (PARMAX) model, and to the achievement of a canonical periodic realization in the state-space of such these models. Finally in Chapter 9 the proposed analysis is performed on a detailed high fidelity multibody model of a 6MW wind turbine.

## Developed tools

---

The main goals of this work couldn't be achieved without a suitable development of specific tools. In particular it is possible to mention three softwares: `BEst` (**B**lade **E**stimation) and `IdeA` (**I**dentification of **A**erodynamic properties), which are concerned with the estimation of structural and aerodynamic properties of blades, and `PSI-tool` (**P**eriodic **S**tability analysis by **I**dentification) which refers to the identification and the analysis of periodic input-output models.

`BEst` and `IdeA` codes implement the methodologies described in the first part of this thesis and are written using the Matlab computer language. Both codes should be interfaced with an external computer program providing a suitable implementation of a the mathematical model of reference, which is a beam model for the structural case and a BEM (Blade Element Momentum) model, for the aerodynamic case. Currently, `BEst` and `IdeA` are interfaced with the program `Cp-Lambda` (Code for Performance, Loads, Aero-Elasticity by Multi-Body Dynamic Analysis) [16]; however, both codes have been written in such a way to allow for the interfacing with other beam and BEM simulators.

`PSI-tool` is a tool for performing the identification of periodic input-output models and the stability analysis of the identified models according

to the Floquet theory and is implemented in Matlab language. The tool consists in a series of Matlab functions which mainly solve the identification problem of the PARMAX (Periodic AutoRegressive Moving Average with eXogenous input) model from measurements of suitable input and output time series using the prediction error algorithm as described in the second part of the thesis. The software package is moreover completed by a set of other functions providing the realization in the state space of identified input-output models and the periodic stability analysis.





---

**Part I**

**Identification of properties of  
wind turbine models**



---

# CHAPTER 1

---

## Introduction

---

**T**he first part of the thesis is concerned with the development of *model update* procedures [17] applicable to wind turbine rotors. The update of models from experimental measurements is part of the broader problem of *system identification* [18, 19] of wind turbines, which finds applicability in the validation and verification of mathematical models for both design and certification, and in wind turbine active control applications, [20].

Modern comprehensive aero-servo-elastic high fidelity models of wind turbines are based on first principles, and include sophisticated mathematical sub-models of the various components, as blades, tower and drive-train [21]. The structural models are also coupled with aerodynamic models, which, depending on the application at hand, can range from classical blade element inflow models (BEM), to time-accurate dynamic inflow [22] and free-wake models, all the way to first principle computational fluid dynamics (CFD). Comprehensive models also include many other sub-models related for example to generators, actuators and sensors, and are coupled furthermore with the system controllers, including supervisors of the operating states and blade pitch and torque controllers. Hence, wind turbine

analysis codes are typically based on complex, non-linear, multi-field models which are formulated in the time domain.

The fidelity of overall models depends on the fidelity of sub-models and of their couplings, whereas the accuracy of sub-models depends on their ability to capture the relevant physics and on the correct tuning of their parameters. Since modern models, based for example on multibody formulations are actually able to reproduce opportunely the relevant physics and the couplings between the various sub-systems, great attention must be deserved to the tuning of the model parameters.

From this last consideration we can state the first important application of parameter identification in the field of wind turbine system modeling: to calibrate the parameters of wind turbine models to ensure the best possible fidelity to reality, given an assumed mathematical model.

Parameter estimation for wind turbines is still in its infancy and much needs to be done before suitable techniques which work in practice can be effectively used by industry. Moreover, it appears that, given the complexity of wind turbine models and of the problem of system identification in general, a practical approach to accomplish the goal would be to use a divide-and-conquer method to incrementally estimate the parameters of the various sub-models. Such a practice would proceed in two main steps: a first concerns the sub-system identification, followed by a second step which concerns the coupled system identification.

In the first step the parameters of the sub-models (e.g. blades, tower, actuators, etc.) are estimated using specific experimental observations of each sub-model behavior. For example, considering the estimation of structural models, many experiments, which may include the measurement of mode frequencies and shapes, structural deflections under known loads, etc., can be often performed in a controlled environment with good accuracy and low noise levels, as a laboratory. Moreover, one may consider also the identification of aerodynamic models, such as sectional properties (e.g. lift and drag coefficients), dynamic stall models and the measurement of rotor performances in the wind tunnel.

Next, the identification can be conducted for the whole wind turbine operating in closed-loop, in order to estimate those parameters which can not be estimated in the first step, including for example the coupling terms, such as those related to the inflow or to the blades-tower interference models.

Within this general framework, this part is concerned with the sub-model identification step. More specifically, it describes the use of the parameter estimation formulated according to the maximum likelihood in order to update the blade structural beam models and the aerodynamic prop-

---

erties of wind turbine rotors.

It is anyway important to emphasize the fact that the same methods developed in this work still remain effective tools to use for the updating procedures of other sub-models.

## **Organization of Part I**

---

The work described in this part is organized as follows.

First an outline of the estimation problem is described in Chapter 2. The maximum likelihood approach is presented as well as all those statistical metrics using to evaluate the goodness of the identified models.

Chapter 3 and 4 is concerned with the identification respectively of the structural and of the aerodynamic properties of wind turbine blades. The developed procedures are described and tested by some identification trials using real data provided by experimentation in laboratory and in wind tunnel.

Finally, Chapter 5 summarizes the conclusions and the possible improvements of both the proposed estimation approaches.



---

# CHAPTER 2

---

## The estimation problem

---

### 2.1 Formulation

---

#### 2.1.1 Maximum Likelihood Estimation

Consider a parametric version of the model, noted  $\mathcal{M}(\mathbf{p})$ , where  $\mathbf{p} \in \mathbb{R}^n$  is a vector of parameters, related to the properties of the analyzed system.

Define a set of output quantities  $\mathbf{y} = \mathbf{h}(\mathbf{p})$ , where  $\mathbf{y} \in \mathbb{R}^m$ . An experimental measurement (observation) of the outputs  $\mathbf{y}$  can be expressed as

$$\mathbf{z} = \mathbf{y} + \mathbf{r}, \quad (2.1)$$

where the error  $\mathbf{r}$  is due to measurement and/or modeling errors, the latter generated by modeling approximations and unmodeled or unresolved physical processes in  $\mathcal{M}$  with respect to the reality.

Considering a sample of observations  $S = \{z_1, z_2, \dots, z_N\}$ , the likelihood function is defined as

$$f(S, \mathbf{p}) = \prod_{i=1}^N p(z_i | \mathbf{p}), \quad (2.2)$$

where  $p(z_i|\mathbf{p})$  is the probability of the observed variable  $z_i$  given  $\mathbf{p}$ . Maximum likelihood estimation seeks to find the most likely vector  $\mathbf{p}$  for model  $\mathcal{M}$  by maximizing function  $f(S, \mathbf{p})$ , i.e. it identifies the vector  $\mathbf{p}$  that gives the maximum probability of realizing the measurements. Given the exponential nature of probability densities, the problem is re-formulated as the minimization of the negative logarithm of the likelihood function:

$$\mathbf{p}^* = \arg \min_{\mathbf{p}} J, \quad (2.3)$$

with  $J = -\ln f(S, \mathbf{p})$ .

Assuming a normal (Gaussian) distribution with zero mean for the residuals  $\mathbf{r}_i$ ,  $i = 1, N$ , and further assuming that the residuals are statistically independent from one another, the likelihood function can be expressed as

$$f(S, \mathbf{p}) = ((2\pi)^m \det \mathbf{R})^{-N/2} \exp \left( -\frac{1}{2} \sum_{i=1}^N \mathbf{r}_i^T \mathbf{R}^{-1} \mathbf{r}_i \right), \quad (2.4)$$

where

$$E[\mathbf{r}_i \mathbf{r}_j^T] = \mathbf{R} \delta_{ij}, \quad (2.5)$$

$E[\cdot]$  being the expected value operator,  $\mathbf{R}$  the error covariance and  $\delta_{ij}$  the Kronecker delta symbol. The optimization cost function of problem (2.3) then becomes

$$J = \frac{mN}{2} \ln 2\pi + \frac{N}{2} \ln \det \mathbf{R} + \frac{1}{2} \sum_{i=1}^N \mathbf{r}_i^T \mathbf{R}^{-1} \mathbf{r}_i. \quad (2.6)$$

Notice that, when modeling errors are present, the assumptions of zero mean of the residuals  $\mathbf{r}$  might not be fully satisfied, although they appear to be routinely adopted in practical applications [18].

A robust numerical implementation of problem (2.3), as proposed in Ref. [23], can be based on the following iteration, termed here Adaptive Covariance Maximum Likelihood (ACML) method:

1. For a given error covariance  $\mathbf{R}$ , assumed temporarily frozen, minimize with respect to the free parameters  $\mathbf{p}$  the cost function

$$\tilde{J} = \frac{1}{2} \sum_{i=1}^N \mathbf{r}_i^T \mathbf{R}^{-1} \mathbf{r}_i, \quad (2.7)$$

which is obtained from Eq. (2.6) by neglecting all irrelevant constant terms.



---

## 2.2. Identifiability and singular values decomposition

2. For the parameters  $\mathbf{p}^*$  obtained at step 1, minimize with respect to  $\mathbf{R}$  the cost function  $J$ . The solution is obtained in closed-form, leading to the update of the error covariance matrix (see Ref. [18], Appendix E, for details):

$$\mathbf{R} = \frac{1}{N} \sum_{i=1}^N \mathbf{r}_i \mathbf{r}_i^T. \quad (2.8)$$

If not enough samples are available to reconstruct an estimate of the error covariance  $\mathbf{R}$ , one can further assume the statistical independence of the residual components, so that the covariance becomes

$$\mathbf{R} = \text{diag}(\dots, r_j^2, \dots), \quad j = 1, m. \quad (2.9)$$

3. Return to step 1, and repeat until convergence.

This approach should be contrasted with the classical weighted least squares approach, which amounts to performing just step 1 once, by assuming  $\mathbf{R}$  known and frozen.

---

## 2.2 Identifiability and singular values decomposition

The evaluation of the identifiability of the parameters is a critical step of all identification problems, since it is important to select the parameters that are going to be identified and to consider the outputs which can be used in order to maximize the informative content of the measures. There exist several issues which could lead to ill-posed identification problems.

For example, as simply deducible, the use of measures affected by a high level of noise or poorly influenced by a set of parameters, leads irremediably to not accurate estimates. Moreover, it is also possible to consider two or more parameters which involve similar effects on outputs: even if we try to solve as best as possible the estimation problem, there will be at least one combination of the parameters, which is actually not-identifiable.

Fortunately, in many cases a bit of practice and simple physic considerations are enough to formulate a well-posed problem. In any case, the system identification theory gives several rigorous and useful *a priori* and *a posteriori* criteria to formulate and solve coherently an identification problem and to evaluate the identifiability level of the unknowns. All these criteria become essential for those problems characterize by low identifiability of some parameters, which are actually harder to solve.

The basic concept for evaluating the accuracy of the estimates is the so-called Cramér-Rao lower bound.

Indicating as  $\bar{\mathbf{p}}$  the true but unknown deterministic parameters to be estimated from measurements, it can be shown [18, 23] that the Cramér-Rao bounds on the covariance of their estimates  $\mathbf{p}^*$  is given by

$$\text{Var}(\bar{\mathbf{p}} - \mathbf{p}^*) \geq \mathbf{D}, \quad (2.10)$$

where  $\mathbf{D} = \mathbf{F}^{-1}$ ,  $\mathbf{F}$  is the Fisher information matrix

$$\mathbf{F} = \sum_{i=1}^N \mathbf{G}_i^T \mathbf{R}^{-1} \mathbf{G}_i, \quad (2.11)$$

and  $\mathbf{G}_i = \partial \mathbf{y}_i / \partial \mathbf{p}$  the sensitivity of the observations of the  $i$ th experiments with respect to the parameters. The  $j$  element of the diagonal of  $\mathbf{D}$ , noted  $d_{j,j}$  is the variance of the  $j$ th parameter, and in turn  $\sqrt{d_{j,j}}$  is its deviation.

This result shows that the identified parameters are stochastic variables too, and that an estimation of their variance is achievable a priori and a posteriori using the sensitivity matrix computed respectively with the model before and after the identification. In order to bridge mathematics with physics, consider two simple examples in which the identifiability is completely lost. First, if a given parameter does not affect the outputs a column of  $\mathbf{G}$  would be always equal to zero leading to a singular Fisher information matrix and to an ill-posed problem. Second, if two or more parameters have similar effects on outputs, in the sense that the sensitivity of a parameter is equal to a linear combination of the sensitivity of the others, there would be one column of  $\mathbf{G}$  that is a linear combination of the other columns leading again to a singular information matrix. What happens in this case is that, intuitively, it is impossible to understand how to change the parameters because there are infinite possible solutions which actually minimize the cost functions. Of course between the completely not-identifiability and the perfect identifiability there are infinite levels, and the Cramér-Rao bound can measure such levels.

In addition, the correlation matrix  $\mathbf{X}$  is another important tool for measuring the collinearity between two parameters. The element  $(p, q)$  of  $\mathbf{X}$  noted  $\chi_{p,q}$  is computed by the following equation

$$\chi_{p,q} = \frac{d_{p,q}}{\sqrt{d_{p,p}d_{q,q}}}, \quad (2.12)$$

where  $d_{u,v}$  is the element of matrix  $\mathbf{D}$  located in position  $(u, v)$ . It is clear that the correlation matrix  $\mathbf{X}$  is symmetric and has all the diagonal elements equal to 1. For the other elements, the values 1 or -1 indicate a perfect collinearity whereas 0 a perfect decoupling. If the modulus of an

## 2.2. Identifiability and singular values decomposition

extra-diagonal element  $|\chi_{\bar{p},\bar{q}}|$  is greater than a certain level (typically set equal to 0.90 or 0.95) the  $\bar{p}$ th and  $\bar{q}$ th parameters are actually considered not identifiable.

Although the Cramér-Rao inequality and the correlation matrix are important indications of the goodness of the identified model, and in general of the well-posedness of the estimation problem, the need of a rigorous approach to follow in the case of low identifiability still remains. One of the possible answers arises from the singular values decomposition.

Consider the matrix  $\mathcal{G}$  made by stacking the sensitivity matrices  $\mathbf{G}_i$ , multiplied to the left by  $\mathbf{R}^{-1/2}$ , for all  $i = 1, N$  as

$$\mathcal{G} = \begin{bmatrix} \mathbf{R}^{-1/2}\mathbf{G}_1 \\ \mathbf{R}^{-1/2}\mathbf{G}_2 \\ \vdots \\ \mathbf{R}^{-1/2}\mathbf{G}_N \end{bmatrix}, \quad (2.13)$$

and consider the singular values decomposition (SVD) of  $\mathcal{G}$

$$\mathcal{G} = \mathbf{U}\mathbf{S}\mathbf{V}^T. \quad (2.14)$$

where  $\mathbf{U}$  and  $\mathbf{V}$  are the left and right square orthogonal unit matrices of the decomposition, and  $\mathbf{S}$  is constructed as

$$\mathbf{S} = \begin{bmatrix} \mathbf{\Sigma} \\ \mathbf{0} \end{bmatrix}, \quad (2.15)$$

where  $\mathbf{\Sigma}$  is a diagonal matrix whose elements  $\sigma_i$  are the singular values typically sorted so as  $\sigma_1 \geq \sigma_2 \geq \dots \geq \sigma_n \geq 0$ .

It is simple to rewrite Eq.( 2.11) using Eq. (2.13) as

$$\mathbf{F} = \mathcal{G}^T \mathcal{G}, \quad (2.16)$$

or alternately, using the right singular matrix  $\mathbf{V}$  and singular values  $\mathbf{\Sigma}$ ,

$$\mathbf{F} = \mathbf{V}\mathbf{\Sigma}^2\mathbf{V}^T. \quad (2.17)$$

From Eq. 2.17, the inverse of  $\mathbf{F}$ ,

$$\mathbf{F}^{-1} = \mathbf{V}\mathbf{\Sigma}^{-2}\mathbf{V}^T, \quad (2.18)$$

is simply derivable.

Furthermore, by pre- and post-multiplying (2.10) by  $\mathbf{V}$  and  $\mathbf{V}^T$ , the Cramér Rao inequality holds true, since  $\mathbf{V}$  is a full rank matrix. Therefore

$$\text{Var}(\mathbf{V}^T \bar{\mathbf{p}} - \mathbf{V}^T \mathbf{p}^*) \geq \mathbf{V}^T \mathbf{F}^{-1} \mathbf{V}, \quad (2.19)$$

which, recalling (2.18), leads to the following

$$\text{Var}(\bar{\Theta} - \Theta^*) \geq [\Sigma^2]^{-1}, \quad (2.20)$$

where

$$\Theta = V^T p \quad (2.21)$$

is a new set of unknowns computed as a particular linear combination of the original parameters  $p$ . Notice that  $V$  is an orthonormal matrix and therefore it could be viewed as a rotation tensor.

The inequality (2.20) means that  $\Sigma^{-2}$  represents the lower bounds of the variance of the identification of the parameter  $\Theta$ . Reminding that  $\Sigma$  is a diagonal matrix, the Cramér Rao inequality could be written in the scalar form for the  $j$ th component of the vector  $\Theta$ , noted  $\theta_j$  as

$$\text{Var}(\bar{\theta}_j - \theta_j^*) \geq \frac{1}{\sigma_j^2}. \quad (2.22)$$

A certain parameter  $\theta_j$  for which the corresponding Cramér Rao lower bound ( $1/\sigma_j^2$ ) is smaller than a suitable amount, can be considered reliably identifiable. The threshold of the variance for which a particular parameters  $\theta_j$  could be selected as identifiable or not has to be chosen depending on the problem at hand.

According to the SVD, the estimation problem could be reformulated in order to consider only the identifiable parameter, [24].

To this end define the vector of identifiable parameters as  $\Theta_{\text{ID}} = \{\theta_1, \theta_2, \dots, \theta_{N_{\text{ID}}}\}^T$ , where  $N_{\text{ID}}$  is the number of identifiable parameters and the vector of not identifiable parameters  $\Theta_{\text{NID}} = \{\theta_{N_{\text{ID}}+1}, \theta_{N_{\text{ID}}+2}, \dots\}^T$ . Consequently, the right singular matrix can be divided as  $V = [V_{\text{ID}} \ V_{\text{NID}}]$ , where  $V_{\text{ID}} = [v_1, v_2, \dots, v_{N_{\text{ID}}}]$  and  $V_{\text{NID}} = [v_{N_{\text{ID}}+1}, v_{N_{\text{ID}}+2}, \dots]$ .

The minimization of the maximum likelihood cost function (2.6) is then performed with respect to the vector  $\theta_{\text{ID}}$ . Then the physical parameters  $p$  are computed simply according to the definition in Eq. (2.21), as

$$p = V_{\text{ID}} \Theta_{\text{ID}}. \quad (2.23)$$

Moreover, the SVD provides even more information on the system identifiability through the matrix  $U$ , because its columns show which of the available measurements actually contribute to identify the parameters.

---

# CHAPTER 3

---

## Identification of blade beam models

---

**T**HE formulation of beam elements has received considerable attention in the literature. Some complex applications, such as anisotropic helicopter and wind turbine rotor blades, are solved using geometrically exact formulations [25] whose fully-populated stiffness matrices are obtained either by the use of sectional analysis theories (see for example Ref. [26] and references therein), or directly by 3D finite elements [27, 28]. The resulting blade models are used for performing simulations in all necessary operating conditions using a plethora of multi-disciplinary aero-servo-elastic modeling tools, with the purpose of estimating loads, stability boundaries, vibration levels and other quantities of interest, as well as for the tuning and verification of control laws.

The rotor blades of modern wind turbines, being realized using composite materials and designed under a number of aero-elastic and manufacturing constraints, are typically characterized by complex distributions of their stiffness, mass and inertial properties along the span. Often, manufactured blades present characteristics that differ in a non negligible way from their theoretical design values. The reasons for this are numerous, and include manufacturing processes, uncertain material properties, modeling approxi-

mations, etc.

To understand the nature of the discrepancies between designed and manufactured blades, and to provide updated high fidelity mathematical beam models to be used in aero-elastic simulations, it is useful to devise procedures that provide estimates of the physical parameters of the blade on the basis of experimental measures obtainable on the manufactured items [29–32].

This chapter describes the development of model update procedures [17] applicable to wind turbine blades; this problem is part of the broader task of system identification of wind turbines. The formulation is based on an output-error maximum-likelihood constrained parameter estimation approach [18, 23, 33, 34]. The free parameters of the estimation problem are represented by the structural and mass characteristics of a beam model of the blade. An ad hoc interpolation scheme is used to keep the number of free parameters to a minimum, while at the same time accounting for the rapidly varying and often discontinuous distributions of physical properties along the span of typical modern wind turbine blades.

The parameter estimation is formulated as a constrained optimization problem, solved using a Sequential Quadratic Programming (SQP) approach [35]. The cost function is formulated in terms of the maximum likelihood function and considers multiple kind of measurements, which may include natural frequencies, mode shapes, static deflections and dynamic responses. The use of the maximum likelihood function allows one to account for the stochastic nature of the problem, due to the inevitable presence of noise and uncertainties in the measurements.

The definition of the estimation problem is complemented by a number of equality and/or inequality constraints, which may include bounds on the physical parameters, knowledge of the total mass and of the location of the center of gravity of the blade, and the requirement that the updated model improves the metric quality measure provided by the Modal Assurance Criterion with respect to the initial baseline model.

Although most published methods in finite element model updating use exclusively modal data (cf. for example Refs. [2–5] and references therein), we argue here that one should use all possible sources of information for increasing the reliability of model update procedures. A better identifiability of the parameters is typically obtained only when enough information is contained in the experimental measurements. To this reason, the present approach is formulated so that multiple measures are fused simultaneously together to yield more accurate estimates of the unknown parameters. To robustify the solution of the identification problem, which is often difficult

---

given its high dimensionality, an iterative approach in which the estimation problem is divided into smaller sub-problems and repeated until convergence is developed. Such algorithm greatly eases convergence, without however affecting the quality of the results.

The idea of combining multiple sources of information for the calibration of wind turbine beam models is not new. Static deflections under gravity and applied loads were used in Ref. [36] to estimate the stiffness and mass distributions, while modal data was used for a final consistency check of the estimates. Static deflections and modal data were fused together using an unconstrained optimization approach in Ref. [37] to estimate the Young modulus distribution along the blade, while the mass distribution was assumed to be known or measured directly by cutting the blade into sections. The same method was then further evaluated on multiple blade estimation problems in Refs. [38, 39].

The present proposed approach differs from these related methods in a number of ways. First, the identification of Young modulus, as opposed to the identification of elements of the stiffness matrix as used here, requires a precise knowledge of the cross section geometry that one must either assume or measure by cutting the blade into sections. Second, a contribution of our work is to show that one can identify the blade mass properties with a good level of confidence together with the stiffness ones thanks to the use of a constrained optimization, in which additional information (e.g., total mass, center of gravity location, etc.) is infused, avoiding to make assumptions a priori or to cut the blade and weigh the resulting sections. Third, the method is based on a statistical approach through a maximum likelihood cost function. This has important practical implications. In fact, the effects of noise in the measurements are accounted for, and there is an automatic and physically-based way of weighting the different data sets that enter into the process; furthermore, one can evaluate the confidence intervals of the estimates. Fourth, we propose a specially devised divide and conquer approach that, without affecting the quality of the results, eases convergence of these high dimensionality constrained optimization problems.

The proposed formulation is demonstrated first on simulated data regarding a large wind turbine blade, and then using real experimental measures obtained on two small wind turbine blades.

The procedures and the results shown in this chapter are based on those presented in [40]

### 3.1 Model Updating of Blade Beam Models

---

#### 3.1.1 Model Updating Including Modal and Static Response Data

Typically, multiple experiments can be conducted on a blade, including measurement of the eigenfrequencies, of the eigenvectors, of static deflections under concentrated or distributed known loads, and temporal responses under suitable excitations. Conceptually, all this data can be profitably used in a single unified model updating procedure, in order to estimate the beam properties that best fit the available experimental measurements.

Since parameter estimation of complex models is a problem hard to solve, the possibility of introducing in the estimation process all the available experimental data results to be interesting in order to improve the informative content of the measures. To this reason the proposed maximum likelihood approach is formulated to account for multiple experiments.

The output vector is here defined as

$$\mathbf{y} = (\mathbf{y}_M^T, \mathbf{y}_S^T)^T, \quad (3.1)$$

where  $\mathbf{y}_M$  is the set of outputs accounting for modal data (frequencies and, possibly, modal shapes), and  $\mathbf{y}_S$  the set of outputs accounting for static deflections.

More precisely,  $\mathbf{y}_M$  is defined as

$$\mathbf{y}_M = (\dots, \omega_k, \boldsymbol{\phi}_k^T, \dots)^T, \quad k = 1, N_M, \quad (3.2)$$

where  $\omega_k$  is the  $k$ th natural modal frequency,  $\boldsymbol{\phi}_k$  its associated modal shape and  $N_M$  the number of modes, obtained from the solution of the corresponding eigenvalue problems on model  $\mathcal{M}$ :

$$[\omega_k, \boldsymbol{\phi}_k] = \text{eig}(k, \mathbf{p}). \quad (3.3)$$

If the eigenvectors are not experimentally available, then the set of outputs simply contains the modal frequencies, i.e.  $\mathbf{y}_M = (\dots, \omega_k, \dots)^T$ . In both cases, we write  $\mathbf{y}_M \in \mathbb{R}^{m_M}$ , where in the first case  $m_M = (1 + N_{\text{nodes}}N_{\text{dc}})N_M$ , being  $N_{\text{nodes}}$  the number of nodes in the FEM model of the blade and  $N_{\text{dc}}$  the number of displacement components in the modal vector, while  $m_M = N_M$  in the second case. The associated maximum likelihood cost function of Eq. (2.7) is noted  $J_M$ .

Consider now the static response of model  $\mathcal{M}$ . The vector of structural deflections at the mesh nodes, noted  $\mathbf{d}$ , can in general be computed by



solving the following system of governing equilibrium equations

$$\mathbf{g}(\mathbf{d}, \mathbf{u}, \mathbf{p}) = \mathbf{0}, \quad (3.4)$$

where  $\mathbf{u}$  is the input (representing either point and/or distributed loads on the structure). Clearly, the governing equations depend on the model parameters  $\mathbf{p}$ . For each given loading condition  $\mathbf{u}_k$  of the  $N_S$  available ones, the corresponding static deflections are noted  $\mathbf{d}_k$  and the outputs are defined as

$$\mathbf{y}_{S_k} = \mathbf{h}_S(\mathbf{d}_k), \quad k = 1, N_S, \quad (3.5)$$

$\mathbf{y}_{S_k} \in \mathbb{R}^{m_y}$ , i.e. they are given by some function  $\mathbf{h}_S(\cdot)$  of the beam response (for example, they might represent the displacement components at the tip of the beam or at some other given location along the span). Then, the outputs for all loading conditions are gathered together to define the vector of outputs accounting for static deflections, i.e.

$$\mathbf{y}_S = (\dots, \mathbf{y}_{S_k}^T, \dots)^T, \quad k = 1, N_S, \quad (3.6)$$

where  $\mathbf{y}_S \in \mathbb{R}^{m_S}$ ,  $m_S = m_y N_S$ . The associated maximum likelihood cost function of Eq. (2.7) is noted  $J_S$ .

#### 3.1.2 Model Updating by Constrained Optimization

For the practical solution of realistic problems, the model parameter estimation given by (2.3) is reformulated here as the following constrained optimization

$$\min_{\mathbf{p}} J(\mathbf{y}, \mathbf{z}), \quad (3.7a)$$

$$\text{s.t.: } \mathbf{c}(\mathbf{y}, \mathbf{p}) \leq \mathbf{0}, \quad (3.7b)$$

$$\mathbf{y}_{\text{lb}} \leq \mathbf{y} \leq \mathbf{y}_{\text{ub}}, \quad (3.7c)$$

$$\mathbf{p}_{\text{lb}} \leq \mathbf{p} \leq \mathbf{p}_{\text{ub}}, \quad (3.7d)$$

where the outputs  $\mathbf{y}$  were given in (3.1) and are functions of the unknown parameters  $\mathbf{p}$  as detailed in §3.1.1. Assuming that modal and static measurements are uncorrelated, the maximum likelihood cost  $J$  in (3.7a) can be written as the sum of two terms as

$$J = \frac{1}{m_M} J_M + \frac{1}{m_S} J_S, \quad (3.8)$$

where  $J_M$  and  $J_S$  are the maximum likelihood costs expressed by Eq. (2.7) for, respectively, the modal and static deflection data. Notice that the two

cost contributors are scaled by the number of available measures,  $m_M$  and  $m_S$ , since the two are typically quite different between each other (e.g., tens of static deflections and only a few eigenfrequencies, as in the examples shown later on).

The formulation of the problem is completed by a number of constraint conditions. Equations (3.7b) represent possible linear and/or non-linear equality and/or inequality constraints on the outputs and/or the parameters, as detailed further below. Furthermore, Eqs. (3.7c,3.7d) specify possible lower and upper bounds on the outputs and the parameters, respectively.

Problem (3.7) is a Non-Linear Programming Problem (NLP), which can be solved effectively with a number of methods, most notably SQP [35] and Interior Point (IP) [41]. In this work, the former of the two methods was used, with gradients of cost function and constraints computed by finite differences. When eigenvalues and eigenvectors are included in the definition of the problem outputs, their gradients can be computed efficiently by the technique described in Ref. [42], although for other outputs the gradients will in general have to be computed by numerical perturbation means.

As for most optimization problems, it is better to scale all quantities appearing in (3.7) so as to improve conditioning. To this end, we define scaled outputs  $\hat{\mathbf{y}} = (\dots, \hat{y}_i, \dots)^T$ , obtained by dividing each output by its corresponding measure

$$\hat{y}_i = \frac{y_i}{z_i + \delta}, \quad i = 1, m, \quad (3.9)$$

and in the same way the scaled measures  $\hat{\mathbf{z}} = (\dots, \hat{z}_i, \dots)^T$

$$\hat{z}_i = \frac{z_i}{z_i + \delta}, \quad i = 1, m, \quad (3.10)$$

where  $m$  is the number of available measures and  $\delta = \|\mathbf{z}\|_2$  is used to avoid divisions by zero; similarly, we define scaled parameters  $\hat{\mathbf{p}} = (\dots, \hat{p}_i, \dots)^T$  as

$$\hat{p}_i = \frac{p_i}{p_i^0}, \quad i = 1, n, \quad (3.11)$$

where  $n$  is the number of parameters and  $p^0$  are values related to the baseline (initial) model; typically, these values are never equal to zero. With

these new definitions, the scaled parameter estimation problem becomes

$$\min_{\hat{\mathbf{p}}} J(\hat{\mathbf{y}}, \hat{\mathbf{z}}), \quad (3.12a)$$

$$\text{s.t.: } \mathbf{c}(\hat{\mathbf{y}}, \hat{\mathbf{p}}) \leq \mathbf{0}, \quad (3.12b)$$

$$\hat{\mathbf{y}}_{\text{lb}} \leq \hat{\mathbf{y}} \leq \hat{\mathbf{y}}_{\text{ub}}, \quad (3.12c)$$

$$\hat{\mathbf{p}}_{\text{lb}} \leq \hat{\mathbf{p}} \leq \hat{\mathbf{p}}_{\text{ub}}, \quad (3.12d)$$

which in general exhibits superior convergence and robustness when compared to the unscaled problem (3.7).

Several different constraint types can be appended to the optimization problem by means of Eqs. (3.12b), so as to account for further sources of knowledge about the solution other than the measurements  $\mathbf{z}$ .

For example, when identifying the mass properties of the blade, the measured total mass and center of gravity locations can be enforced as constraints as

$$\mathbf{c} = \begin{pmatrix} 1 - \frac{1}{M} \int_0^L m(s) \, ds \\ 1 - \frac{1}{s_G M} \int_0^L m(s)s \, ds \end{pmatrix} = \mathbf{0}, \quad (3.13)$$

where  $M$  is the measured total blade mass,  $m(s) = m(\mathbf{p}(s))$  is the mass per unit span,  $s \in [0, L]$  is a coordinate measured along the beam reference line, being  $L$  the beam length, and  $s_G$  the center of gravity location along the span. Notice that here again the equations were written in non-dimensional form for scaling reasons.

To ensure that the eigenvectors computed on the updated model improve the metric quality measure provided by the Modal Assurance Criterion (MAC) with respect to the initial baseline model, the following inequality constraints can be included in the definition of Eqs. (3.12b):

$$\mathbf{c} = (\dots, \text{MAC}(\phi_i^0, \mathbf{z}_{\phi_i}) - \text{MAC}(\phi_i, \mathbf{z}_{\phi_i}), \dots) \leq \mathbf{0}, \quad i = 1, N_M, \quad (3.14)$$

where  $\phi_i^0$  is the  $i$ th eigenvector computed on the initial baseline model,  $\mathbf{z}_{\phi_i}$  the corresponding measured eigenvector, and the operator  $\text{MAC}(\cdot, \cdot)$  is defined as

$$\text{MAC}(\mathbf{a}, \mathbf{b}) = \frac{(\mathbf{a}^T \mathbf{b})^2}{(\mathbf{a}^T \mathbf{a})(\mathbf{b}^T \mathbf{b})}. \quad (3.15)$$

#### 3.1.3 Definition of Model Parameters

More often than not, the property distributions of wind turbine blades are quite complex, and present high gradients or jump discontinuities, for ex-

ample in correspondence of the beginning and ending of shear-webs. In order to accurately represent such complex property distributions, beam analysis codes for wind turbine applications typically define a large number of sectional properties along the blade span. The direct use of such sectional properties as unknown parameters in the model update processes described above is impractical for a number of reasons. First, a large number of sections would imply a large number of unknown parameters, which in turn would imply large computational costs. Second, and more importantly, the use of a large number of unknowns to represent beam properties along the span will decrease the observability of the problem.

To address these problems, the identification parameters  $\mathbf{p}$  of problem (3.7) are here defined in terms of interpolated multiplicative shape functions that deform a given baseline property distribution, as detailed next.

First, the blade span is divided into  $N_{\text{segm}}$  segments, the  $k$ th segment being defined for  $s_k \leq s \leq s_{k+1}$ , where the values  $0 = s_1, s_2, \dots, s_{N_{\text{segm}}+1} = L$  identify segment boundaries. Smooth interpolations are defined on each segment, while one may or may not impose a desired level of continuity between segments through constraints on the parameters to be included in Eqs. (3.12b). With no inter-segment constraints, one has a simple way to account for discontinuities in the blade property distributions.

Next, the  $i$ th property at station  $s$  along the span of the updated model, noted  $\pi_i(s)$ , is expressed as

$$\pi_i(s) = \alpha_i(s) \pi_i^0(s), \quad (3.16)$$

where  $\pi_i^0(s)$  is the value of the  $i$ th property for the initial model (baseline), while  $\alpha_i(s)$  is the multiplicative deforming factor of the baseline. The number of identified properties is noted  $N_{\text{prop}}$ , and  $\pi_i(s)$  can represent any one of the parameters of the beam model, as for example mass per unit span, sectional inertias, bending, torsional, axial and shear (according to the assumptions of the model) stiffnesses. For  $s$  in the  $k$ th segment, i.e.  $s \in [s_k, s_{k+1}]$ , the span-wise varying deforming factors are defined by the following interpolation

$$\alpha_i(s) = \sum_{j=1}^{N_{\text{nodes}}^k} n_j(\xi) \alpha_{i,j}^k, \quad (3.17)$$

where  $n_j(\xi)$  are shape functions expressed in terms of the non-dimensional abscissa  $\xi \in [0, 1]$ ,

$$\xi = \frac{s - s_k}{s_{k+1} - s_k}, \quad (3.18)$$

### 3.2. Preliminary results using simulated data

and  $\alpha_{i_j}^k$  are the associated  $N_{\text{nodes}}^k$  nodal values for segment  $k$ . There is ample freedom in the choice of the shape functions; in the examples we have used linear functions, but other choices (e.g., cubic splines) are certainly possible and could be dictated by the specific problem at hand. While it is clearly possible to use additive corrections to the baseline, the present multiplicative approach was preferred here because it allows, for the same number of degrees of freedom, for a richer representation of the distribution. For example, assuming for the sake of argument a cubic baseline, a linear correction gives a quartic description with the multiplicative approach, while only a cubic description with the additive one.

Finally, the optimization parameters are defined as the nodal values of the shape function, i.e.

$$\mathbf{p} = (\dots, \alpha_{i_j}^k, \dots)^T, \quad i = 1, N_{\text{prop}}, \quad j = 1, N_{\text{nodes}}^k, \quad k = 1, N_{\text{segm}}. \quad (3.19)$$

### 3.2 Preliminary results using simulated data

At first, we consider the application of the proposed procedures to a simulation case, with the goal of verifying the well-posedness of the problem and the identifiability of the unknown parameters.

To this aim, we consider the 61.5 meter long wind turbine blade of Ref. [43]. For simplicity of this preliminary study, the identification parameters were chosen as constants defined on three segments of equal length, as shown in Figure 3.1, for each structural property (i.e. flap-wise, edge-wise and torsional stiffnesses, and mass per unit span).

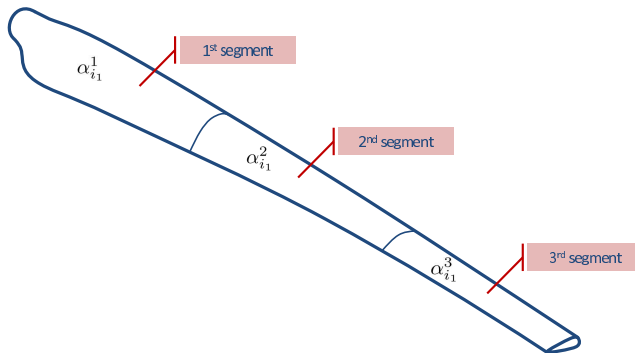


**Figure 3.1:** Definition of identification parameters for the preliminary simulation study.

The blade, clamped at the root and subjected to gravity, was loaded first with a tip force in the flap-wise direction, then in the edge-wise direction,

and finally with a tip torsional moment. The outputs included the displacements and rotations of ten uniformly spaced sections along the blade span, as well as the lowest five modal frequencies. All measures were added to a zero-mean Gaussian white error with standard deviation equal to 0.5% of their maximum value. For displacements, such values are typical of the case of wire transducer measurements, used later in one of the experimental tests, see section 3.3.

Eigenvectors were not included in this simulated example, for two reasons. First, in actual laboratory experiments eigenvectors are more difficult to measure than eigenvalues and they are often associated with higher levels of noise and uncertainty [17]. Second, eigenvectors often carry a smaller informational content than eigenvalues; this can be explained, for example, by recalling that the modal shapes of a beam of constant properties do not depend on the beam properties but only on the boundary conditions. This fact was confirmed by numerical experiments, which showed that the use of eigenvectors brings little benefit to the quality of the property estimates of wind turbine blades that are obtained by the sole use of eigenvalues and static deflections.

To ease convergence and robustify the procedure, the identification was conducted using a divide and conquer approach, where each set of properties (flap-wise, edge-wise, torsional stiffness and mass) is identified separately, while keeping the others temporarily frozen, and then iterating until convergence. The iteration is necessary to correctly capture all couplings, since all parameters have some influence on all outputs, although small in some cases.

The procedure, used here and in the following, can be summarized as follows:

1. Estimate flap-wise, edge-wise and torsional stiffnesses, one at a time, keeping the other ones frozen at their last updated values.
2. Maintaining the blade stiffness properties fixed, estimate the mass distribution, while enforcing constraints on measured total mass and center of gravity position, as well as MAC constraints if mode shapes are available.
3. Return to step 1 and repeat until convergence.

All steps are performed by solving an optimization defined by the same cost function, i.e. using always all available measurements (static test deflections and modal information) and, in this sense, this approach can be in-

terpreted as a Gauss-Seidel-like iteration on the original fusion-based problem.

Notice that in step 1, being the blade in general twisted and coupled, the result of each identification (e.g. of flap-wise stiffness) will be felt in the next (e.g., edge-wise stiffness). Similarly, the modifications of the stiffness distributions achieved by step 1 will be felt in step 2 when modifying the mass mainly through their effects on the modes. Finally, when iterating and repeating step 1, the modified mass will affect the solution because it will change the blade deflection due to gravity and the modes.

Notice that this procedure is just a way to simplify convergence, but it will not alter the results, so that the identification still remains a fusion approach where all available measurements contribute to the estimation of the unknown parameters. In other words, if one were to solve the problem in one shot (i.e., without divide and conquer), provided that one could make such one shot solution converge, then one would get exactly the same results that are obtained with the proposed divide and conquer iteration at convergence. This is so because the various steps in which the identification is broken, are repeated multiple times and iterated until convergence.

Table 3.1 summarizes the results of this identification exercise; the table column labeled “Initial” reports the initial guesses for the unknown parameters, which were arbitrarily set to  $\pm 10 \div 20\%$  of the real ones. The results show that the properties associated with the central part of the blade are more precisely identifiable than the ones towards the root, which in turn are more precisely identifiable than the ones of the tip region. This is due to the fact that the central part of a wind turbine blade is usually the one that contributes the most to the rigidity of the structure. Considering the central part of the blade, one can also observe that the flap-wise stiffness is more precisely identifiable than the edge-wise stiffness, which in turn is more precisely identifiable than the torsional stiffness. This can be explained by the fact that the three stiffnesses have decreasing (in the order flap-wise, edge-wise and torsion) effects on the displacement response of the blade, as expected.

Next, we consider the identification of the structural properties of two real wind turbine blades using experimental data, named in the following blades A and B, respectively.

### 3.3 Model Update of “Blade A”

---

The blade was tested by a consultant of the manufacturer for the purpose of verifying the resistance of the blade. Although these tests were not de-

## Chapter 3. Identification of blade beam models

**Table 3.1:** Identified parameters for the preliminary study using simulated data.

Parameters		Real	Initial	Identified
Flap-wise	$\alpha_{1_1}^1$ (root)	1.0	1.2	1.011
	$\alpha_{1_1}^2$ (central)	1.0	1.2	1.001
	$\alpha_{1_1}^3$ (tip)	1.0	1.2	1.011
Edge-wise	$\alpha_{2_1}^1$ (root)	1.0	0.8	0.996
	$\alpha_{2_1}^2$ (central)	1.0	0.8	0.997
	$\alpha_{2_1}^3$ (tip)	1.0	0.8	1.007
Torsional	$\alpha_{3_1}^1$ (root)	1.0	0.9	1.002
	$\alpha_{3_1}^2$ (central)	1.0	0.9	0.994
	$\alpha_{3_1}^3$ (tip)	1.0	0.9	0.991
Mass	$\alpha_{4_1}^1$ (root)	1.0	1.1	1.013
	$\alpha_{4_1}^2$ (central)	1.0	1.1	0.995
	$\alpha_{4_1}^3$ (tip)	1.0	1.1	0.969

signed for identifying the blade structural properties, it was found that the collected data was of sufficient quality and informational content even for this purpose, although with the limitations and problems noted here below.

### 3.3.1 Description of experimental plant

In order to perform the static tests, the blade was bolted at the root and equipped with five saddles placed along its span. Loads were applied at each saddle in the vertical direction at three different points labeled  $C_0$ ,  $C_1$  and  $C_2$ , as shown in Figure 3.2, via cables equipped with load cells and connected to an overhead traveling crane. Wire distance transducers were attached at points  $A_1$  and  $A_2$  on each saddle, as shown in Figure 3.2; an additional wire transducer was attached at the blade tip.

Static test data are collected loading blade in different points along blade span and in different points of the load applicators to involve mostly flap deflections and torsional rotations. For each load condition the available measures are the elongations of the eleven thread transducers (two transducers for each saddle and one connected to the blade tip). It's important to note that for each section, having only at best 2 transducers, there is no way to compute without approximations all the 6 displacement components.

Table 3.2 reports the weight of each saddle. Note that such this mass are



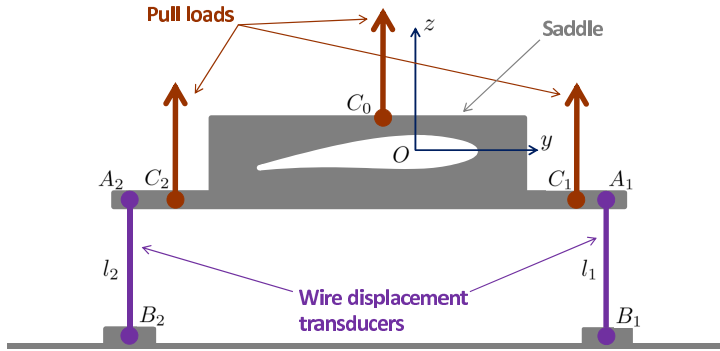


**Figure 3.2:** Sketch of saddle used for the loading of blade A.

not negligible compared to the blade mass, and therefore must be considered in the beam model during the identification.

**Table 3.2:** Mass of the load saddles.

	Load saddle 1	Load saddle 2	Load saddle 3	Load saddle 4	Load saddle 5
Mass [kg]	37.2	30.6	19.0	14.9	12.6

#### Static tests

Figure 3.3 shows a schematic view of the experiments: for each load case  $F_i$  represents the force applied to the  $i$ th section then  $C_j$  the  $j$ th point at which the load have been applied.

The details of the flap experiments (*i.e.* values of forces and their own points of application) are in reported in Table 3.3. Then Figure 3.4 show the measures of the transducers. The corresponding data for the torsional experiments are presented in Table 3.4, and in Figure 3.5.

From the measures provided by the wire transducers, the vertical deflections  $\delta_s$  and the torsional rotations  $\delta_r$  of each sections were obtained under the assumption of small deviations from the reference configuration, which holds in the case of the present measurements.

Notice that some of these load cases are far from optimal from the point of view of the identification of blade structural properties. In fact, whenever

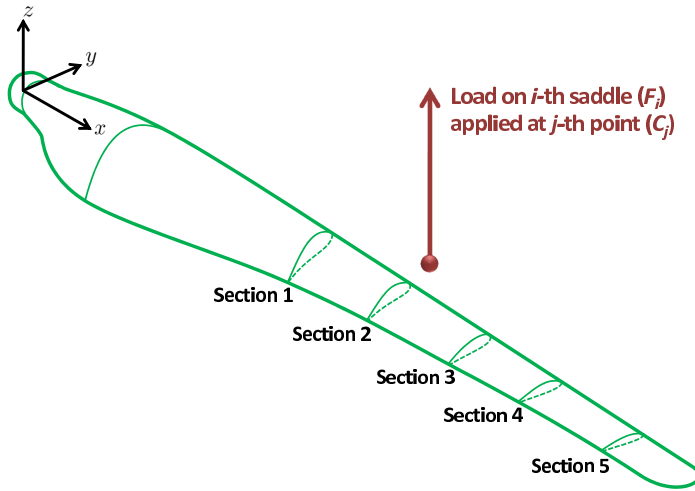


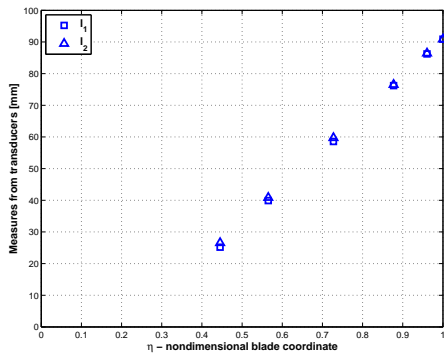
Figure 3.3: Notation for the definition of the load conditions of Blade A.

Table 3.3: Flap experiment: loads. Forces are in kN.

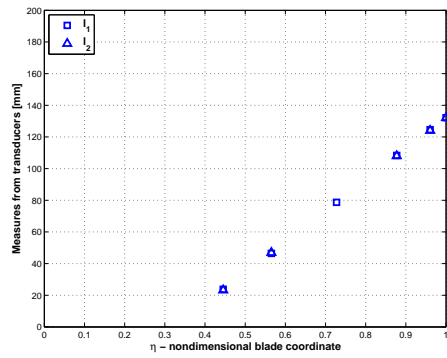
Load case	Section 1		Section 2		Section 3		Section 4		Section 5	
	$F_i$	$C_j$	$F_i$	$C_j$	$F_i$	$C_j$	$F_i$	$C_j$	$F_i$	$C_j$
1	5.40	$C_0$	0	-	0	-	0	-	0	-
2	0	-	3.24	$C_0$	0	-	0	-	0	-
3	0	-	0	-	2.03	$C_0$	0	-	0	-
4	0	-	0	-	0	-	0.99	$C_0$	0	-
5	0	-	0	-	0	-	0	-	0.40	$C_0$

Table 3.4: Torsional experiment: loads. Forces are in kN.

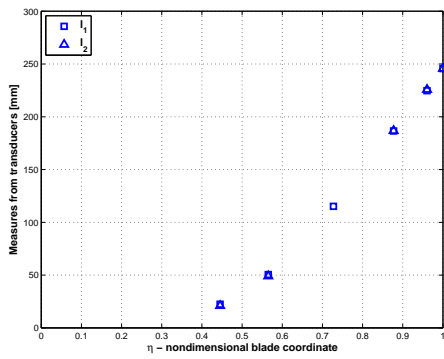
Load case	Section 1		Section 2		Section 3		Section 4		Section 5	
	$F_i$	$C_j$	$F_i$	$C_j$	$F_i$	$C_j$	$F_i$	$C_j$	$F_i$	$C_j$
1	4.32	$C_1$	0	-	0	-	0	-	0	-
2	0	-	1.66	$C_1$	0	-	0	-	0	-
3	0	-	0	-	1.07	$C_2$	0	-	0	-
4	0	-	0	-	0	-	0.56	$C_1$	0	-
5	0	-	0	-	0	-	0	-	0.30	$C_1$



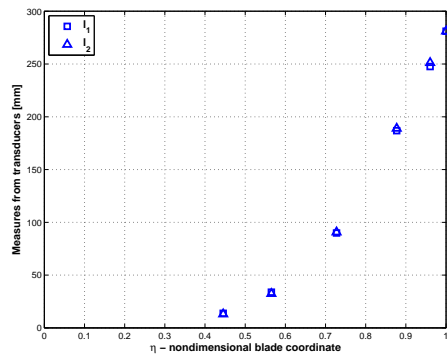
(a) Experiment 1.



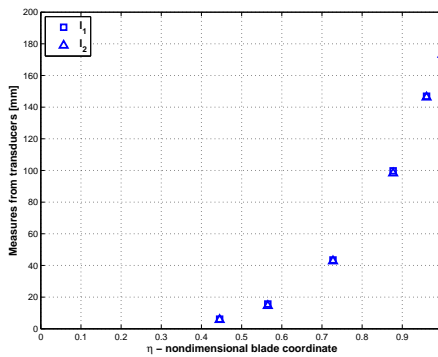
(b) Experiment 2.



(c) Experiment 3.



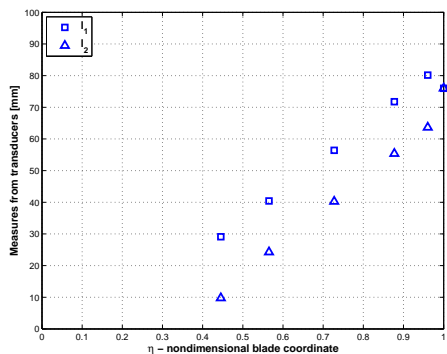
(d) Experiment 4.



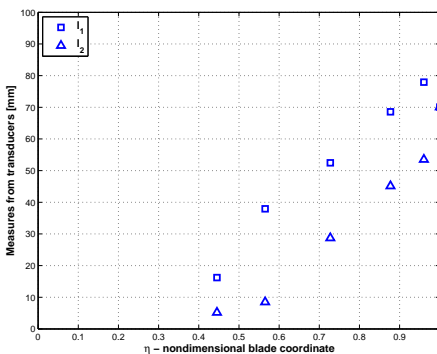
(e) Experiment 5.

**Figure 3.4:** Measures coming from transducers.

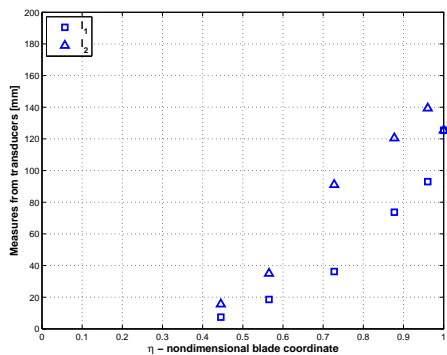
### Chapter 3. Identification of blade beam models



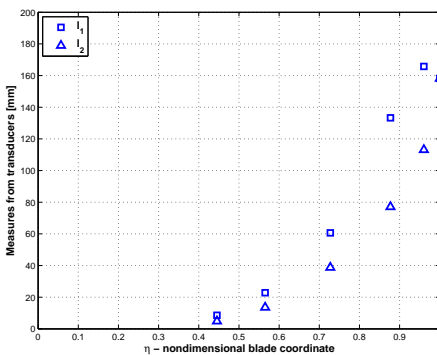
(a) Experiment 1.



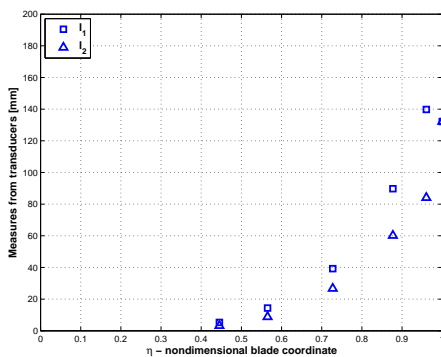
(b) Experiment 2.



(c) Experiment 3.



(d) Experiment 4.



(e) Experiment 5.

**Figure 3.5:** Torsional experiment: measures coming from transducers.

outboard saddles remain unloaded, a complete section of the blade behaves as a rigid body. Therefore, displacement measures along it carry no informational content on its stiffness characteristics. Furthermore, only few measurements were made, and this prevented us from reserving a part of the data set for the validation of the identified model, as commonly done.

#### Modal tests

Several dynamic trials have been done in order to define the natural frequencies of the blade.

Modal frequencies were found putting two monoaxial accelerometers PCB393B12 of 0.23 kg weight on a section located at 4510 mm from root and impacting the blade using a shock hammer test (SHT) PCB086B20. The accelerometers were placed with the axes orthogonal to each other so as to measure approximately the flapwise acceleration with the first and the edgewise with the second accelerometer. Table 3.5 reports the first 4 natural frequencies of the blade.

**Table 3.5:** *Natural frequencies of the blade.*

Mode	I flapwise	I edgewise	II flapwise	II edgewise
Frequencies [Hz]	3.65	7.43	10.89	27.34

#### Total mass and center of gravity position

In order to measure the total mass and the center of gravity position, the blade was weighted 32 times using two load cells placed in several known positions. From each of the 32 weighting it is possible to estimate simply the total mass,  $M$ , and the center of gravity position,  $r_{CG}$ , imposing the equilibrium of the systems. The mean values of  $M$  and  $r_{CG}$ , other than the measured blade length are reported in Table 3.6.

#### 3.3.2 Estimation of beam properties

Piecewise linear shape function were used for all unknown distributions. By performing a few tests until satisfactory results were obtained, it was determined to use five nodes for the flap-wise and torsional stiffnesses, three nodes for the mass distribution, two nodes for the edge-wise stiffness. The reduced number of edge-wise degrees of freedom is due to the lack of tests

### Chapter 3. Identification of blade beam models

---

**Table 3.6:** *Total mass and blade center of gravity position.*

Length [m]	Total mass [kg]	CG position [m]
6.2	74.14	1.93

with edge-wise loading, which does not allow for an accurate estimation of this stiffness distribution. Notice also that, since the total mass and the center of gravity position are included as constraints in the identification process, the number of nodes of the corrective function of the mass distributions must be greater than 2; otherwise there would be no ways to modify the mass distribution without violating the constraints.

For some of the load cases, Figure 3.6 shows the measured deflections (triangular symbols), the deflections computed with the model prior to identification (dashed lines), and the ones after identification (solid lines), plotted as a function of the non-dimensional blade span  $\eta = s/L$ . Table 3.7 reports the measured eigenfrequencies, as well as the ones prior to and after identification. For all outputs, the initial large discrepancies are markedly reduced after identification, and the identified model appears to be well correlated with the experimental data.

**Table 3.7:** *Lowest natural frequencies of blade A.*

Mode	I Flap	I Edge	II Flap	II Edge
Initial model	3.79	6.94	12.72	22.86
Identified model	3.62	7.50	11.73	25.29
Measures	3.65	7.43	10.89	27.34

The estimated blade properties are displayed in Figure 3.7. Each figure shows the initial (dashed lines) and the identified (solid lines) properties, as well as their Cramér-Rao standard deviations. Because a nominal torsional rigidity was not available prior to identification, Figure 3.7(c) shows only the identified one. Notice that the edge-wise stiffness and mass distributions have a lower level of confidence than the other quantities; for the former

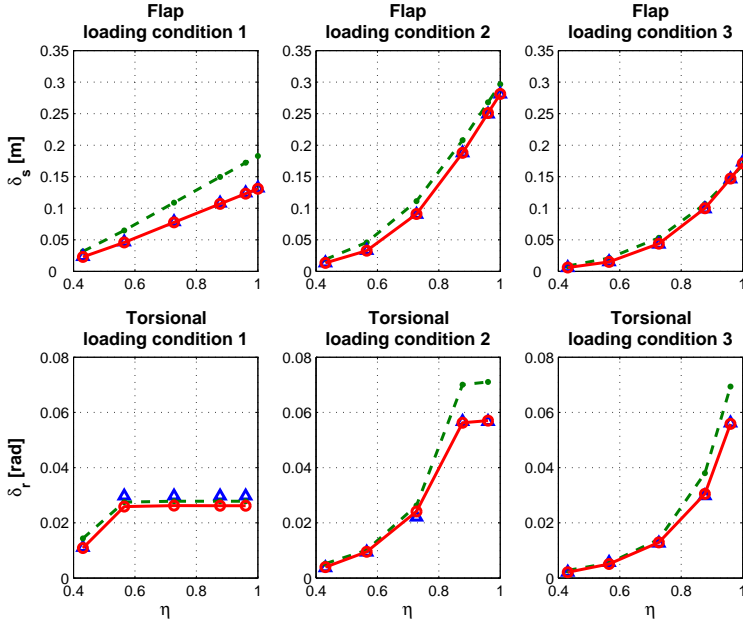


**Figure 3.6:** Static deflections for some loading conditions of blade A. Triangle symbols: experimental data; dashed lines: initial model; solid lines: identified model.

quantity, this is due to the lack of specific edge-wise load cases, as noted above.

## 3.4 Model update of “Blade B”

### 3.4.1 Description of experiments

A second, different, wind turbine blade was tested by its manufacturer; these tests were specifically aimed at supporting a model update activity.

#### Length, total mass and center of gravity position

The blade was initially measured and weighted multiple times, by suspending it at different span-wise locations using two cables equipped with load cells. The blade length and the average values of mass  $M$  and span-wise location  $x_{CG}$  of the center of gravity along the blade pitch axis are reported in Table 3.8.

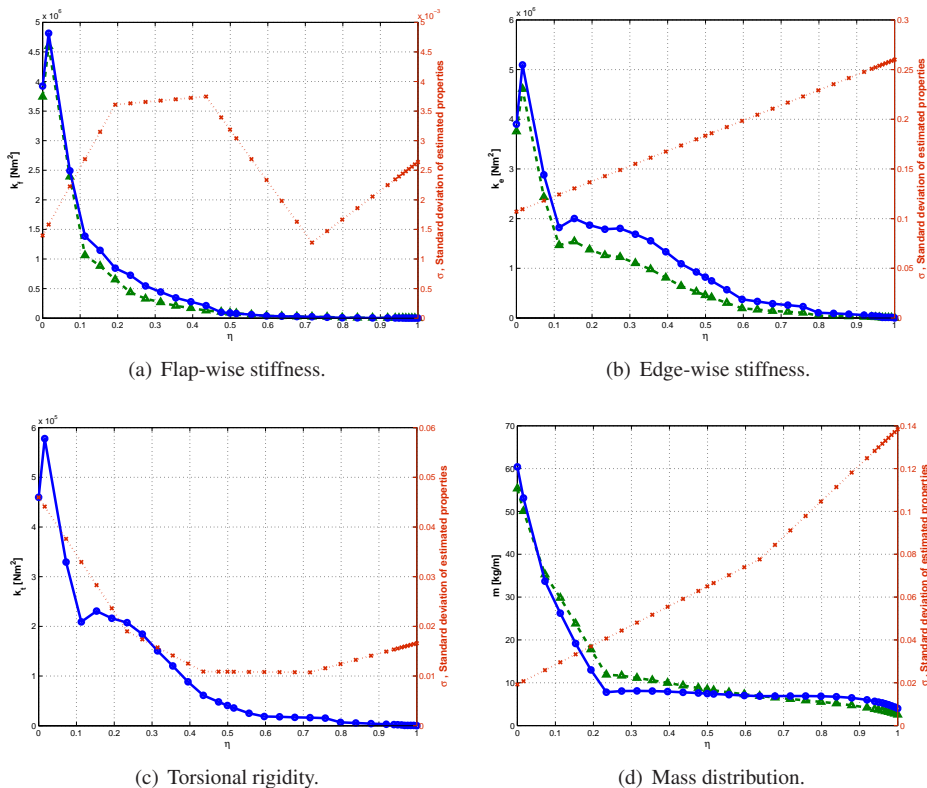


Figure 3.7: Blade A: span-wise distribution of initial (dashed lines) and identified (solid lines) properties, and their Cramér-Rao standard deviations (dotted lines).

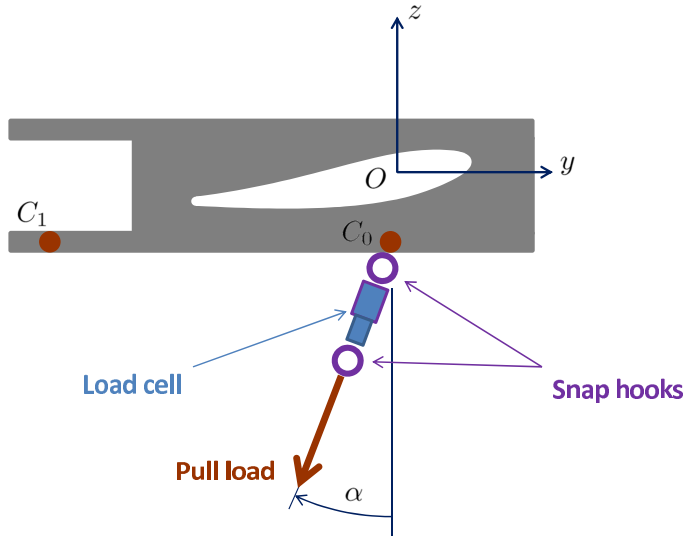
Length [m]	Total mass [kg]	CG position [m]
7.52	140.2	2.577

Table 3.8: Length, mass and center of gravity position of blade B.



### Static tests

The blade was bolted at the root and equipped with three saddles placed along its span. Loads were applied at each saddle in a direction making an angle  $\alpha$  with respect to the vertical, at two different points labeled  $C_0$  and  $C_1$  (cf. Figure 3.8), via a cable equipped with a load cell connected by means of snap hooks.



**Figure 3.8:** Sketch of saddle used for the loading of blade B.

Table 3.9 reports the mass and geometric characteristics of the saddles. The location of the saddles from the blade root is labeled  $x_O$ , while the position of the load application points are given in the reference frame of axes  $x, y, z$  of Fig. 3.8, with origin at the center of the blade root circle.

Separate load cases involving mainly flap-wise, mainly edge-wise and mainly torsional responses were considered. For each case (mainly flap, edge or torsional), three different load conditions were considered, two of which were used for conducting the identification, while the third one was used for the validation of the estimated model parameters. For the first load condition all three saddles were loaded, while for the second condition only the two saddles closer to the tip were loaded; finally, for the third condition loads were applied only at the tip saddle. Such conditions are linearly independent, so that the use of one of them for validation after identification constitutes a meaningful verification of the goodness and generality of the

	Saddle 1	Saddle 2	Saddle 3
Mass [kg]	25.4	21.8	20.3
$x_O$ [mm]	3017.0	5085.0	6503.0
$y_{C_0}$ [mm]	0.0	0.0	0.0
$z_{C_0}$ [mm]	215.0	-159.0	-150.0
$y_{C_1}$ [mm]	-1025.0	-1200.0	-1185.0
$z_{C_1}$ [mm]	215.0	-159.0	-150.0

**Table 3.9:** *Saddle mass and geometric characteristics.*

identified model.

Load magnitudes were chosen not to exceed maximum allowed ones, but also large enough to excite not too small responses, given the fact that the present blade is short and rather stiff.

The vertical and horizontal components of the loads applied at each blade section are computed considering the angle  $\alpha$  between the vertical and the direction of loads and including also the weight of the snap hooks and of the load cell as simply deducible from Figure 3.8.

The deflection of the blade was measured using a Leica Scan Station C10 laser scanner [44]. Black markers were placed on the blade surface at nineteen equally spaced sections along the blade span as shown in Fig. 3.9. Scan data was processed with the Leica Cyclone 7.1 software, that allows one to obtain the marker coordinates in a given reference frame. Measurements were also performed on the unloaded blade, so as to obtain the deflected configuration under the sole action of the gravitational field. Figure 3.10 shows some typical blade scan images obtained during the laboratory experiments.

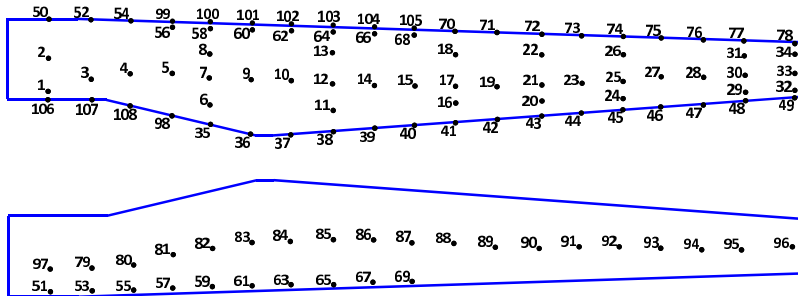
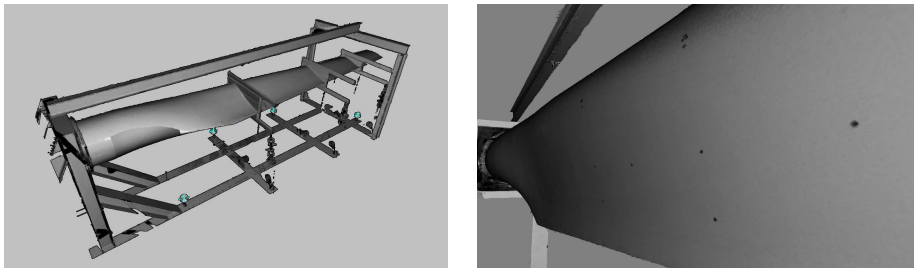
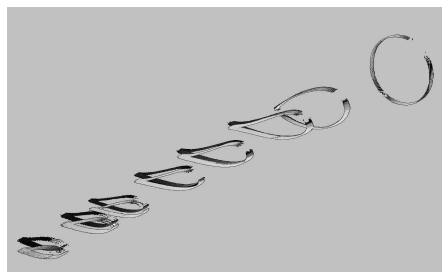


**Figure 3.9:** Marker IDs and their location on the blade surface.



(a) Scanner image of a torsional static test.

(b) Detail of a blade section and of its markers.



(c) Unloaded (dark) and loaded (light) blade cross sections, for one of the torsional loading conditions.

**Figure 3.10:** Laser scanner images of blade and supporting frame.

Once the coordinates of markers had been computed using the laser scanner software, the motion of each blade section was obtained by a non-linear least squares fit. With reference to Figure 3.11, the blade pitch axis is located at point  $H$  in the unloaded configuration, and at point  $K$  in the loaded one; similarly, the  $m$ th marker is located at  $P_m$  in the unloaded case, and at  $Q_m$  in the loaded one. The relationship between the two configurations can be written as

$$(Q_m - H) = \mathbf{T}(P_m - H) + \mathbf{s}, \quad (3.20)$$

where  $\mathbf{s}$  is the unknown sectional translation vector, and  $\mathbf{T}(\psi)$  the rotation tensor parameterized in terms of the unknown rotation vector  $\psi = \varphi \mathbf{k}$ , with rotation angle  $\varphi$  and rotation axis  $\mathbf{k}$ . Finally, the sectional motion is computed as

$$\{\mathbf{s}, \psi\} = \arg \min_{\mathbf{s}, \psi} \sum_{m=1}^{N_{\text{mark}}} \epsilon_m^T \epsilon_m, \quad (3.21)$$

where  $N_{\text{mark}}$  is the number of markers for the considered blade section and  $\epsilon_m = (Q_m - H) - \mathbf{T}(P_m - H) - \mathbf{s}$ .

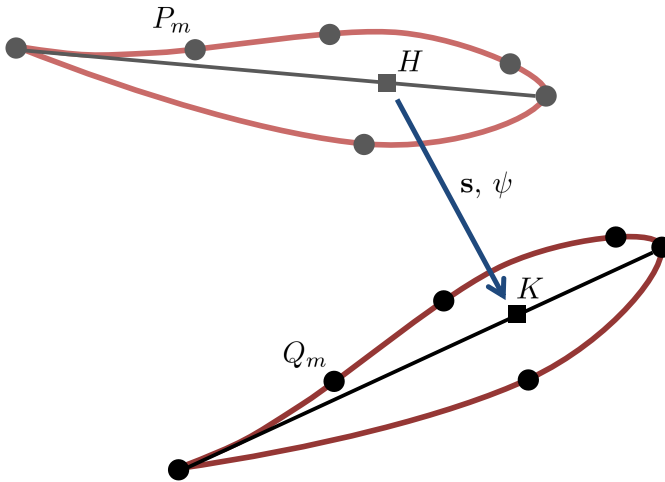


**Figure 3.11:** Computation of translation and rotation of a blade section from its marker coordinates.

The lowest modal frequencies of the blade were estimated by impacting the blade with a shock hammer, and measuring the response with fifteen mono-axial accelerometers. Fourteen accelerometers were placed along the span in orthogonal pairs, one aligned with flap and the other with edge

motions, while the last one was placed in the blade tip region away from the pitch axis to better resolve the torsional response. Figure 3.12 shows the FFT for accelerometers #1, #2 and #3 (i.e. those at the blade tip) as well as #15 (placed at the root bolted connection, on the frame side), for excitations in the flap-wise (at left) and edge-wise (at right) directions. The shock hammer tests were repeated twenty times, and the first four blade natural frequencies, computed as the mean values of all trials, were used as modal outputs in the identification process.

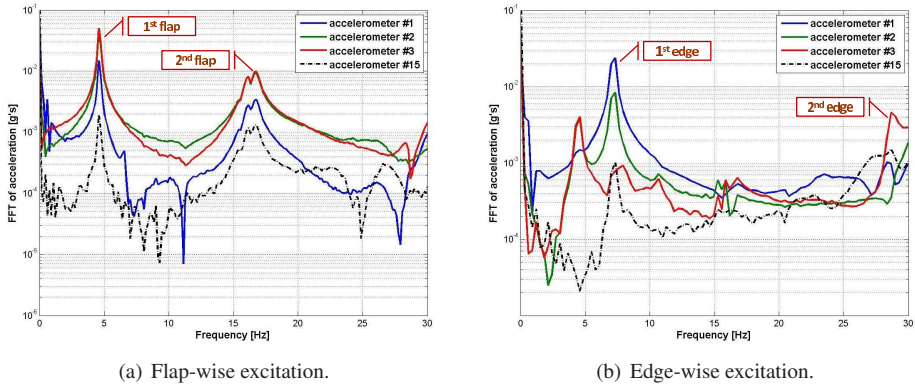


**Figure 3.12:** *FFT of some blade accelerometers for shock hammer tests.*

It appears that the root constraint is not perfectly rigid, and in fact the supporting frame is subjected to vibrations as indicated by accelerometer #15; the flexibility of the frame will be further confirmed by the static test measures (see Figure 3.13 later on). This will be taken into account during the estimation of the blade model parameters, by introducing unknown stiffnesses at the root boundary condition so as to model this effect. The effects of flexibility of the boundary conditions in the calibration of blade models has been previously considered, as described in Ref. [45].

### 3.4.2 Estimation process

All nominal blade properties showed a marked discontinuity at the 4% span location, due to a change in the lamination sequence in the root region. Accounting for this, the identification parameters were also allowed to jump at that location by using two segments (see definition of model parameters in §3.1.3). The root segment was associated with a single (span-wise) constant identification unknown; the same constant was used in the flap-wise and edge-wise directions, to account for the cylindrical shape of the blade

at the root. For the rest of the blade we used piecewise linear shape functions, with two nodes for the flap-wise and edge-wise distributions, one for the torsional rigidity, and three nodes for the mass distribution; such values were determined by performing the identification for an increasing number of them, until satisfactory results were obtained.

In order to model the flexibility of the supporting frame of the blade, three (flap-wise, edge-wise and torsional) torsion springs of unknown stiffness were added to the blade model at the root clamp, and included in the set of identification parameters. It was observed that the addition of these unknowns rendered the problem harder to solve, since they tended to produce effects on the outputs that were highly correlated with the ones due to the parameters modeling the blade root region. A detailed study of the Fisher information matrix showed that the couple of spring/root parameters related to the edge-wise stiffnesses had a better level of identifiability than the flap-wise pair.

For all loading conditions, Figure 3.13 shows the measured deflections (triangular symbols), the deflections computed with the model prior to identification (dashed lines), and the ones after identification (solid lines); measured torsional rotations of the blade sections appear to be quite noisier than displacements. The rightmost column, labeled loading conditions 3, shows validation results, in the sense that the data was not used for the identification of the blade properties. All plots, including the validation ones, show a good quality of the identified model.

Notice, as mentioned previously, the flexibility of the supporting frame: in fact, the slopes of the measured deflections at the blade root ( $\eta = 0$ ) are clearly different from zero, indicating a flexible root boundary condition.

Table 3.10 reports the eigenfrequencies. Two sets of estimates are given here. Following the initial values, shown in the first line of the table, the second line reports the values obtained by using a non-fusion approach, where stiffnesses were identified first by using all static deflections, and mass was identified next by using the measured eigenfrequencies, mass and center of gravity, while keeping stiffness frozen. The third line reports the values identified by using the proposed and previously explained fusion approach, and associated with the static deflections that were shown in Figure 3.13. By comparing with the fourth row, which reports the measured values, it appears that the estimates of the fusion-based approach are better than the ones of the non-fusion-based approach. On the other hand, by comparing the results in terms of displacements, which are not reported here for brevity, one can observe a very slight better correlation of the non-fusion-based results with the measures. This is expected, since the fusion

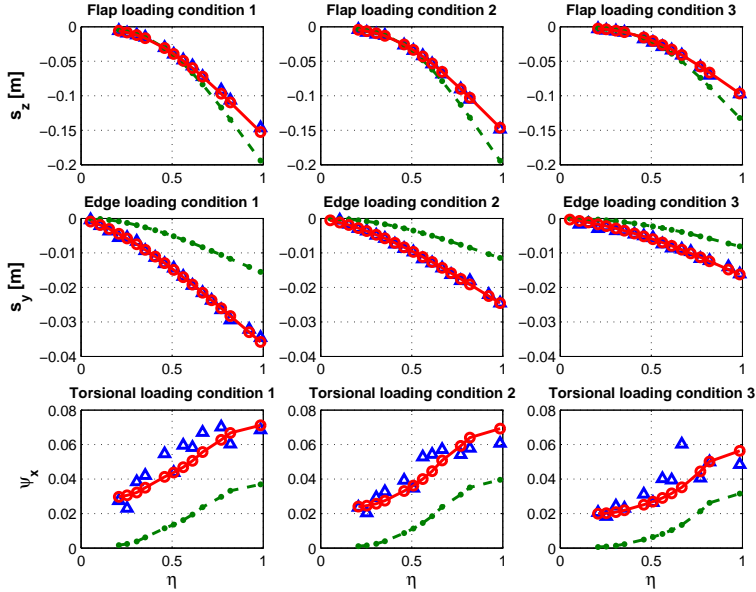


**Figure 3.13:** Static deflections for the loading conditions of blade B. Triangle symbols: experimental data; dashed lines: initial model; solid lines: identified model. The rightmost column shows validation data, and was not used in the identification process.

approach tries to fit the model parameters to all available measures, while accounting for their relative accuracy through the adaptive error covariance. Therefore, the non-fusion approach may appear to better fit a sub-set of the data, but this is just an artifact of its locality and lesser generality.

**Table 3.10:** Lowest natural frequencies of blade B.

Mode	I Flap	I Edge	II Flap	II Edge
Initial model	4.677	8.994	18.71	39.56
Identified model (non-fusion)	4.579	6.876	16.06	29.51
Identified model (fusion)	4.579	7.168	16.75	28.70
Measures	4.578	7.172	16.78	28.69

The fusion-based estimated blade properties are displayed in Figure 3.14. Each figure shows the initial (dashed lines) and the identified (solid lines) properties, as well as their Cramér-Rao standard deviations. Notice the very large discrepancy between the nominal and identified mass

### Chapter 3. Identification of blade beam models

properties; the former were affected by large errors, as also readily shown by the initial weighing of the blade. This large discrepancy between the weight of the nominal and the manufactured blade can be justified by the low accuracy in the unsophisticated and low cost manufacturing process and in particular to the excessive presence of non structural mass, like resin and filler, which was not accurately controlled by the manufacturer.

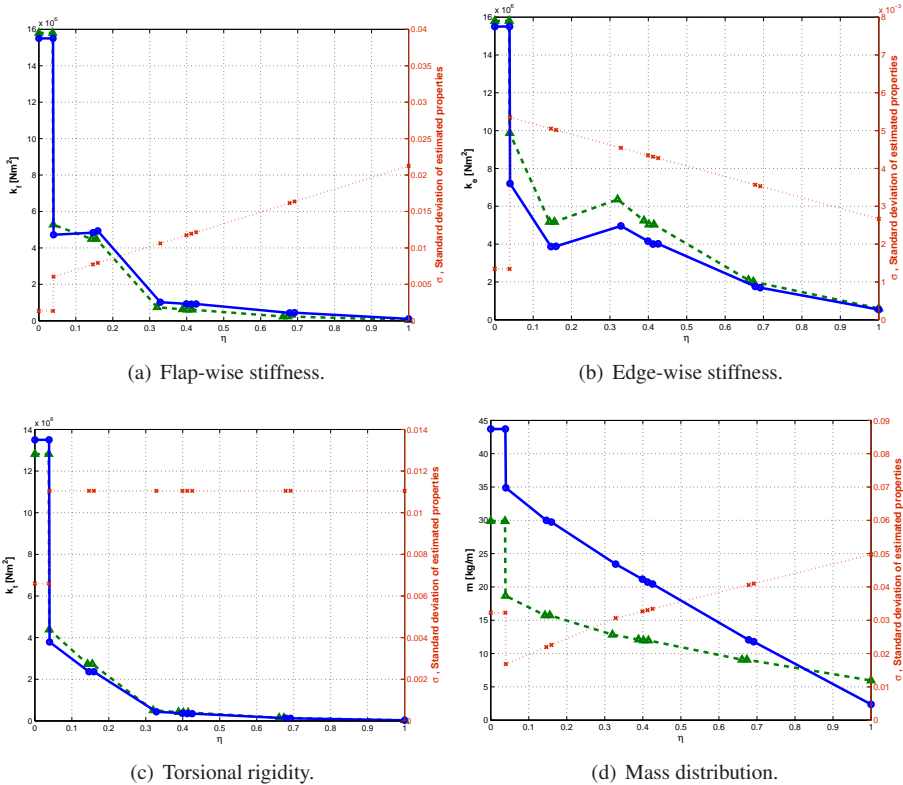


**Figure 3.14:** Blade B: span-wise distribution of initial (dashed lines) and identified (solid lines) properties, and their Cramér-Rao standard deviations (dotted lines).



---

## CHAPTER 4

---

### Identification of aerodynamic properties of blades

---

**T**HE behavior of wind turbines is principally influenced by the aerodynamics of the rotor. This elementary and basic fact is enough to emphasize the importance of having an accurate description of the aerodynamic properties of the blades of wind turbines. Without a correct characterization of the rotor aerodynamics, the predictive capabilities of any wind turbine model are dramatically reduced.

At present, several aerodynamic models of wind turbines and rotarywing aircraft are based on the lifting line theory, which represents an excellent compromise between accuracy of results and computational costs.

According to the lifting line theory, a lifting body, as a wing or a blade, is associated to a line on which several airfoils are collected. The aerodynamic characteristics of each airfoil are stored in three look-up tables describing the lift, the drag and the moment coefficients as functions of the angle of attack, Reynolds number and Mach number. At each station along the lifting line, the aerodynamic loads of the local airfoil are computed interpolating conveniently the aerodynamic look-up tables starting from the local chord length, the local angle of attack and the local Reynolds and

Mach number, which are computed considering the wind speed and the rotor rotation as well as the motion involved by the flexibility of the body linked to the lifting line.

Typically, aero-servo-elastic multibody models of wind turbines use lifting lines coupled with static or dynamic inflow models to model the aerodynamics of blades, nacelles and towers, introducing often in the computation the effects of the dynamic stall, the tip and hub losses, tower shadow in order to make the simulation the more realistic as possible, [46,47].

The use of aerodynamic models based on lifting lines is not limited to multibody simulations: with the growth of interest in wind farms modeling, the attention of many wind engineers has moved to the study of turbine wakes through *large eddy simulations* (LES) codes, in which the aerodynamics of turbines is typically described by three rotating lifting lines, [48].

As simply deducible, the accuracy of the results obtained using any kind of code implementing lifting line theory, depends essentially and strongly on two factors. First, on how the look-up tables with the aerodynamic coefficients are accurately tuned and second on how the flow around the lifting body has a two dimensional behavior.

Considering the first factor, it's important to know that lift, drag and moment coefficients of airfoils are generally extracted from wind tunnel tests, [49,50], or computed using aerodynamic softwares as X-Foil, [51]. It's reasonable to imagine, therefore, that experimentation uncertainties, manufacturing processes and computational approximations would affect the goodness of such aerodynamic properties.

But the second factor above mentioned results to be more critical, especially in the field of wind turbine modeling. In some working conditions the flow around the blades is far from being two dimensional, especially in the root region where the flow is almost always stalled because of the presence of very thick or cylindrical airfoils. In a rotating blade the stalled flow, by interacting with the radial pressure gradient due to blade rotation, tends to run along the blade span, increasing the lift of the stalled part of the blade. This effects is called "centrifugal pumping". Moreover, the radial flow induced by the centrifugal pumping, accelerates under the action of the Coriolis force toward the trailing edge delaying in this way the stall. These three-dimensional effects, which often manifest themselves up to the fifty percent of the blade, are detailed explained in [52].

The possibility to reproduce the complex aerodynamics of rotating blades within the lifting line framework, less onerous from the computational point of view, in order to have models which better predicts the behavior of a real wind turbines is currently an important topic of research.

Exploit the fact that CFD codes are able to model suitably the three-dimensional flow around a rotating wing, in literature several methods have been proposed to recover the three-dimensional effects in the two-dimensional properties of the airfoils, [6–10].

On the other hand, the use of system identification techniques to extract the aerodynamic properties of the airfoils of wind turbines, could actually fill the gap between the predictions of the models based on the lifting line theory and the real behavior of turbines, but unexpectedly, in literature there are not many examples related to this important topic. Ref. [11] is one of the few examples in which an attempt of computing airfoil properties through identification procedures is presented. The work developed in this chapter tries to cover this lack, suggesting two approaches of parametric estimation and showing a rigorous analysis of the problem.

The chapter is divided into three sections. Section 4.1 describes two possible approaches to solve the estimation problem: in the first, noted here as *direct approach*, the unknowns represent corrective functions to be applied directly to the aerodynamic properties of the airfoils belonging the blades. In the second approach, at contrary, the estimation problem is reformulated using the singular values decomposition in order to achieve a better conditioned problem. This second approach is noted here as *SVD-based approach*.

Section 4.2 shows, for both the approaches, the results obtained from the identification of the aerodynamics of the scaled wind turbine model V2 from wind tunnel test data.

Finally in Section 5.2, conclusions and possible future developments of the identification of the aerodynamics of wind turbine rotors are presented.

---

## 4.1 Estimation process

### 4.1.1 Identification using power thrust coefficients and blade loads

Consider now a wind turbine model in which the aerodynamics is modeled by a parametric version of the well-known BEM (Blade Elementum Momentum) theory. The dynamics of the system is generally computing solving a non linear set of equations as

$$\mathbf{g}_d(\mathbf{x}, \dot{\mathbf{x}}, \mathbf{w}, \mathbf{p}) = 0, \quad (4.1)$$

where  $\mathbf{p}$  is the parameter vector, used to parametrize the aerodynamic properties,  $\mathbf{x}$  is the state vector and  $\mathbf{w}$  is the input vector, composed of wind speed, and wind turbines controls, i.e. pitch angles of the blades and electrical torque. Together with the dynamic equations (4.1), the output equation

are given

$$\mathbf{q} = \mathbf{h}_d(\mathbf{x}, \dot{\mathbf{x}}, \mathbf{w}, \mathbf{p}), \quad (4.2)$$

where  $\mathbf{q} \in \mathbb{R}^l$  is the output vector.

Consider now the stationary regime on which the system, if asymptotically stable, converges after an initial transitory under the action of constant, non turbulent and axial wind, constant pitch angles and constant electrical torque. In order to compute such this regime, it is possible to solve a more efficient static problem, in which the rotating parts of the turbine are clamped while the air flow due to the rotation of the blades and the centrifugal acceleration are reproduced for a given rotor speed according to the Galilean relativity. This equilibrium condition is computing solving the following static problem

$$\mathbf{g}_s(\mathbf{x}, \mathbf{u}, \mathbf{p}) = 0, \quad (4.3)$$

where the input  $\mathbf{u}$  is now determined by the wind speed  $V_\infty$ , the rotor speed  $\Omega$  and the pitch angle  $\beta$  such that  $\mathbf{u} = \{V_\infty, \Omega, \beta\}^T$ . Together with (4.3) the output equations is defined as

$$\mathbf{y} = \mathbf{h}_s(\mathbf{x}, \mathbf{u}, \mathbf{p}), \quad (4.4)$$

where  $\mathbf{y} \in \mathbb{R}^m$  is the output vector.

In the development of this work, only stationary working conditions are considered. This simplification allows to perform the estimation using the outputs of static simulations, which in general require less computational time than the dynamic computations, leading to estimation processes performed in reasonable time.

The working conditions of a real wind turbines are often far from being constant, because the presence of rotor uptilt, wind shear and turbulence involve periodic and in general non constant working regimes. To this reason measures of the inputs and outputs above mentioned have to be intended as obtained by averaging over a suitable number of rotor revolutions. This simplification is generally considered valid especially when the test experiments are performed in a low turbulent wind tunnel as the case analyzed in this chapter.

Consider  $N$  test conditions (or experiments), the input of the  $i$ th experiment, with  $i = 1, N$ , is defined as  $\mathbf{u}_i = \{V_{\infty i}, \Omega_i, \beta_i\}^T$ .

For a wind turbine in which the structure is considered infinitely rigid, the couple of variables  $V_\infty$  and  $\Omega$ , could be substituted by the tip-speed-ratio (TSR)  $\lambda$  defined as  $\lambda = \Omega R / V_\infty$ , with  $R$  the rotor radius. Of course for a flexible structure, the aeroelasticity plays an important role in the determination of the performances of the turbines. In such these cases, the use

of  $V_\infty$  and  $\Omega$  in the input vector is preferable to reproduce correctly also the deformations of blades.

A large number of measurements, which can be useful for the identification purpose, can be extracted from a wind turbines.

In particular, the torque (or alternately power) and thrust measurements, which are typically available in most of the operative turbines, represent the first sources of information regard the rotor aerodynamics. Moreover, also the loads measured at different locations along blade span can be considered. Unfortunately, the possibility of having also the blade loads as output involves important modifications to the blades commonly used because they must be opportunely equipped with strain gages, which in turns need accurate calibration procedures.

The treatment made in this section is related to the case of having also the blade loads as measures but the proposed estimation approaches are tested considering only thrust and torque measured because the wind turbine scaled model V2 was at the moment not equipped with blade load sensors.

Because the measures of torque  $T$  and power  $P$  have the same informative content, since they are linked together by the rotor speed  $\Omega$ , which is measured, it is possible to consider as output only one of them. In the following the use of the power measure is preferred.

The output vector  $\mathbf{y} \in \mathbb{R}^m$  related to the  $i$ th test condition, noted here  $\mathbf{y}_i$  is defined as

$$\mathbf{y}_i = \{P_i, F_i, \dots, M_x^{(j)}{}_i, M_y^{(j)}{}_i, M_z^{(j)}{}_i, \dots\}^T, \quad j = 1, N_{sec} \quad (4.5)$$

where the subscript  $i$  indicates values related to the  $i$ th test condition,  $P_i$  and  $F_i$  are respectively power and thrust,  $M_x^{(j)}{}_i$ ,  $M_y^{(j)}{}_i$  and  $M_z^{(j)}{}_i$  represent respectively the edgewise, flapwise and torsional blade bending moment measured at the  $j$ th station along blade span and  $N_{sec}$  is the number of sections in which the load sensors are located.

Rather than power  $P$  and thrust  $F$ , it is better to use the relative coefficients  $C_P$  and  $C_F$

$$\begin{aligned} C_{P_i} &= \frac{P_i}{\frac{1}{2}\rho_i V_{\infty_i}^3 \pi R^2}, \\ C_{F_i} &= \frac{F_i}{\frac{1}{2}\rho_i V_{\infty_i}^2 \pi R^2}, \end{aligned} \quad (4.6)$$

where  $\rho_i$  the air density of the  $i$ th experiment. As power and thrust coefficients it is possible to introduce also the moment coefficients as

$$C_{M_{x,y,z_i}}^{(j)} = \frac{M_{x,y,z_i}^{(j)}}{\frac{1}{2}\rho_i V_{\infty_i}^2 \pi R^3}, \quad (4.7)$$

which lead to the definition of a new non dimensional output

$$\mathbf{y}_i = \{C_{P_i}, C_{F_i}, \dots, C_{M_x}^{(j)}{}_i, C_{M_y}^{(j)}{}_i, C_{M_z}^{(j)}{}_i, \dots\}^T, \quad j = 1, N_{sec}. \quad (4.8)$$

The associated maximum likelihood cost functions of Eq. (2.6) is noted  $J_A$ ,

$$J_A = \frac{mN}{2} \ln 2\pi + \frac{N}{2} \ln \det \mathbf{R} + \frac{1}{2} \sum_{i=1}^N (\mathbf{z}_i - \mathbf{y}_i)^T \mathbf{R}^{-1} (\mathbf{z}_i - \mathbf{y}_i), \quad (4.9)$$

with  $\mathbf{R}$  the variance of the measurement noise.

Finally the estimation problem is formulated as this bounded optimization problem

$$\min_{\mathbf{p}} \quad J_A(\mathbf{y}, \mathbf{z}), \quad (4.10a)$$

$$\text{s.t.} \quad \mathbf{y}_{lb} \leq \mathbf{y} \leq \mathbf{y}_{ub}, \quad (4.10b)$$

$$\mathbf{p}_{lb} \leq \mathbf{p} \leq \mathbf{p}_{ub}, \quad (4.10c)$$

According to the Adaptive Covariance Maximum Likelihood (ACML) method just described in Section 2.1.1, the minimization of  $J_A$ , if the matrix  $\mathbf{R}$  is unknown, can be perform with a two step iteration which considers the alternate estimation of  $\mathbf{p}$  and  $\mathbf{R}$ . In this case the cost function for a given fixed  $\mathbf{R}$ , noted  $\tilde{J}_A$  is defined as

$$\tilde{J}_A = \frac{1}{2} \sum_{i=1}^N (\mathbf{z}_i - \mathbf{y}_i)^T \mathbf{R}^{-1} (\mathbf{z}_i - \mathbf{y}_i). \quad (4.11)$$

#### 4.1.2 Identification with direct approach

Modeling the aerodynamic properties of a blade through lifting line theory is not trivial. Typically, the external shape of wind turbine blades is defined by lofting some suitable airfoils, noted here as reference airfoils, according to chord and twist distributions of the blade, generally designed to optimize the aerodynamic performances in an iterative process, [53, 54].

The two-dimensional aerodynamic properties of the airfoils located at a generic station along blade span are computed interpolating the properties of the reference airfoils generally known from wind tunnel test or from numerical computations.

The method described in this sections, noted *direct approach*, is based on the estimation of additive unknown corrective functions, which modify

directly the baseline of the reference airfoils,

$$C_k^i(\alpha) = C_k^{i0}(\alpha) + \Delta_k^i(\alpha) \quad (4.12)$$

where  $C_k^i(\alpha)$  is the  $k$ th aerodynamic property, (i.e. lift, drag or moment coefficients), of the  $i$ th airfoil of reference,  $C_k^{i0}(\alpha)$  is the same properties but related to the baseline model, while  $\Delta_k^i(\alpha)$  is the corrective additive function. The number of aerodynamic properties is noted  $N_{\text{aerprop}}$  whereas the number of reference airfoils  $N_{\text{airf}}$ .

Each corrective function is defined by the following interpolation

$$\Delta_k^i(\alpha) = \sum_{j=1}^{N_{\text{nodes}}^{k,i}} \eta_j(\alpha) \delta_{i_j}^k \quad (4.13)$$

where  $\eta_j(\alpha)$  are suitable shape functions and  $\delta_{i_j}^k$  are the associated  $N_{\text{nodes}}^{k,i}$  nodal values of the  $k$ th property of the  $i$ th airfoil.

The optimization parameters are then defined as the nodal values of the shape functions.

$$\mathbf{p} = \{ \dots, \delta_{i_j}^k, \dots \} \quad i = 1, N_{\text{airf}} \quad k = 1 : N_{\text{aerprop}} \quad j = 1 : N_{\text{nodes}}^k \quad (4.14)$$

It is important to underline that this estimation approach is very similar to that used for identifying the blade structural properties, see Chapter 3. A substantial difference is due to the different kind of corrective functions used, multiplicative for the structural and additive for the aerodynamic identification. In the aerodynamic case it is better to use additive functions as unknown because the lift coefficient  $C_L$  could assume a null value for a certain angle of attack. For that angle of attack the lift coefficient would be permanently equal to 0 if a multiplicative corrections are used.

### 4.1.3 Identification with the SVD-based approach

The identification of the aerodynamic properties of rotors is a very complex problem especially if the available measures are only related to power and thrust obtained in some working condition. As it will be underlined in Section 4.2.2 dedicated to the results of the direct approach, the difficulty arises first because the airfoils closer to the root have low level of identifiability and second the number of parameters to-be-identified grows as the number of reference airfoils increases, leading to a dramatic reduction of the accuracy of the estimates. Even for simple cases, as for example the one

related to the estimation of V2 rotor properties, which has only two reference airfoils, the need of developing a method more robust, able to handle problems with low level of identifiability, is important. Of course such this method can be formulated according to the singular values decomposition, and it is noted here *SVD-based approach*.

First of all, it is necessary to consider the  $k$ th aerodynamic property, with  $k = 1, N_{\text{aerprop}}$  and  $N_{\text{aerprop}}$  the number of aerodynamic properties to-be-identified, as a function of the angle of attack  $\alpha$  and of a variable  $\xi$  linked in a bijective way to the non-dimensional blade span  $\eta$ . The  $k$ th aerodynamic coefficient  $C_k$  is then defined as

$$C_k = C_k(\alpha, \xi(\eta)), \quad (4.15)$$

The variable  $\xi$  could be equal for example to the non-dimensional blade span or to the thickness of the blade, on the basis of the specific needs. As example, choosing  $\xi(\eta) = \eta$ , according to Equation 4.15 the lift coefficient of the airfoil located at  $\eta = \bar{\eta}$  related to the angle  $\alpha = \bar{\alpha}$  is indicated with  $C_L(\bar{\alpha}, \bar{\eta})$ .

The  $k$ th identified property is defined in the same way as

$$C_k(\alpha, \xi(\eta)) = C_k^0(\alpha, \xi(\eta)) + \Delta_k(\alpha, \xi(\eta)) \quad (4.16)$$

where  $C_k^0(\alpha, \xi(\eta))$  is the nominal property and  $\Delta_k(\alpha, \xi(\eta))$  is the  $k$ th unknown corrective function.

The range of interest of the two variables  $\alpha$  and  $\eta$  defines the two-dimensional domain  $\mathcal{D} = \mathcal{D}(\alpha, \xi(\eta))$ . For each properties  $N_{\text{nodes}}^k$  nodes are defined in the domain  $\mathcal{D}$ .

Each corrective function is described by means of suitable shape functions  $\phi_{kj}(\alpha, \xi(\eta))$  with  $j = 1, N_{\text{nodes}}^k$ ,

$$\Delta_k(\alpha, \xi(\eta)) = \sum_{j=1}^{N_{\text{nodes}}^k} \phi_{kj}(\alpha, \xi(\eta)) \delta_j^k \quad (4.17)$$

where  $\delta_j^k$  are the nodal values of the  $k$ th aerodynamic properties. As for the previous case, several kind of shape functions, linear, quadratic, cubic, *etc.*..., can be chosen according to the specific problem at hand. In the development of this work, linear shape functions have been chosen.

All the nodal values for each aerodynamic properties are collected in a vector  $\mathbf{t}$  of length  $N_t$ , named physical parameters, as

$$\mathbf{t} = \{ \dots, \delta_j^k, \dots \}^T \quad k = 1, N_{\text{aerprop}}, \quad j = 1, N_{\text{nodes}}^k, \quad (4.18)$$



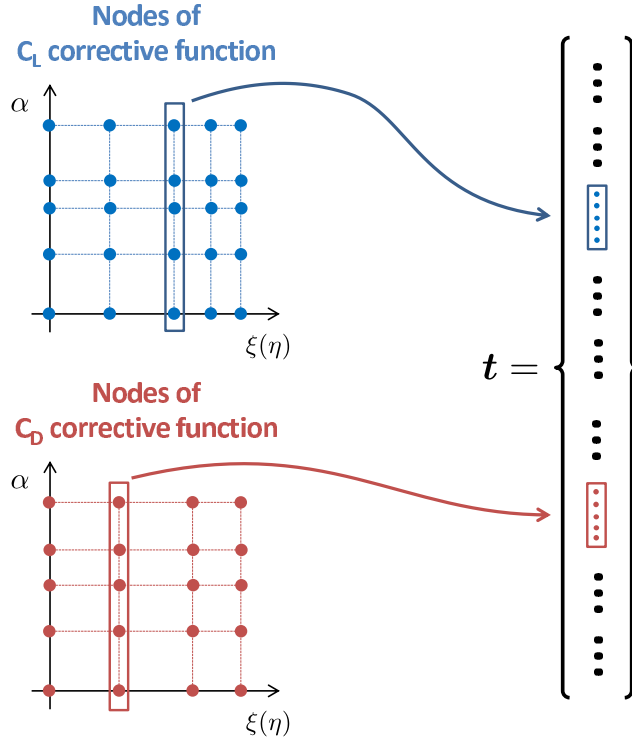


**Figure 4.1:** Stacking of the nodal values in a vector. Only  $C_L$  and  $C_D$  are displayed for clarity, but it is also possible to include for example  $C_m$ .

as symbolically depicted in Figure 4.1

Since the vector  $\mathbf{t}$  contains different kind of variables, for example lift and drag coefficients, which may assume values of different magnitude, it's essential to scale each element of  $\mathbf{t}$ ,  $\delta_j^k$ , by an suitable reference value  $\delta_{j \text{ ref}}^k$ . All these scaled values are collected in the vector  $\hat{\mathbf{t}}$ ,

$$\bar{\mathbf{t}} = \{ \dots, \delta_j^k / \delta_{j \text{ ref}}^k, \dots \}^T \quad k = 1, N_{\text{aerprop}}, \quad j = 1, N_{\text{nodes}}^k. \quad (4.19)$$

The sensitivity matrix for the  $i$ th experiment is computed as  $\mathbf{G}_i = \partial \mathbf{y} / \partial \bar{\mathbf{t}}$ .

Eventually, compute the matrix  $\mathcal{G}$ , stacking matrices  $\mathbf{R}^{-1/2} \mathbf{G}_i$  as in

Eq. 2.13

$$\mathcal{G} = \begin{bmatrix} \mathbf{R}^{-1/2} \mathbf{G}_1 \\ \mathbf{R}^{-1/2} \mathbf{G}_2 \\ \vdots \\ \mathbf{R}^{-1/2} \mathbf{G}_N \end{bmatrix}, \quad (4.20)$$

and compute its singular values decomposition,  $\mathcal{G} = \mathbf{U} \mathbf{\Sigma} \mathbf{V}^T$ .

According to what stated in Section 2.2, this decomposition can be used to reformulate the identification problem in a more robust and identifiable way. Define then the new orthogonal parameters  $\boldsymbol{\theta}$

$$\boldsymbol{\theta} = \mathbf{V}^T \bar{\mathbf{t}}, \quad (4.21)$$

or alternately for the  $w$ th component of the  $\boldsymbol{\theta}$ , noted  $\theta_w$ ,

$$\theta_w = \mathbf{v}_w^T \bar{\mathbf{t}}, \quad (4.22)$$

where  $\mathbf{v}_w$  is the  $w$ th column of the right singular matrix  $\mathbf{V}$ . The Cramèr Rao variance of the orthogonal parameter  $\theta_w$ , noted  $\sigma_w^2$  is computed according to Eq. (2.20) as

$$\sigma_w^2 = \frac{1}{\Sigma_{w,w}^2}, \quad (4.23)$$

where  $\Sigma_{w,w}$  is the  $w$ th element of the diagonal of matrix  $\mathbf{\Sigma}$ , which actually corresponds to the  $w$ th singular value.

Since the vector  $\bar{\mathbf{t}}$  is scaled, the standard deviation  $\sigma_w$  could be interpreted as the normalized deviations with respect to the reference values used to scaled the parameter vector  $\mathbf{t}$ . This remark allows to select simply a threshold of identifiability  $\sigma_d$  for accepting or discarding a particular orthogonal parameter  $\theta_w$  if its deviation  $\sigma_w$  is lower (accept) or greater (discard) than  $\sigma_d$ . A typical values for  $\sigma_d$  is 0.05.

The vector of parameters to-be-identified  $\mathbf{p}$  is thus composed by all the parameters  $\theta_w$  which  $\sigma_w \leq \sigma_d$ ,

$$\mathbf{p} = \{\dots, \theta_w, \dots\} \quad w \leq N_{\text{ID}}, \quad (4.24)$$

where  $N_{\text{ID}}$  is the number of identifiable parameters. All the other  $\theta_w$  for  $w > N_{\text{ID}}$  are discarded since their level of identifiability is too low.

The estimation problem is then solved by minimizing the cost function defined in (4.9).

Indicating the identified parameters with  $\hat{\boldsymbol{p}}$ , the physical scaled parameters  $\bar{\boldsymbol{t}}$  can be computed from equation (4.22) as

$$\bar{\boldsymbol{t}} = \sum_{w=1}^{N_{\text{ID}}} \boldsymbol{v}_w \hat{\boldsymbol{p}} \quad (4.25)$$

The treatment hitherto exposed is strictly related to the particular needs of the analyzed problem, but clearly estimation approaches based on the SVD are very common especially in robotics: a general review of the use of SVD in an identification procedures is presented in [24, 55–57].

It is interesting to observe that the identifiable part of the right singular matrix  $\mathbf{V}_{\text{ID}}$ , could be interpreted as an orthonormal basis of the identifiable space of the parameters, whereas the not identifiable part  $\mathbf{V}_{\text{N}}$  is related to the null space. Any change of the parameters proportional to  $\mathbf{V}_{\text{N}}$  does not produce significant changes in the outputs, so as to make identifiable that set of parameters.

Consider now a vector  $\boldsymbol{v}_m$  with  $1 \leq m \leq N_{\text{ID}}$  between the identifiable basis vectors. The  $i$ th element of  $\boldsymbol{v}_m$  is associated to the shape functions related to the  $i$ th element of the vector  $\boldsymbol{t}$  as defined in Eq. (4.17). As a consequence of that, the vector  $\boldsymbol{v}_m$  can be resorted, by proceeding in the inverse way with respect to what depicted in Figure 4.1, restoring the physical meaning of the parameters, since each element of  $\boldsymbol{v}_m$  is associated to a particular node in the domain  $\mathcal{D}(\alpha, \xi(\eta))$  and to a particular aerodynamic properties. From each  $\boldsymbol{v}_m$ , with  $m = 1, N_{\text{id}}$  is then possible to extract  $N_{\text{Aerprop}}$  shapes, noted here *SVD-modal shapes*,  $\psi_{m_k}(\alpha, \xi(\eta))$  with  $k = 1, N_{\text{Aerprop}}$ , defined in the two dimensional domain  $\mathcal{D}(\alpha, \xi(\eta))$ . In addition the corrective functions of the  $k$ th aerodynamic properties can be expressed in a more intuitively way by means of these SVD-modal shapes, as

$$\Delta_k(\alpha, \xi(\eta)) = \sum_{m=1}^{N_{\text{id}}} \theta_m \psi_{m_k}(\alpha, \xi(\eta)). \quad (4.26)$$

The definitions of the vector of unknown  $\boldsymbol{p}$  and of the estimation problem as in Eq.(4.24) conclude the SVD-based approach formulation.

From the Eq. (4.26) its also clearly visible that coupled corrections of more aerodynamic properties (e.g.  $C_L$  and  $C_D$ ) are involved together, since the same unknown  $\theta_m$  acts on the whole set of  $\psi_{m_k}(\alpha, \xi(\eta))$ . This is true as long as in a vector  $\boldsymbol{v}_m$  of the identifiable basis, parameters related to different aerodynamic properties are present. Of course this fact is absolutely coherent with the physics due to the coupled nature of the problem.

Finally, due to the intrinsic nonlinearity of the system, the sensitivity matrices  $\mathbf{G}_i$ ,  $i = 1, N$ , computed with the nominal model, could be significantly different respect those computed at the end of the estimation algorithm. For this reason it is opportune to repeat the optimization algorithm, until convergence, updating at every turn the sensitivity matrices, and in turn the SVD-modal shapes. Notice that, together with the updating of the SVD-modal shapes, also the covariance matrix  $\mathbf{R}$  has to be recomputed, according to the adaptive covariance maximum likelihood algorithm (see Section 2.1.1). This leads to the following iteration:

1. Compute the sensitivity matrices  $\mathbf{G}_i$  and the SVD-modal shapes  $\psi_{m_k}(\alpha, \xi(\eta))$  using the nominal model;
2. Perform the estimation;
3. Update the SVD-modal shapes  $\psi_{m_k}(\alpha, \xi(\eta))$  and the error covariance matrix  $\mathbf{R}$ , then return to step 2 until convergence.

## 4.2 Results from wind tunnel test data

---

### 4.2.1 Description of experiments

The estimation techniques for the aerodynamic parameters of wind turbine rotors, described in Section 4.1, have been performed in order to update the aerodynamic model of the wind tunnel scaled model V2. The V2 turbine is the first aeroelastically-scaled wind tunnel model of a real wind turbine Vestas V90, [58]. The V2 turbine was tested during the last three years for more than 100 hours in the wind tunnel of the Politecnico di Milano (see a schematic view of the wind tunnel in Figure 4.2), which is one of the largest one in Europe, in order to design and prove advanced control laws, to perform wake measurements, to study the interactions between turbines and several other applications.

Two airfoils, the AH79-100C (see Ref. [49]) and the WM006 (see Ref. [59]) have been chosen as reference airfoils to design the aerodynamic shape of V2 in order to achieve high aerodynamic performances even at the low Reynolds numbers at which the V2 works. Table 4.1 and Figure 4.3 shows the locations of these airfoils with respect to the blade span.

The V2 model was tested in the aeronautical section, see Figure 4.2, at several working conditions in order to explore as much as possible the TSR-pitch domain. Each condition was opportunely chosen to maintain the highest possible average Reynolds number on blades without exceeding the maximum rotor speed and the maximum torque available. As a

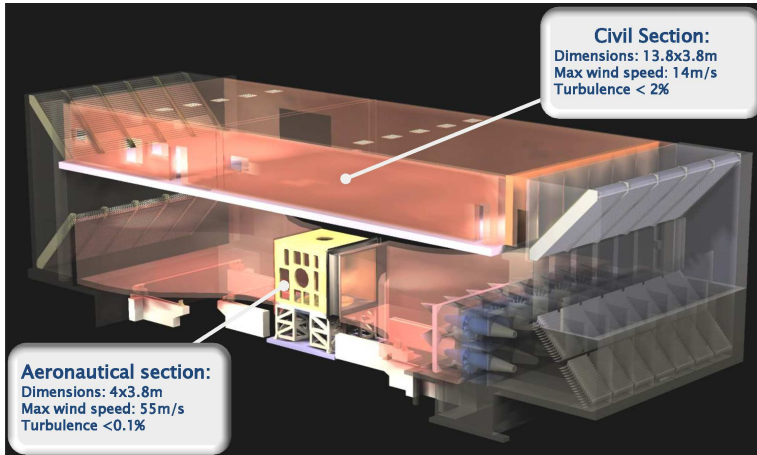


**Figure 4.2:** Schematic view of the wind tunnel of Politecnico di Milano.

**Table 4.1:** Location of the airfoils of the V2 wind turbine.

Distance from root [m]	Non-dimensional blade span $\eta$	Airfoil	Thickness ratio [%]
0.0000–0.0196	0.00–0.02	Cylinder	100
0.0196–0.1315	0.02–0.14	Cylinder → AH79-100C	variable
0.1315–0.4067	0.14–0.42	AH79-100C	10
0.4067–0.6733	0.42–0.70	AH79-100C → WM006	variable
0.6733–0.9622	0.70–1.00	WM006	9

consequence of that the differences between the average Reynolds number of all the trials are very low.

The torque of the rotor was measured by means of strain gages located on the rotor shaft and previously calibrated by suitable test bed trials; the rotor speed was computed from the encoder data. The longitudinal force generated by the turbine was measured by a balance located at the tower root. The outputs of the balance was also corrected removing the drag of the group tower-nacelle, obtained by a dedicated experimentation testing the turbine without the blades in the same wind tunnel. The wind speed was measured by accurate pressure measurements system downstream and upstream the test section. In addition the air density was computed from air pressure, temperature and humidity during the whole set of tests.

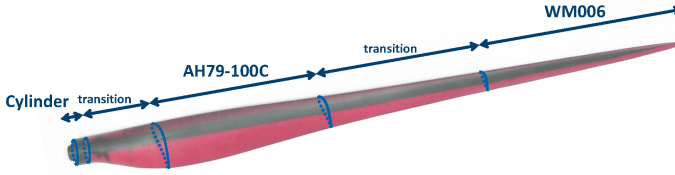


**Figure 4.3:** Location of the airfoils of the V2 wind turbine. Schematic view.

The measured force and power coefficients,  $C_{F_m}$  and  $C_{P_m}$  was computed according to the following equations,

$$C_{F_m} = \frac{F_m}{\frac{1}{2}\rho_m V_{\infty m}^2 \pi R^2}, \quad C_{P_m} = \frac{T_m \Omega_m}{\frac{1}{2}\rho_m V_{\infty m}^3 \pi R^2} \quad (4.27)$$

where  $F_m$  is the measured force,  $T_m$  the measured torque,  $\Omega_m$  the measured rotor speed,  $V_{\infty m}$  the measured wind speed and  $\rho_m$  the measured air density.

The force and power coefficients, as well as the TSR was also corrected to consider the effects of the blockage of the wind tunnel using Eq. 4.28,

$$C_{F_c} = C_{F_m} \left( \frac{V_{\infty m}}{V'} \right)^2 \quad (4.28a)$$

$$C_{P_c} = C_{P_m} \left( \frac{V_{\infty m}}{V'} \right)^3 \quad (4.28b)$$

$$\lambda_c = \lambda_m \frac{V_{\infty m}}{V'} \quad (4.28c)$$

where  $V'$  is the equivalent free airspeed, computed according to a suitable blockage correction method. Among the plethora of blockage correction methods, see for example Refs. [60–62], the *BMCB* method, [61], was chosen after having compared the results of such these methods with those obtained by CFD simulations of V2 in free air and in wall boundary conditions [10], performed with the code *ROSITA*, [63], which solves RANS equations on Chimera grid with Spallart-Allmaras turbulence model.

The vector of measurements of the  $i$ th test condition, noted  $z_i$  is then defined as  $z_i = \{C_{P_{c_i}}, C_{F_{c_i}}\}^T$ , where the subscript ‘c’ indicates the corrected measures.

Table 4.2 summarizes the 33 test conditions and the related measures, used in the estimation approach.

**Table 4.2:** Test conditions and measures used for the identification of the aerodynamic properties of V2.

Trial #	$\beta$ [deg]	TSR	$V_\infty$ [m/s]	$C_P$	$C_T$	Trial #	$\beta$ [deg]	TSR	$V_\infty$ [m/s]	$C_P$	$C_T$
1	-1.0	5.84	6.74	0.255	0.425	20	2.0	4.97	7.71	0.218	0.316
2	-1.0	6.76	6.29	0.314	0.509	21	2.0	5.89	6.69	0.277	0.400
3	-1.0	7.63	5.58	0.340	0.595	22	2.0	6.80	6.26	0.309	0.446
4	-1.0	8.44	5.04	0.334	0.646	23	2.0	7.74	5.50	0.305	0.478
5	-1.0	9.33	4.56	0.308	0.689	24	2.0	8.68	4.90	0.272	0.489
6	-1.0	9.97	4.27	0.276	0.728	25	2.0	9.56	4.45	0.229	0.512
7	0.0	5.84	6.74	0.266	0.417	26	2.0	10.25	4.15	0.171	0.526
8	0.0	6.76	6.30	0.318	0.491	27	3.0	4.97	7.71	0.223	0.308
9	0.0	7.63	5.58	0.340	0.561	28	3.0	5.89	6.68	0.273	0.384
10	0.0	8.51	5.00	0.324	0.599	29	3.0	6.80	6.26	0.292	0.412
11	0.0	9.38	4.54	0.298	0.632	30	3.0	7.74	5.50	0.273	0.426
12	0.0	9.94	4.28	0.266	0.661	31	3.0	8.71	4.89	0.232	0.431
13	1.0	4.90	7.82	0.203	0.315	32	3.0	9.69	4.39	0.162	0.435
14	1.0	5.89	6.68	0.275	0.412	33	3.0	10.42	4.09	0.080	0.438
15	1.0	6.80	6.26	0.318	0.473						
16	1.0	7.68	5.54	0.329	0.525						
17	1.0	8.59	4.96	0.304	0.546						
18	1.0	9.43	4.51	0.273	0.570						
19	1.0	10.23	4.16	0.222	0.602						

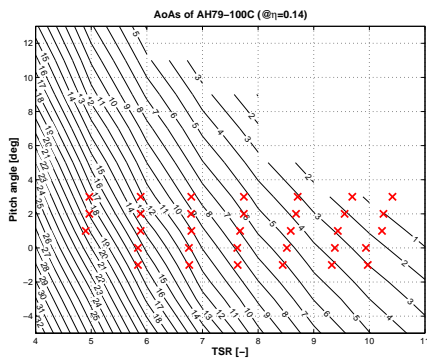
### 4.2.2 Direct approach

The approach named *direct approach*, see Section 4.1.2, was performed in order to estimate the aerodynamic models of V2. First of all, in a preliminary analysis the angles of attack, at which the airfoils work, have been performed by means of BEM simulations. Figure 4.4 shows the contour plot of the angles of attack related to four spanwise stations for varying-pitch angle  $\beta$  and TSR. The ‘x’-marks indicate the test conditions.

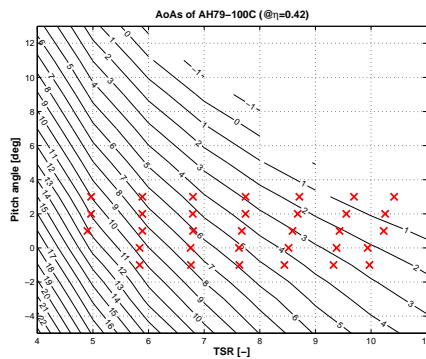
Figures 4.4(a) and 4.4(b) show that the angles of attack range of the AH79-100C airfoil is about  $[-1 \div 20]$  deg, whereas from Figures 4.4(c) and 4.4(d), the range for WM006 is  $[0 \div 10]$  deg. Of course there are no possibilities to obtain accurate results out of these ranges. The nodes of the corrective functions to-be-estimated, for both airfoils, have been chosen according to these indications and after some identification trials. The values of such these nodes are displayed in Table 4.3.

The comparison between identified outputs and measures are displayed in Figure 4.5, which shows the power coefficients, and in Figure 4.6, which shows the thrust coefficients.

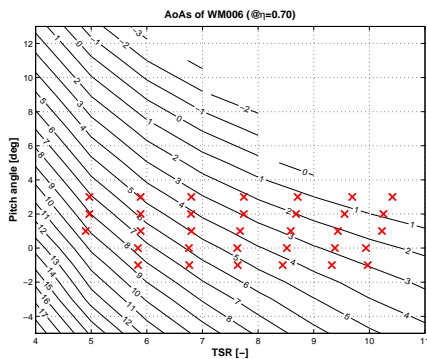
Notice the large discrepancies between the outputs of the nominal model



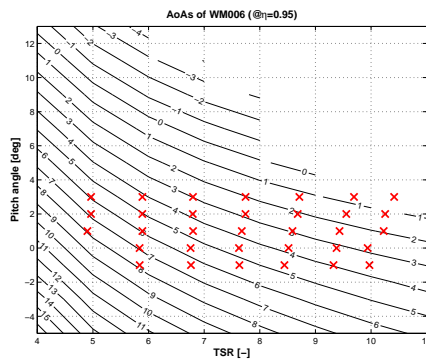
(a) Angles of attack of AH79-100C at  $\eta = 0.14$ .



(b) Angles of attack of AH79-100C at  $\eta = 0.42$ .



(c) Angles of attack of WM006 at  $\eta = 0.70$ .



(d) Angles of attack of WM006 at  $\eta = 0.95$ .

**Figure 4.4:** Angles of attack of the airfoils at the tested conditions. Solid lines: contour plot of the angles of attack; 'x' marks: tested conditions.



**Table 4.3:** *Nodes of the corrective functions to-be-estimated.*

Airfoil	Nodes for $C_L$ corrective functions [deg]	Nodes for $C_D$ corrective functions [deg]
AH79-100C	-1, 4, 8, 11, 14	-1, 4, 8, 11, 14
WM006	1, 4, 7, 10	1, 4, 7, 10

and the measures and, at contrary, the great correlation achieved with the new identified model, for both  $C_P$  and  $C_F$  measurements.

The identified aerodynamic properties are displayed in Figure 4.7. Each figure shows the nominal, dashed lines, and the identified properties, solid lines, as well as the Cramèr Rao standard deviations. In particular, the lift coefficient of the WM006 airfoils are very different from the nominal one: the identified lift curve appears to be shifted downward with respect to the nominal one as the airfoil had a lower camber. Actually, due to the reduced dimensions of the blade, even small imprecisions in the blade manufacturing process could cause considerable dissimilarities in the shape of the airfoils leading in turn to large differences in the aerodynamic properties.

Notice also the different level of standard deviation between the estimated properties of the inner, AH79-100C, and outer airfoil, WM006. Several observations can be outlined. First the standard deviation of the outer airfoils suggest that the properties of WM006 are estimated better than those of AH79-100C. At contrary the inner airfoil shows a very low level of confidence, barely acceptable. This results is actually expected, since typically the global performances of turbines are strongly influenced by the outer part of the blades.

Furthermore, the analysis of the correlation matrix shows a strong collinearity among the airfoil parameters, as highlighted by Table 4.4 and 4.5 which show the correlation matrix  $\mathbf{X}$  between respectively the lift and drag parameters of both the airfoils. The cross-correlation values greater than 0.95 are also marked in bold font. It appears that the properties of the inner airfoil is correlated with the properties of the outer one in the pre-stall range.

Although the quality of the identification, as seen by looking at the comparison between measures and outputs, appears deceptively good, these simple considerations highlight the difficulty of the problem: the sensitivity of the outputs with respect to inner airfoil parameters are low and

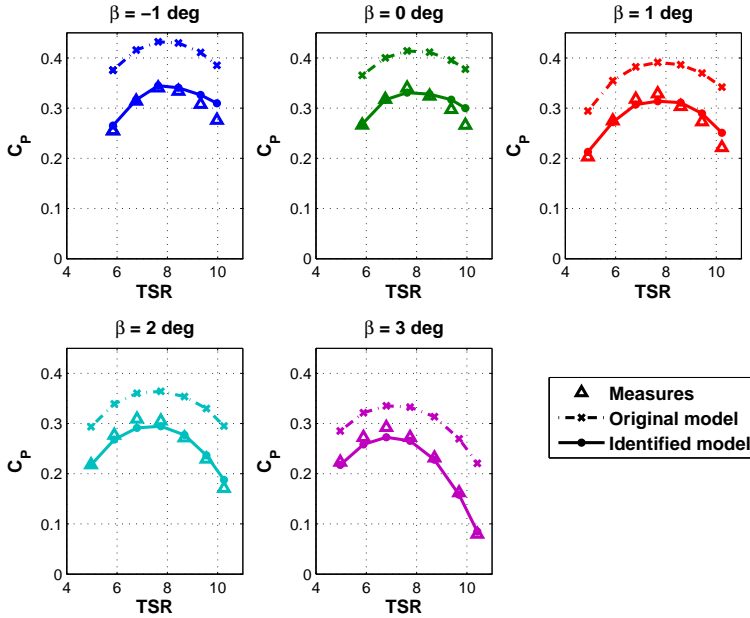


**Figure 4.5:** Comparison of power coefficients for the tested conditions obtained with the direct approach. Triangle symbols: measures; dashed lines: original model; solid lines: identified model.

characterize by a high level of correlations with those of the outer airfoil. As a consequence, the estimate of the properties of the inner airfoil has a very low level of confidence, as also shown by the Cramèr Rao deviations displayed in Figure 4.7. But the most problematic issue arises from the strong correlation between the parameters of the two airfoils: any errors in the identification of the inner airfoil properties affect in a significant and perhaps unpredictable way the estimate of the outer airfoil properties.

Notice that it is easy to imagine that any attempt of identifying the aerodynamic properties of a real wind turbine, whose shape is made by lofting more than two airfoils, has few possibility to give accurate results without the use of local measures, as for example the blade loads at different span-wise.

### 4.2.3 SVD-based approach

The SVD-based approach, described in Section 4.1.3, was performed for repeating the identification of the aerodynamic model of V2 using the same set of measures of Table 4.2.

The aerodynamic properties were considered as a function of the an-

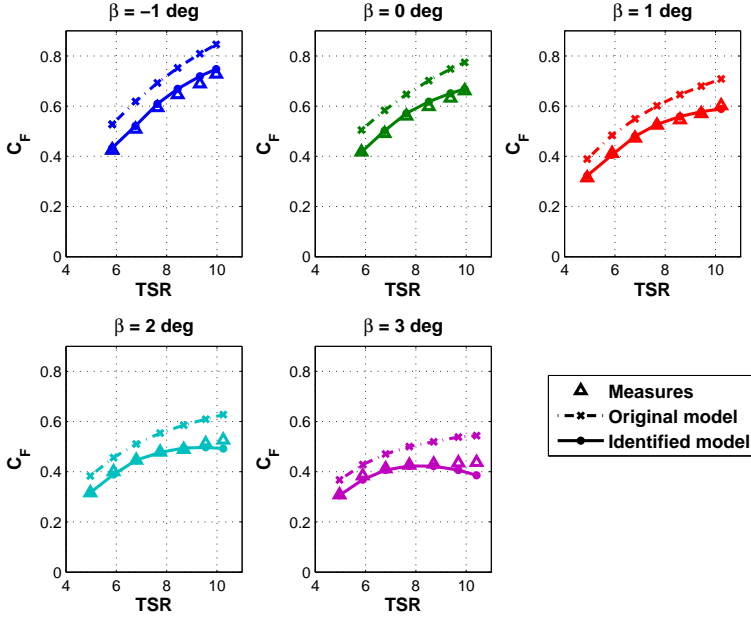
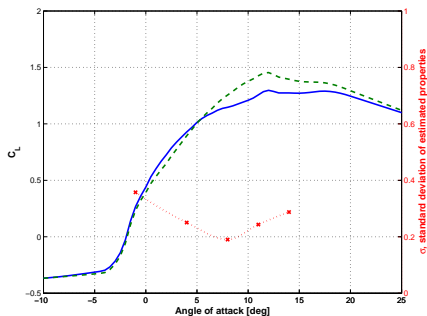


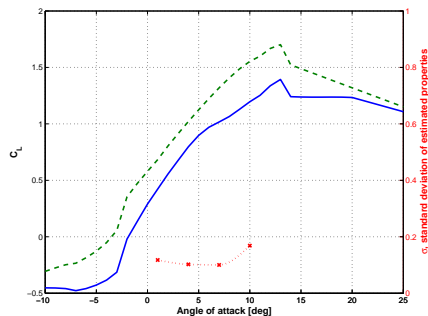
**Figure 4.6:** Comparison of thrust coefficients for the tested conditions obtained with the direct approach. Triangle symbols: measures; dashed lines: original model; solid lines: identified model.

gle of attack  $\alpha$  and of the non-dimensional blade span  $\eta$ . The domain  $\mathcal{D}(\alpha, \eta)$  was discretized with a grid of 42 nodes, defined at each couples  $(\alpha_d(m), \eta_d(n))$ ;  $m = 1, N_\alpha$ ;  $n = 1, N_\eta$ ; where  $\alpha_d = \{-8, 1, 3, 5, 7, 9, 25, \}$  [deg] and  $\eta_d = \{0, 0.2, 0.4, 0.6, 0.8, 1.0\}$  [deg] are the vectors, respectively of length  $N_\alpha = 7$  and  $N_\eta = 6$ , which define the discretization of the variable  $\alpha$  and  $\eta$ . Moreover all corrective functions were imposed to be equal to 0 for all  $\alpha \leq -8$  and  $\alpha \geq 25$  [deg] in order to link the identified with the nominal properties out of the range of identifiability. The same grid was used for both the corrective functions of lift and drag, whereas the moment coefficients of the airfoils were kept fixed to the nominal values due to the lack of specific measures, e.g. the torsional loads along blade span. The reference values, used to scale the unknown parameters, were chosen equal to 1.0 for the unknowns related to the lift coefficients and equal to 0.08 for the parameters related to the drag coefficients.

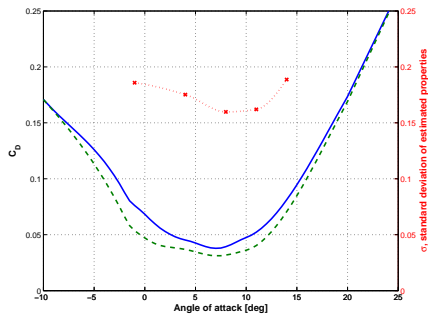
The sensitivity matrices of the outputs with respect to the 60 scaled physical parameters have been computed using finite differences and the matrix  $\mathcal{G}$ , defined in Eq. (4.20) was built for a given noise covariance ma-



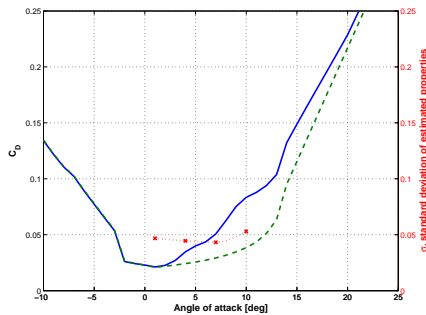
(a) Lift coefficient of AH79-100C.



(b) Lift coefficient of WM006.



(c) Drag coefficient of AH79-100C.



(d) Drag coefficient of WM006.

**Figure 4.7:** Aerodynamic properties estimated with the direct approach. Nominal model: dashed lines; identified model: solid lines; Cramér-Rao standard deviations: dotted lines.

**Table 4.4:** Correlation matrix between lift coefficients  $C_L$  of the airfoils of V2.

Nodes [deg]		AH79-100C					WM006			
		-1	4	8	11	14	1	4	7	10
AH79-100C	-1	1.00	0.88	0.76	0.63	0.45	<b>-0.98</b>	-0.89	-0.75	-0.47
	4	—	1.00	0.85	0.70	0.49	-0.92	<b>-0.99</b>	-0.82	-0.50
	8	—	—	1.00	0.76	0.52	-0.78	-0.86	<b>-0.95</b>	-0.47
	11	—	—	—	1.00	0.53	-0.65	-0.70	-0.85	-0.72
	14	—	—	—	—	1.00	-0.45	-0.50	-0.56	-0.85
WM006	1	—	—	—	—	—	1.00	0.93	0.78	0.48
	4	—	—	—	—	—	—	1.00	0.83	0.51
	7	—	—	—	—	—	—	—	1.00	0.56
	10	—	—	—	—	—	—	—	—	1.00

trix  $\mathbf{R}$  equal to  $\sigma_E^2 \mathbf{I}$ , where  $\sigma_E = 0.005$ , which is an appropriate value for both the  $C_P$  and  $C_F$  measurements according to the experimental accuracy in measuring the thrust and the torque of the rotor.

The computation of the singular values of  $\mathcal{G}$ ,  $\Sigma_{ww}$ , and in turn of the variances of the orthogonal parameters,  $\sigma_w^2 = 1/\Sigma_{w,w}^2$ , shows that there are only ten linear combinations of the physical parameters which are actually identifiable with a good level of accuracy. This is clearly visible from Figure 4.8(a), where the variances of the orthogonal parameters are displayed as well as the threshold of identifiability chosen equal to 0.003, which corresponds to an expected standard deviation of the identified parameters of about the 5.5% of the reference values. After having performed the first estimation process of the ten identifiable orthogonal parameters, the SVD-modal shapes were updated recomputing the sensitivity matrix  $\mathcal{G}$  and then a second optimization was executed. The variances of the orthogonal parameters related to the second estimation process are displayed in Figure 4.8(b). The number of identifiable parameters is now twelve, greater than the previous process. This difference is not surprising since the problem is nonlinear and the aerodynamic properties identified in the first process are actually very different from those of the baseline model.

Looking at Figure 4.9 and 4.10, which show the identifiable SVD-shapes respectively from the first to the sixth and from the seventh to the twelfth, some simple considerations can be done:

## Chapter 4. Identification of aerodynamic properties of blades

**Table 4.5:** Correlation matrix between lift coefficients  $C_D$  of the airfoils of V2.

Nodes [deg]	AH79-100C					WM006				
	-1	4	8	11	14	1	4	7	10	
AH79-100C	-1	1.00	0.98	0.96	0.90	0.70	<b>-0.99</b>	<b>-0.98</b>	<b>-0.95</b>	-0.71
	4	—	1.00	0.98	0.91	0.70	<b>-0.99</b>	<b>-0.99</b>	<b>-0.96</b>	-0.72
	8	—	—	1.00	0.92	0.70	<b>-0.97</b>	<b>-0.98</b>	<b>-0.99</b>	-0.71
	11	—	—	—	1.00	0.70	-0.91	-0.91	-0.94	-0.84
	14	—	—	—	—	1.00	-0.70	-0.71	-0.72	-0.86
WM006	1	—	—	—	—	—	1.00	<b>-0.99</b>	<b>-0.96</b>	0.72
	4	—	—	—	—	—	—	1.00	<b>-0.97</b>	0.72
	7	—	—	—	—	—	—	—	1.00	0.73
	10	—	—	—	—	—	—	—	—	1.00

- Due to the coupled physics of the problem, each shape is associated to both  $C_L$  and  $C_D$  parameters.
- As expected, the root region, up to the 20% of the blade length, is characterized by little identifiability, since the  $C_P$  and  $C_F$  measures are not sufficiently influenced by the airfoils near the root, as simply predictable.
- Most shapes present sharp variations in the  $\alpha$  direction; this highlights the ability of the various shapes in distinguishing the effects generated at different angles of attack. On the other hand, the changes in the  $\eta$  direction is typically more modest showing that it is harder to separate the effects of the various spanwise sections with a good level of confidence. These remarks show actually that the considered measures allows to estimate the behavior of the aerodynamic properties as a function of the angle of attack and, at contrary, the difficulty of having a better spanwise identifiability, as just noted in Section 4.2.2.
- The parameters related to the lift coefficient and to the outer part of the blades are mostly involved in the first three identifiable shapes. This actually demonstrates what was just noticed in Section 4.2.2 that the properties related to the lift coefficients of the outer airfoil are the most identifiable.

## 4.2. Results from wind tunnel test data

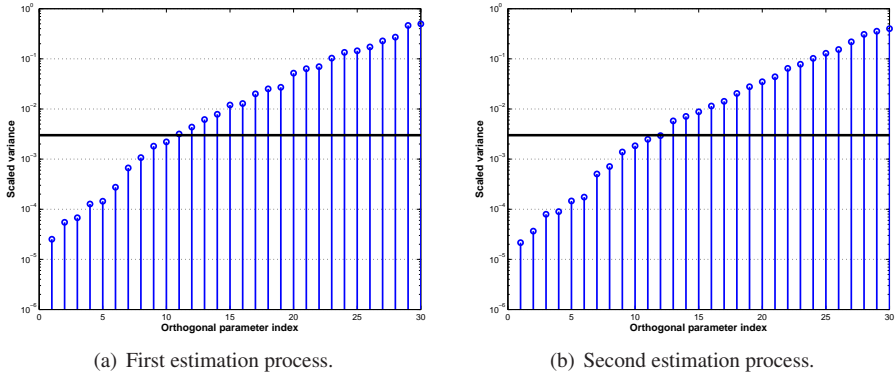


**Figure 4.8:** *Variances of the orthogonal parameters for the first (left) and second (right) estimation process. The black horizontal solid line indicates the threshold of identifiability.*

It is interesting to note that the analysis performed by means of the SVD gives the important mathematical demonstration of all the limits of the direct approach, highlighted by an extensive practice and just noted in Section 4.2.2.

Figures 4.11 and 4.12 display the comparison between the measures and the outputs prior to and after the identification. All plots show an excellent correlation of the estimated model, which seems even better than the one obtained with the direct approach. In addition, notice that only 12 unknowns have been used in the SVD-based estimation, less than the 18 parameters related to the direct approach. This fact newly is not surprising since the SVD, by selecting the most identifiable combinations of the parameters, acts also in order to optimize the number of unknowns to-be-identified to have the best correlation with the experimental measures together with a suitable confidence of the estimates.

The new identified properties are displayed in Figures 4.13 to 4.17, which show the  $C_L$  (left) and  $C_D$  (right) coefficients for the airfoils located at some sections along blade span. All plots show the nominal (dashed line) and the identified (solid line) properties, as well as the related standard deviations (dotted line). Moreover in Figure 4.16, together with the properties of the airfoil at the 86% of the blade also the properties identified with the direct approach are displayed: the similarity between the results achieved by the two approaches are quite similar. Despite its limits, the direct approach, regarding this section of high identifiability, gives results coherent and comparable to those obtained with the more rigorous SVD-based approach.

## Chapter 4. Identification of aerodynamic properties of blades

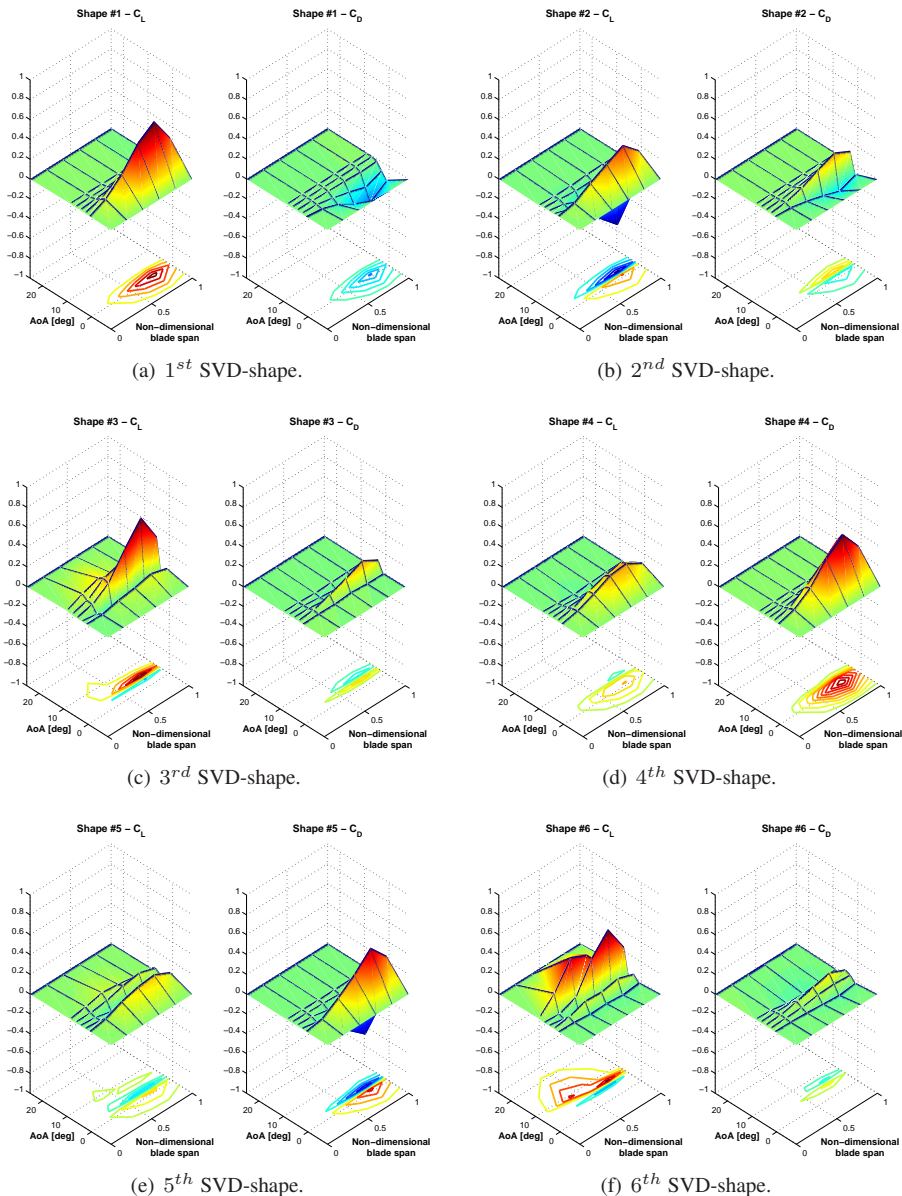


Figure 4.9: First to sixth identifiable SVD-shapes.



## 4.2. Results from wind tunnel test data

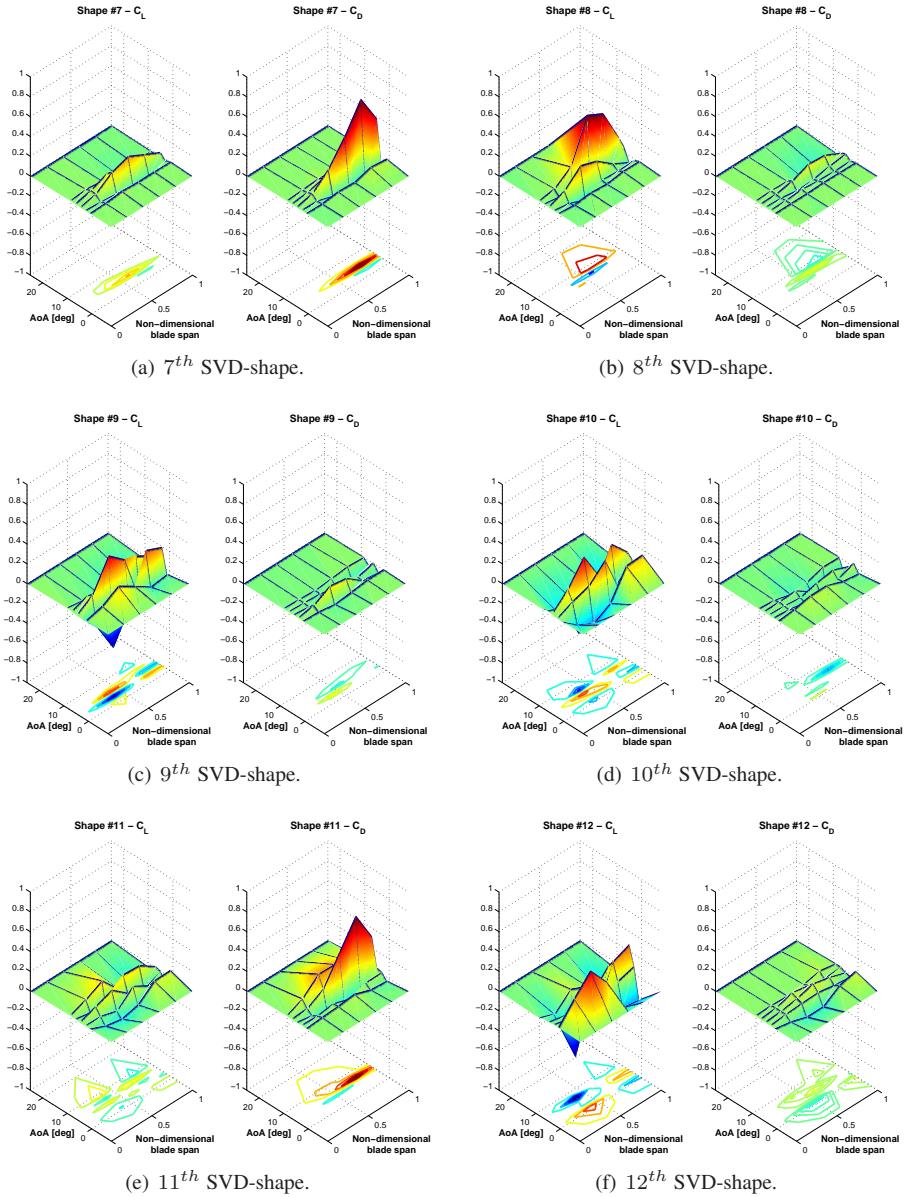
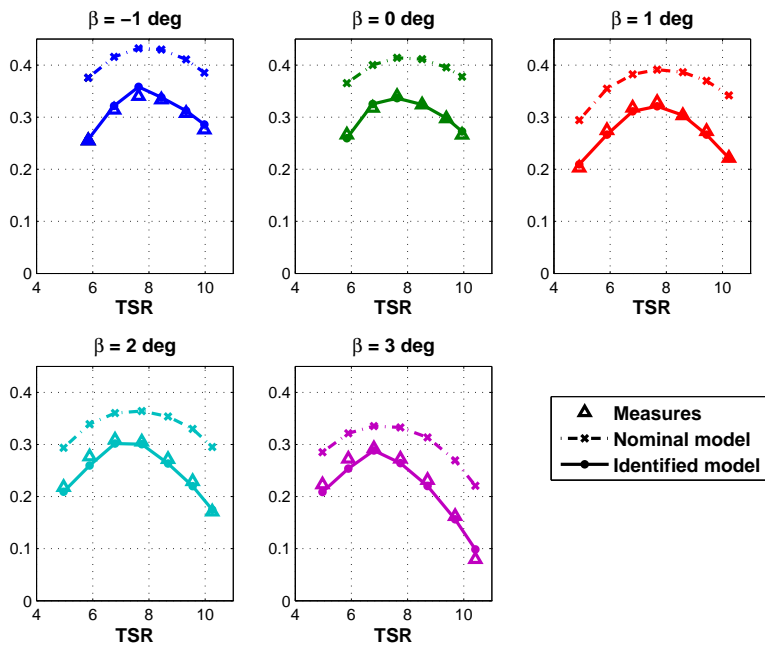
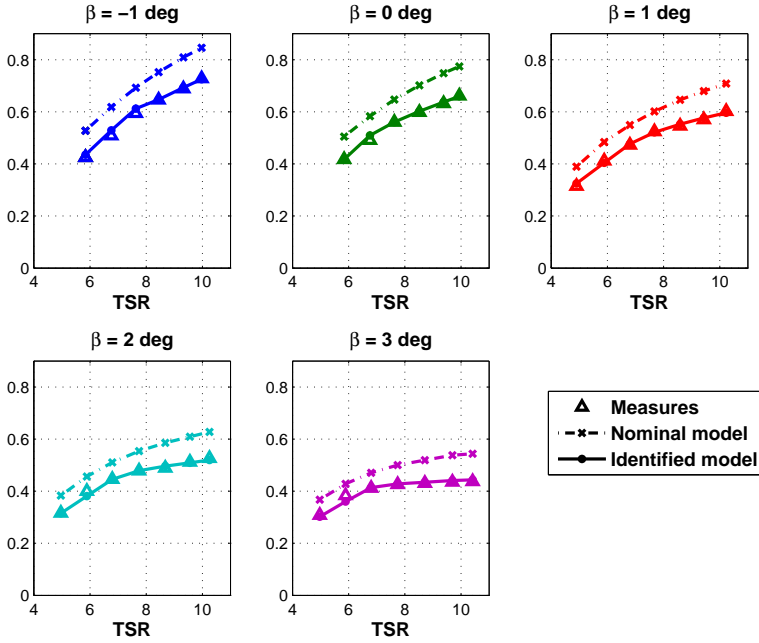


Figure 4.10: Identifiable SVD-shapes.



**Figure 4.11:** Comparison of power coefficients for the tested conditions obtained with the SVD-based approach. Triangle symbols: measures; dashed lines: original model; solid lines: identified model.



**Figure 4.12:** Comparison of thrust coefficients for the tested conditions obtained with the SVD-based approach. Triangle symbols: measures; dashed lines: original model; solid lines: identified model.

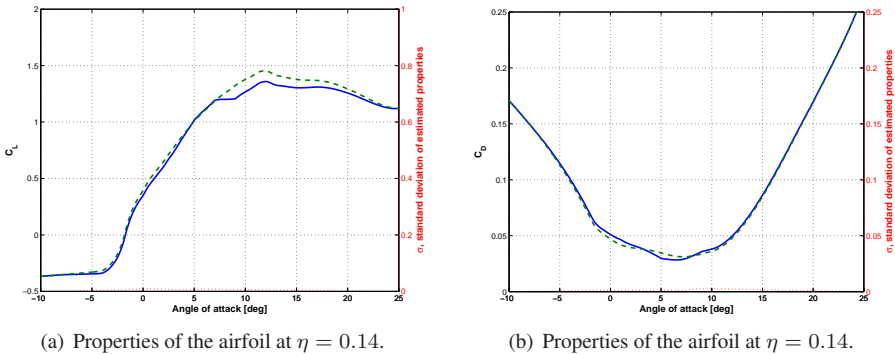
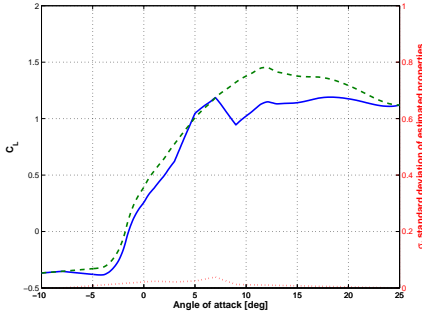
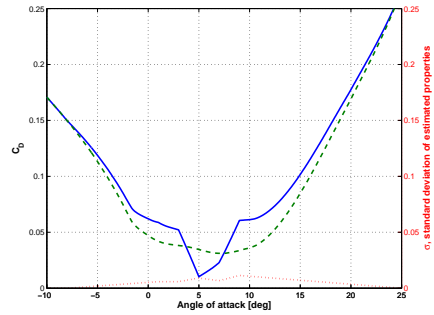


**Figure 4.13:** Aerodynamic properties of the airfoil located at  $\eta = 0.14$ . Solid lines: identified properties; dashed lines: nominal properties; dotted lines: standard deviations.

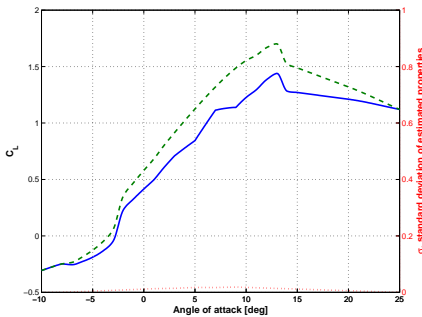


(a) Properties of the airfoil at  $\eta = 0.40$ .

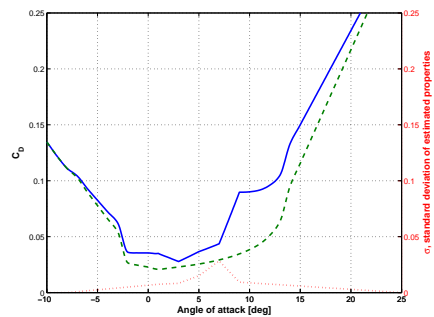


(b) Properties of the airfoil at  $\eta = 0.40$ .

**Figure 4.14:** Aerodynamic properties of the airfoil located at  $\eta = 0.40$ . Solid lines: identified properties; dashed lines: nominal properties; dotted lines: standard deviations.

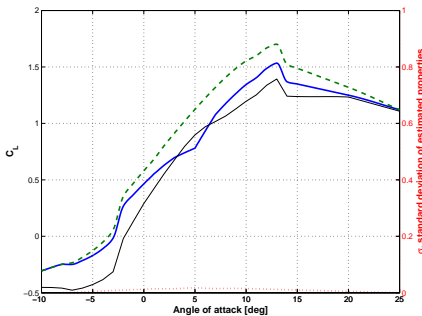


(a) Properties of the airfoil at  $\eta = 0.72$ .

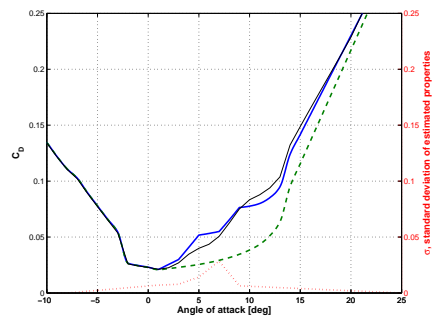


(b) Properties of the airfoil at  $\eta = 0.72$ .

**Figure 4.15:** Aerodynamic properties of the airfoil located at  $\eta = 0.72$ . Solid lines: identified properties; dashed lines: nominal properties; dotted lines: standard deviations.



(a) Properties of the airfoil at  $\eta = 0.86$ .



(b) Properties of the airfoil at  $\eta = 0.86$ .

**Figure 4.16:** Aerodynamic properties of the airfoil located at  $\eta = 0.86$ . Thick solid lines: properties identified with the SVD-based approach; Thin solid lines: properties identified with the direct approach; dashed lines: nominal properties; dotted lines: standard deviations of the SVD-based estimates.

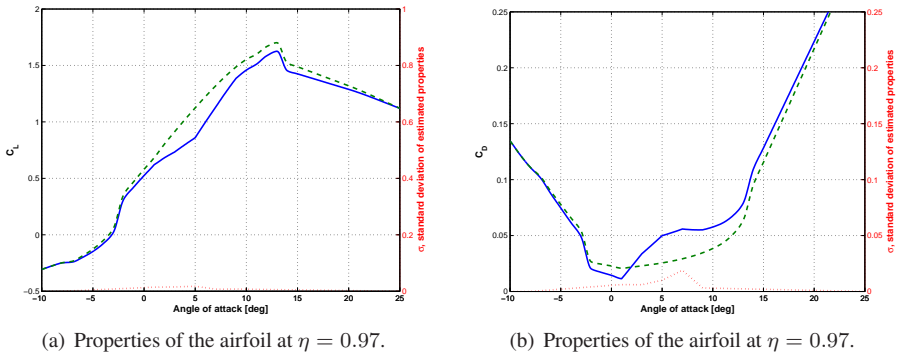


**Figure 4.17:** Aerodynamic properties of the airfoil located at  $\eta = 0.97$ . Solid lines: identified properties; dashed lines: nominal properties; dotted lines: standard deviations.



---

# CHAPTER 5

---

## Conclusions

---

**I**N this part of the thesis some methods for estimating the blade structural and aerodynamic properties from experimental data are described. The proposed procedures can be used for identifying rotor properties of wind turbines, so as to improve the predictive capabilities of aero-elastic simulations. Furthermore, the same procedures can be used for understanding the nature of discrepancies between nominal design characteristics of the blade and the manufactured item, which in turn may have positive feedbacks which include improvements in the manufacturing process or new design solutions to optimize the rotor performances.

In the next two sections the conclusions for both the structural and aerodynamic identification processes will be summarized.

### 5.1 Identification of beam models

---

The proposed procedure for estimating the blade structural properties was tested with the help of simulated and real experimental data. From the results presented in Chapter 3, as well as extensive testing with other blade identification problems not reported here for brevity, the following conclu-

sions can be drawn:

- Using multiple experiments in a measurement fusion approach, as the one pursued here, improves the quality of the estimates; specifically, we found that the use of static load tests can lead to better estimates of the blade structural parameters than those obtained by the sole use of measured natural frequencies, as also observed in Ref. [37].
- The inclusion of equality and inequality constraints is an effective way of including all available information in the estimation problem. Furthermore, the use of bounds on the estimation parameters can help in assuring that the results are within physically admissible limits.
- As for all parameter estimation problems, great care has to be taken to ensure the well posedness of the problem, and the identifiability of unknown parameters. This issue was considered here by studying the Fisher information matrix.
- The use of a divide and conquer approach can greatly robustify the procedure. In fact, breaking the identification parameters into groups leads to smaller and better conditioned problems. All couplings among the various groups can be recovered by iteratively repeating the sub-identification problems for each group. Such iterations were found to converge very quickly.
- The adaptive estimation of the error covariance leads to an iterative solution of least-squares-like problems with given weighting. The maximum likelihood formulation relieves the user from the choice of the weighting factors, which are computed automatically. This proved to be useful especially when considering multiple diverse measurements, as in the present case. Furthermore, the method allows one to define bounds on the covariance of the estimates.
- Experiments aimed at providing data for parameter estimation should be carefully designed so as to provide complete results with a sufficient level of accuracy. Incomplete load cases, imperfect clamp conditions, partial recording of blade section motions and other limitations were found here to complicate the identification process of the tested blades.
- The use of gradient-based methods, SQP in the present case, leads to relatively fast execution times, high precision solutions and an exact handling of linear and non-linear constraints. On the other hand, one



can not guarantee the achievement of the global optimum, and trapping in local minima is possible. The use of global optimizers, possibly coupled to the present local one for efficiency, should be pursued in the continuation of this research.

## 5.2 Identification of aerodynamic properties

---

Two different approaches for the identification of the aerodynamic properties of wind turbine rotors from experimental data have been presented in Chapter 4. In the first approach, noted *direct approach*, the direct estimation of lift and drag coefficients is performed. In the second approach, noted *SVD-based approach*, the singular values decompositions of the sensitivity matrix, performed before each identification, is used to recast the problem in order to restrict the estimation of only those quantities which are actually identifiable with a suitable level of accuracy, improving in this way the goodness of the achieved results.

Both these approaches have been performed in order to identify the aerodynamic model of the scaled wind turbine model V2, using thrust and power measurements obtained from a wind tunnel experimentation. From the achieved results the following conclusions can be stated:

- The problem of estimating the rotor aerodynamics is very hard, especially if compared with the structural one presented in Sections 3. Thrust and power measures, which are typically available in all wind turbines, have a great informative content but not enough to distinguish the effects of many airfoils along blade span, and therefore to identify their properties with a good level of accuracy. The computation of the Cramèr Rao lower bound of the unknowns and the study of the correlation of the Fisher information matrix have highlighted heavy collinearity between the properties of the inner and outer airfoils, particularly evident in the drag coefficients. This issue leads to an identification problem for which it is difficult to assure the well-posedness.
- The SVD-based approach, at least for the author's opinion, appears to be the sole able to solve rigorously the estimation problem, getting rid of all the troubles related to the low identifiability of some parameters and then helping the user to formulate correctly the optimization problem. The model achieved with the SVD-based approach is actually better correlated with measures than the one resulting from the

direct approach, and moreover presents lower and acceptable deviations of the estimates.

Even if the work here illustrated represents a great innovation in the literature related to the modeling of wind turbine rotors, there are some aspects which deserve to be opportunely studied in the next future developments.

First of all the use of loads measurements along the blade span could improve the informative content of the experimental data, leading to the possibility of identifying the aerodynamic properties of many airfoils along blade span. In such these conditions also the direct approach might have more possibility of producing results with a suitable level of confidence.

Rather than the introduction of the blade loads as outputs in the estimation process, the possibility of identifying a model from experimental data provided by a wind turbine operating in a real environment must be carefully considered.

First of all, since turbines operate according to a regulation trajectory, which forces the blade airfoils to work in a narrow range of angle of attack, one needs to suitably extend such range. This demand would require the machine to be operated at varying partialized set points.

Second, the methods described here assume steady operating conditions. In practice such these regimes do not exist because of wind variability and turbulence. Avoiding the use of transient model instead of the steady one, which probably would incur in a non-reasonable computational effort, one could compute averages over suitable time windows and use some careful data processing.

In any case, it seems that the extension to real field data requires that the design of the experiments and the collection of test data be carefully studied. Probably, for performing as best the aerodynamic updating process of a real wind turbine, three conditions must be satisfied:

- The tested wind turbine must be equipped with two or more load sensors located at opportune blade stations;
- The controller of the turbine must be designed in order to allow the trimming of the machine at several partialized set points;
- Although not mandatory, the test data might be collected in low turbulence conditions.

An application of the present formulation to field test data, which accounts for the above mentioned points, is currently under investigation.

---

**Part II**

**Stability analysis and  
identification of periodic wind  
turbine models**



---

# CHAPTER 6

---

## Introduction and motivation

---

**T**HE estimation of damping is useful in a variety of tasks related to the design and verification of a wind turbine, for example for explaining the causes of observed vibration phenomena, for assessing the proximity of the flutter boundaries to the operating envelope of the machine, for evaluating the efficacy of control laws in increasing the damping of low-damped modes, etc. It is expected that the design of the future large and very large wind turbines which are being proposed for the exploitation of off-shore resources will further increase the importance of stability analysis. In fact, new designs will explore rotors of low solidity with long, slender and light-weight blades operating at high tip-speed-ratios, whose response will not only be affected by the drive-train/nacelle/tower flexibility, but also by the additional couplings induced by the hydro-elastic characteristics of the submerged, and possibly floating, structure and by its interaction with the marine environment.

Stability analysis methods use some appropriate linear model of the system, capable of representing with sufficient fidelity its response in the proximity of a given operating condition. If the model is assumed to be linear time invariant (LTI), then stability can be readily assessed by LTI stability

theory, for which a variety of methods is readily available [12, 64–67].

However, wind turbine models are more appropriately characterized by *periodic* rather than time invariant coefficients [68]. In fact, periodic effects are caused by gravitational and aerodynamic loads, the latter due to rotor-in-plane wind components, vertical and horizontal wind shears, and the interaction with the tower. Therefore linear time periodic (LTP) models, whose stability characteristics are described by Lyapunov-Floquet theory [69, 70], are customarily employed.

Rather than directly applying Floquet theory on a LTP model to study its stability, one can first turn the LTP model into an equivalent LTI one by a coordinate transformation, and then perform a standard LTI stability analysis. The infinitely numerous Lyapunov-Floquet state transformations make this possible by achieving the exact cancellation of all periodic terms in the model. However, a more common approach [14, 71] is to use the multi-blade coordinate (MBC) transformation of Coleman and Feingold [13, 72] (cf. also the review given in reference [73]). This transformation, which can be interpreted as an approximation of one of the exact Lyapunov-Floquet transformations [14, 15], expresses the model rotating degrees of freedom into an inertial frame with the effect of a strong reduction, but in general not an exact elimination, of the periodic content of the state matrix. The remaining periodicity is either neglected or removed by averaging, so that the resulting invariant model can at this point be analyzed using standard invariant techniques. We will call this approach in the following *MBC-LTI*. The neglected periodicity is more relevant for anisotropic rotors (i.e. when blades are aerodynamically or structurally different), for anisotropic wind conditions (i.e. with shears and/or cross-flow), and in the presence of gravity; the effects of such approximations on the stability analysis, although often acceptable in many cases, are however in general difficult to assess and quantify a priori.

According to what stated in [74–76], which are three original works on which the results shown here are mainly based, there are two main aspects in the stability analysis of wind turbines: periodicity and the dependence on a model. In this part of the thesis a new approach that accounts for both in ways that try to overcome some limitations of current methods is proposed.

### 6.1 Periodicity

---

Regarding periodicity, the proposed method rigorously accounts for the periodic nature of the problem, building on Floquet stability theory of LTP systems [77, 78]. The motivation behind this approach lies in the fact that

the approximate treatment of periodic terms of contemporary methods implies approximations that invariably neglect some aspects of the behavior of the system. Although such approximations may have been usually acceptable for the current wind turbines, they may become more questionable as industry explores modern controllers and designs of increasing size that try to beat the cubic weight growth curve.

In fact, the use of stability theory shows a richer picture than the one customarily obtained by the use of the standard approximate transformation methods described above, as first noticed in reference [74]. For each of the harmonics computed by the MBC-LTI approach (e.g., first tower fore-aft, first blade flap, first blade edge, second blade flap, etc.), the fully periodic approach reveals the presence of a *fan* made by an infinite number of harmonics of varying “strength”.

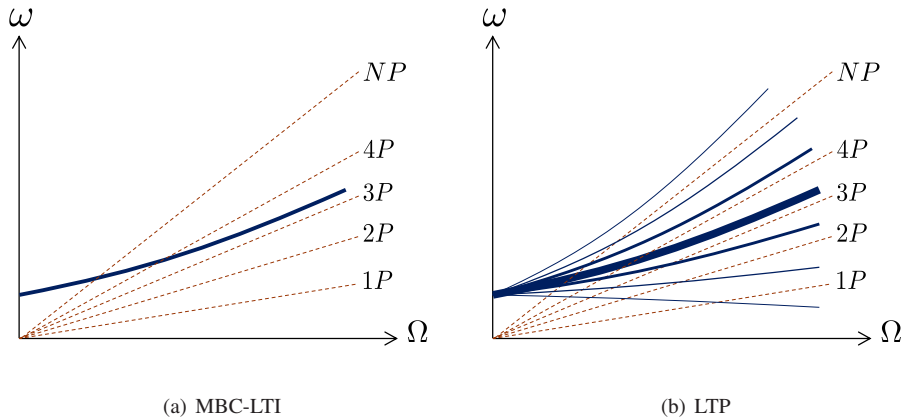


**Figure 6.1:** *Qualitative standard (at left) and periodic (at right) Campbell diagrams (for clarity, one single mode is shown for the standard diagram, and the corresponding single fan for the periodic one).*

To better illustrate this concept, Figure 6.1 shows at left a Campbell diagram obtained by the MBC-LTI approach, and at right its fully periodic version. As customarily done, the plot represents the system harmonics  $\omega$  vs. the rotor speed  $\Omega$ ; the plot also reports the per-rev excitation harmonics indicated as straight dashed lines emanating from the origin. For simplicity of exposition, and not to clutter the figure, the plot on the left shows only one single frequency, which by its shape and location in this qualitative image might represent the first flap blade frequency, slightly increasing with respect to the rotor speed due to centrifugal stiffening. The one on the left part of the figure is the Campbell diagram representation that would

normally be obtained by using a classical approach, and which represents an important design tool since it readily illustrates the possible intersections between system eigenfrequencies and per-rev excitation harmonics.

In reality, a rigorous LTP analysis reveals the picture shown on the right part of the same Figure 6.1. Here, for that same first blade flap mode, we observe not only the principal harmonic already visible in the left plot, but also an infinite number of associated *super-harmonics* fanning out from the principal one at about  $\pm k\Omega$ ,  $k = 1, \dots, \infty$ . All harmonics in the fan have a varying degree of “strength”, indicated in the picture by the thickness of the solid line. These additional super-harmonics are invisible to the classical approach<sup>1</sup>.

These results descend directly from the theory of periodic systems, which shows that the stability of the solution is contained in the monodromy matrix, i.e. the matrix mapping the system states into the states after one period (one rotor revolution). From the characteristic multipliers, which are the eigenvalues of the monodromy matrix, one can readily derive the characteristic exponents. In turn, the characteristic exponents, being the analogues of the eigenvalues in the LTI case, yield the frequency and damping factor of each harmonic of the system. Finally the periodic eigenvectors of the system are computed, which yield *modal participation factors* that measure the relative strength of each harmonic within its fan, as illustrated in the plot above. Modal participation factors rigorously clarify the degree of periodicity of each fan. In fact, the closer the participation of a certain harmonic is to one, the more that fan behaves as invariant (i.e. non periodic); in the limit, if one harmonic has a participation factor of exactly one and all others are zero, then the fan collapses into a single line, yielding the usual picture seen at left in Figure 6.1. On the other hand, if some super-harmonics have significant participation factors, then the fan is strongly affected by periodicity. In such cases, crossing of a significant super-harmonic with a per-rev excitation in conditions where enough energy is present (e.g. high rotor speeds) may results in vibratory phenomena. Notice that these would not be explainable if one try to describe a periodic mode using only one frequency.

---

<sup>1</sup>LTP theory does not allow for the classification of one specific harmonic as the principal one, as the whole fan of harmonics is generated as part of the analysis. However, to ease the bridge between the classical view and the present one, we term here and in the following “*principal harmonic*” the member of the fan that most closely resembles the one that would have been obtained by the MBC-LTI approach; coherently, all other members of the same fan are termed “*super-harmonics*”.



---

## 6.2 Model independence

---

Regarding the dependence on a model for the conduction of a stability analysis, we remark that methods that rely on coordinate transformations, such as the MBC-LTI approach described above, are usually difficult to implement and maintain. In fact, given the software implementation of any suitable mathematical wind turbine model, one would first have to develop its linearization. Next, one would need to implement the Coleman transformation of the rotating degrees of freedom of the model, followed by some specific additional elaboration to remove any remaining periodic term. It is clear that, if the original non-linear model is of high fidelity and hence highly complex, as the ones used in most current comprehensive codes, then the implementation of these software modifications can imply a considerable effort. Even more importantly, it means that every time the non-linear model is improved or expanded, this has to be followed by a similar upgrade of its MBC-LTI derivation.

To overcome such hurdles, in this work periodic stability analysis theory is not applied to the analytical expression of a specific model, but rather it is formulated in terms of input-output discrete-time histories. Such time histories could come from “virtual” experiments performed on any model, from simplified ones to the more advanced contemporary comprehensive multibody-based aero-hydro-servo-elastic models. On the practical side, this implies that one can easily replace the model with a different (new or better) one, without having to modify or adjust in any way the stability analysis procedure. Furthermore, by properly expanding the formulation presented here to include the effects of process noise, the time histories could also come from measurements obtained on the real wind turbine operating in the field.

Using this approach, inputs are represented by either pitch, torque and/or by externally applied force signals, studied so as to excite the response of the mode(s) of interest. On the other hand, outputs are represented by the corresponding measurements of components of the system response (velocities, accelerations, loads, etc.), chosen so as to exhibit a high informational content on the mode(s) of interest. This procedure is graphically depicted in Figure 6.2.

Given such suitable input-output time histories, a Periodic Auto-Regressive Moving Average model with eXogenous inputs (PARMAX) [79] is fitted to the histories using system identification techniques, and more specifically with the prediction error method [80, 81]. Finally, the periodic stability analysis theory of Floquet is applied to the state-space

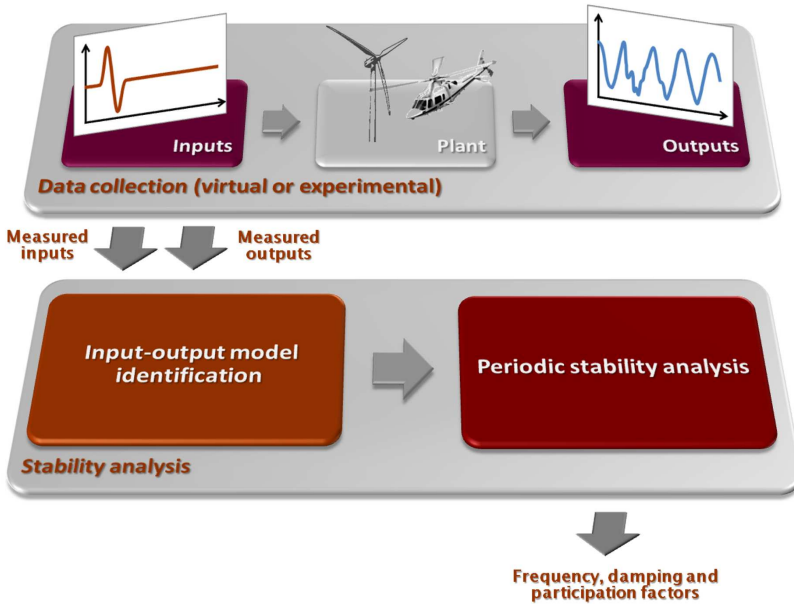


Figure 6.2: Model-independent stability analysis process.

realization of the identified model to yield frequencies, damping and modal participation factors of each harmonic in each fan. From this point of view, this method could be interpreted as an extension to periodic models of the method of Prony [82]. A somewhat related approach is pursued in reference [83], which proposes an output-only modal analysis in the frequency domain, made possible by the identification of the periodic harmonic transfer function of the system [77].

### 6.3 Organization of this part

---

The work presented in this part is organized according to the following plan.

At first, the stability theory of LTP systems is briefly reviewed in Section 7. The continuous and discrete-time formulations in § 7.1 and § 7.2 explain the presence of the frequency fans and lead to the definition of the modal participation factors as periodicity indicators. To better illustrate these concepts, we consider in § 7.3 the simplified model problem of a rotor-tower system in a vacuo, which also clearly establishes the differences between a periodic stability analysis and an approximate MBC-LTI one.

Next, Section 8 describes the process of identifying LTP systems from input-output data using the prediction error method. The identification techniques of three models are described: the equation error approach, is formulated in § 8.1.1, whereas the output error method, in § 8.1.2, and the estimation of PARMAX models in § 8.1.3. Finally, § 8.2 describes the realization of the identified periodic reduced model in state-space form.

The paper is completed by several numerical experiments, reported in Section 9, which illustrate the main findings of this work with the help of the detailed model of a multi-MW wind turbine implemented in a high fidelity aero-servo-elastic simulation code.



---

## Stability analysis of LTP systems

---

### 7.1 Continuous time

---

A generic LTP system in continuous time can be written in state space form as

$$\dot{\mathbf{x}} = \mathbf{A}(t)\mathbf{x} + \mathbf{B}(t)\mathbf{u}, \quad (7.1a)$$

$$\mathbf{y} = \mathbf{C}(t)\mathbf{x} + \mathbf{D}(t)\mathbf{u}, \quad (7.1b)$$

where  $t$  is time,  $\mathbf{x}$ ,  $\mathbf{u}$  and  $\mathbf{y}$  the state, input and output vectors, respectively, while  $\mathbf{A}(t)$ ,  $\mathbf{B}(t)$ ,  $\mathbf{C}(t)$  and  $\mathbf{D}(t)$  are periodic system matrices such that

$$\mathbf{A}(t + T) = \mathbf{A}(t), \quad \mathbf{B}(t + T) = \mathbf{B}(t), \quad (7.2a)$$

$$\mathbf{C}(t + T) = \mathbf{C}(t), \quad \mathbf{D}(t + T) = \mathbf{D}(t), \quad (7.2b)$$

for each  $t$ . The smallest  $T$  satisfying equation (7.2) is defined as the system period. Vector  $\mathbf{u}$  contains the machine control inputs (i.e. blade pitch angles, electrical torque, possibly the yaw angle) as well as exogenous inputs related to the wind states (e.g. wind speed, vertical or lateral shears, cross-flow, etc.). The closed-loop case may be considered by including the effects of the control law in the  $\mathbf{A}(t)$  matrix; in this case, the  $\mathbf{u}$  vector is only related to wind states.

To study the stability of (7.1a), its autonomous version is considered together with the associated initial conditions:

$$\dot{\mathbf{x}} = \mathbf{A}(t)\mathbf{x}, \quad \mathbf{x}(0) = \mathbf{x}_0. \quad (7.3)$$

The state transition matrix  $\Phi(t, \tau)$ , that maps the state  $\mathbf{x}(\tau)$  at time  $\tau$  into the state  $\mathbf{x}(t)$  at time  $t$  through

$$\mathbf{x}(t) = \Phi(t, \tau)\mathbf{x}(\tau), \quad (7.4)$$

obeys a similar equation with its initial conditions

$$\dot{\Phi}(t, \tau) = \mathbf{A}(t)\Phi(t, \tau), \quad \Phi(\tau, \tau) = \mathbf{I}, \quad (7.5)$$

where  $\mathbf{I}$  is the identity matrix. The periodicity of the system, involves the *bi-periodicity* of the transition matrix, such that

$$\Phi(t + T, \tau + T) = \Phi(t, \tau). \quad (7.6)$$

Notice also that the swapping of the indices  $t$  and  $\tau$  in the transition matrix implies its inverse, that is  $\Phi(t, \tau)^{-1} = \Phi(\tau, t)$ . Even if in continuous time the expression of the transition matrix, in general, can't be worked out analytically, it is however possible to figure out its determinant through the *Liouville-Jacoby* formula

$$\det \Phi(t, \tau) = e^{\int_{\tau}^t \text{Tr}(\mathbf{A}(\sigma))d\sigma}, \quad (7.7)$$

which proves also that  $\Phi(t, \tau)$  is invertible  $\forall(t, \tau)$ . This is no more true in the discrete time case, see the first chapter of [77] for the details.

As it will be described in the following, an important role in the stability analysis of the periodic systems is played by the state transition matrix over one period  $\Psi(\tau) = \Phi(\tau + T, \tau)$ , termed *monodromy matrix*. Equations (7.6) and (7.7) entails that in continuous time  $\Psi(\tau)$  is periodic,  $\Psi(\tau) = \Psi(\tau + T)$  and non singular  $\forall\tau$ .

The general behaviour of an LTP system was first formalized by Gaston Floquet and Aleksandr Lyapunov, [69, 70].

The Floquet-Lyapunov problem is the one of finding, if any, a periodic invertible state-space transformation  $\mathbf{y}(t) = \mathbf{Q}(t)\mathbf{x}(t)$  such that the resulting system,

$$\dot{\mathbf{y}} = \mathbf{R}\mathbf{y}, \quad (7.8)$$

is time-invariant, i.e. the matrix  $\mathbf{R}$ , termed also *Floquet factor*, is constant.

In the new coordinates the dynamic matrix  $\mathbf{R}$  is given by

$$\mathbf{R} = \mathbf{Q}(t)\mathbf{A}(t)\mathbf{Q}^{-1}(t) + \dot{\mathbf{Q}}(t)\mathbf{Q}^{-1}(t). \quad (7.9)$$

which shows also that  $\mathbf{Q}(t)$  must obeys the following matrix differential equation

$$\dot{\mathbf{Q}}(t) = \mathbf{R}\mathbf{Q}(t) - \mathbf{Q}(t)\mathbf{A}(t) \quad (7.10)$$

The solution of (7.10) is

$$\mathbf{Q}(t) = e^{\mathbf{R}(t-\tau)}\mathbf{Q}(\tau)\Phi(\tau, t). \quad (7.11)$$

Imposing the periodicity condition  $\mathbf{Q}(\tau + T) = \mathbf{Q}(\tau)$ , one gets

$$\mathbf{Q}(\tau) = e^{\mathbf{R}T}\mathbf{Q}(\tau)\Phi(\tau, \tau + T), \quad (7.12)$$

which gives in turn the important relationship between the monodromy matrix and the Floquet factor as

$$\Psi(\tau) = \mathbf{Q}(\tau)^{-1}e^{\mathbf{R}T}\mathbf{Q}(\tau). \quad (7.13)$$

From (7.13) it is possible to compute the Floquet factor  $\mathbf{R}$  for any invertible initial condition  $\mathbf{Q}(\tau)$ , by the following

$$\mathbf{R} = \frac{1}{T}\log[\mathbf{Q}(\tau)\Psi(\tau)\mathbf{Q}(\tau)^{-1}] \quad (7.14)$$

Notice that there is an infinite number of Floquet factors, and therefore an infinite number of Floquet-Lyapunov transformations, first, because one can choose any invertible initial condition  $\mathbf{Q}(\tau)$ , and second because in the complex domain the matrix logarithm has infinite possible solutions. In particular, this latter remark will be deeply analyzed later on.

Giving  $\mathbf{Q}(\tau)$  and  $\mathbf{R}$ , the transformation matrix  $\mathbf{Q}(t)$  is readily obtained using Equation (7.11).

Starting from (7.11) after simple analytical computations the transition matrix results to be

$$\Phi(t, \tau) = \mathbf{P}(t)e^{\mathbf{R}(t-\tau)}\mathbf{P}(\tau)^{-1} \quad (7.15)$$

where the periodic matrix  $\mathbf{P}(t) = \mathbf{Q}(t)^{-1}$  is also termed *periodic eigenvector*. Equation 7.15 could be simplified, as commonly done, choosing  $\tau = 0$  and  $\mathbf{P}(0) = \mathbf{I}$ , leading to

$$\Phi(t, 0) = \mathbf{P}(t)e^{\mathbf{R}t}. \quad (7.16)$$

Equations (7.15) and 7.16 show also that any periodic system is asymptotically stable if all the eigenvalues of  $\mathbf{R}$ , noted  $\theta_j$ ,  $j = 1, \dots, N_s$ ,  $N_s$  being the order of the system, and termed *characteristic exponents* have negative real part. Rather than in terms of the Floquet factor, the stability

assessment could be done referring to the monodromy matrix. In fact, since the monodromy matrix correlates the state vector of two different time instants separated by one period, it is simply to derive the equation which describes the free motion of the state sampled at time  $\tau + kT$ ,  $k \in \mathbb{N}$ , noted  $\hat{\mathbf{x}}(k) = \mathbf{x}(\tau + kT)$ , as

$$\hat{\mathbf{x}}(k) = \mathbf{\Psi}(\tau)^k \hat{\mathbf{x}}(0). \quad (7.17)$$

Eq. (7.17) is the governing equation of a linear invariant discrete time systems with  $\mathbf{\Psi}(\tau)$  as dynamic matrix. Therefore the system is asymptotically stable if all the eigenvalues of the monodromy matrix,  $\theta_j$ , called *characteristic multipliers* belong to the open unit disk in the complex plane. It is also possible to demonstrate that the eigenvalues of the monodromy matrix and their multiplicity are actually time invariant even if the monodromy matrix is in general time periodic, see [77] for proofs and details. For this reason we can ignore the time instant when referring to the characteristic multipliers. The eigenvalues  $\theta_j$  and associated eigenvectors  $\mathbf{s}_j$ , are obtained by the spectral factorization of the monodromy matrix,

$$\mathbf{\Psi}(\tau) = \mathbf{S} \text{diag}\{\theta_j\} \mathbf{S}^{-1}, \quad (7.18)$$

with  $\mathbf{S} = [\dots, \mathbf{s}_j, \dots]$ .

From the factorization of  $\mathbf{\Psi}$ , recalling (7.13), one gets the factorization of  $\mathbf{R}$  as

$$\mathbf{R} = \mathbf{Q}(\tau) \mathbf{S} \text{diag}\{\eta_j\} \mathbf{S}^{-1} \mathbf{Q}(\tau)^{-1}, \quad (7.19)$$

where the *characteristic exponents*  $\eta_j$  are related to the characteristic multipliers  $\theta_j$  through the following expression:

$$\theta_j = e^{\eta_j T}. \quad (7.20)$$

Equation (7.20) leads to a multiplicity of solutions of characteristic exponents, as

$$\eta_j = \frac{1}{T} \log \theta_j = \frac{1}{T} (\log |\theta_j| + i(\angle(\theta_j) + 2\ell\pi)), \quad (7.21)$$

where  $\ell \in \mathbb{Z}$  is an arbitrary integer. This indeterminacy however does not affect the real frequency content of the response, since the transition matrix is uniquely defined.

To this end, consider for each mode one of the infinite solution of (7.21), for example the one with  $\ell = 0$ , noted  $\hat{\eta}_j$ . Thus, any other characteristic exponents,  $\eta_j$  could be computed from  $\hat{\eta}_j$  as

$$\eta_j = \hat{\eta}_j + i \frac{2m\pi}{T}, \quad m \in \mathbb{Z} \quad (7.22)$$



Inserting (7.19) into (7.15), one can express the state transition matrix as

$$\Phi(t) = \sum_{j=1}^{N_s} \mathbf{Z}_j(t) e^{\hat{\eta}_j t}, \quad (7.23)$$

where  $\mathbf{Z}_j(t) = \mathbf{P}(t)\mathbf{Q}(\tau)\mathbf{S}\mathbf{I}_{jj}\mathbf{S}^{-1}$ , while  $\mathbf{I}_{jj}$  is a matrix with the sole element  $(j, j)$  equal to 1 and all others equal to 0. The periodic matrix  $\mathbf{Z}_j(t)$  can be expanded in a Fourier series as follows

$$\mathbf{Z}_j(t) = \sum_{n=-\infty}^{+\infty} \mathbf{Z}_{jn} e^{i n \frac{2\pi}{T} t}, \quad (7.24)$$

where  $\mathbf{Z}_{jn}$  is the matrix of complex amplitudes of the  $n$ th harmonic of  $\mathbf{Z}_j(t)$ , leading to the following expression of the transition matrix:

$$\Phi(t) = \sum_{j=1}^{N_s} \sum_{n=-\infty}^{+\infty} \mathbf{Z}_{jn} e^{(\hat{\eta}_j + i n \frac{2\pi}{T})t}. \quad (7.25)$$

From Equation (7.25) one can see that, for each mode, an infinite number of exponents, which play the role of eigenvalues of the LTI systems, participates in the response of the system and a single frequency is not sufficient to characterize completely the mode. All the exponents, as symbolically depicted in figure 7.1, have imaginary parts which differ in integer multiples of the  $2\pi/T$  and same real parts, thus all exponents of a given mode, are all together stable or not. This fact of course is not surprising since the stability of the system is just determined from the characteristic multipliers, which are defined without indetermination.

However, in several applications, as for example in wind turbine modeling, it's also interesting to characterize the behaviour of the response of the systems. Therefore the knowledge of the exponents  $\hat{\eta}_j + i n \frac{2\pi}{T}$  becomes important, since they give in turn their own frequencies  $\omega_{jn}$  and the proper damping factors  $\xi_{jn}$ . In addition the amplitudes  $\mathbf{Z}_{jn}$  determine the strengths of the relative harmonics. The measurement of the relative contribution can be obtained introducing the participation factors,  $\phi_{jn}$ , defined as

$$\phi_{jn} = \frac{\|\mathbf{Z}_{jn}\|}{\sum_n \|\mathbf{Z}_{jn}\|}, \quad (7.26)$$

where  $\|\cdot\|$  is a matrix norm. The triads  $\{\omega_{jn}, \xi_{jn}, \phi_{jn}\}$  describe completely the behaviour of the periodic system. The participation of a given output

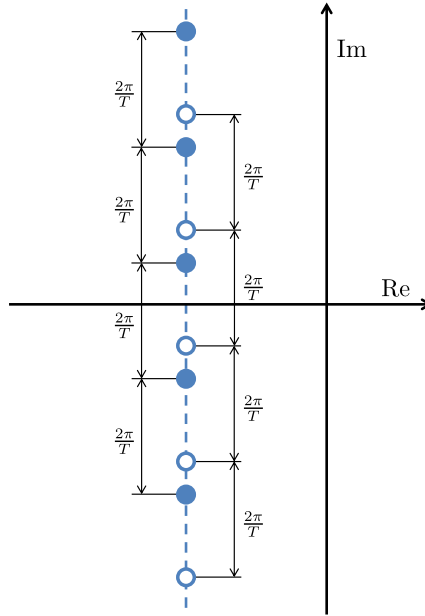


**Figure 7.1:** Representation of the eigenvalues characterizing the response of a periodic continuous-time system. A couple of complex conjugate poles is shown.

$y$  can be measured introducing the *output-specific participation factor*, defined as

$$\phi_{j_n} = \frac{\|CZ_{j_n}\|}{\sum_n \|CZ_{j_n}\|}, \quad (7.27)$$

Moreover, the apparent indeterminacy in the computation of the imaginary part of the logarithm of the characteristic multipliers in equation (7.21) is then understood. In fact, all the exponents that satisfy equation (7.20) are in effect present in the response of the system, as it can be seen from equation (7.25). Since the transition matrix is uniquely defined, any choice of the integer  $\ell$  in equation (7.21) would act as a shift in the frequency content of  $Z_j$ , such that all the triads  $\{\omega_{j_n}, \xi_{j_n}, \phi_{j_n}\}$  remain exactly the same, as first observed in [84] and later discussed in [78].

Sometimes, one of the amplitude matrices  $Z_{j_n}$  is predominant with respect to the others. In such cases, the resulting participation factors will be all close to zero, except that related to the predominant harmonic, which is at contrary close to one. This fact suggest two considerations. First, the harmonic participation factor can be used as a “periodicity indicator”: the closer the participation of a certain harmonic of a given mode is to one, the more that mode behaves as invariant. Second, in practical application, if a

given participation factor is predominant with respect to the others, a single frequency characterization could be accepted.

Often, although not always, the harmonic with the highest participation is very similar in terms of frequency and damping to the one that would result from the invariant analysis of periodic systems based on the Coleman transformation (MBC-LTI approach). As suggested in [76], and previously noted, such harmonic may be called the principal one, while the others may be termed super-harmonics. The formulas however show clearly that such a dichotomy, although useful to bridge the classical and periodic views, is in reality wrong, since periodic modes are not defined by a single frequency but by an infinite multitude, where each frequency is spaced from its two neighbors by plus and minus the rotor speed  $\Omega = 2\pi/T$ . Furthermore, any one of these harmonics could resonate with the external excitations. For this reason the Campbell diagram of a periodic system, noted *periodic Campbell diagram*, should show not only one line per mode, but a fan made by infinite numbers of harmonics with different participation factors as qualitatively depicted in Figure 6.1.

## 7.2 Discrete time

The autonomous dynamic equations of a generic LTP system in discrete time and its initial conditions are

$$\mathbf{x}(k+1) = \mathbf{A}(k)\mathbf{x}(k), \quad \mathbf{x}(0) = \mathbf{x}_0, \quad (7.28)$$

where  $k$  is a generic time instant and  $\mathbf{A}(k)$  is a periodic matrix of period  $K$  such that  $\mathbf{A}(k+K) = \mathbf{A}(k) \forall k$ . Similarly, the transition matrix obeys the following equations and initial conditions

$$\Phi(k+1, \kappa) = \mathbf{A}(k)\Phi(k, \kappa), \quad \Phi(\kappa, \kappa) = \mathbf{I}. \quad (7.29)$$

In this work we consider only reversible systems, i.e. those for which  $\det(\Phi(k, \kappa)) \neq 0 \forall (k, \kappa)$ . Notice that in the continuous-time case the reversibility is always guaranteed (cf. Sections 7.1 and reference [77, 85] for the detailed treatment).

For reversible discrete-time systems, the state transition matrix  $\Phi(k, \kappa)$  can be decomposed in periodic and contractive factors as

$$\Phi(k, \kappa) = \mathbf{P}(k)\mathbf{R}^{(k-\kappa)}\mathbf{P}(\kappa)^{-1}, \quad (7.30)$$

where  $\mathbf{P}(k)$  is periodic and  $\mathbf{R}$  is constant. Here again, the monodromy matrix is defined as the transition matrix over one period, i.e.

$$\Psi(\kappa) = \Phi(\kappa+K, \kappa) = \mathbf{P}(\kappa)\mathbf{R}^{(K-\kappa)}\mathbf{P}(\kappa)^{-1}, \quad (7.31)$$

whose spectral decomposition yields its characteristic multipliers  $\theta_j$  and eigenvectors  $\mathbf{S}$ :

$$\Psi(\kappa) = \mathbf{S} \operatorname{diag}\{\theta_j\} \mathbf{S}^{-1}. \quad (7.32)$$

As in the continuous time case, the characteristic multipliers and their multiplicity are in effect independent by the index  $\kappa$ .

The relationship between characteristic multipliers and characteristic exponents becomes then

$$\theta_j = \eta_j^K. \quad (7.33)$$

In the discrete-time case, the apparent multiplicity of the characteristic exponents appears as a phase indetermination since

$$\eta_j = \sqrt[K]{|\theta_j|} \left( \cos \left( \frac{\angle(\theta_j) + 2\ell\pi}{K} \right) + i \sin \left( \frac{\angle(\theta_j) + 2\ell\pi}{K} \right) \right), \quad (7.34)$$

where  $\ell = 0, \dots, K - 1$  is an arbitrary integer, see Figure 7.2 for a schematic representation. As in the continuous-time case, this does not in reality generate any inconsistency since frequencies, damping and participation factors of the various harmonics are unaffected by this apparent arbitrariness.

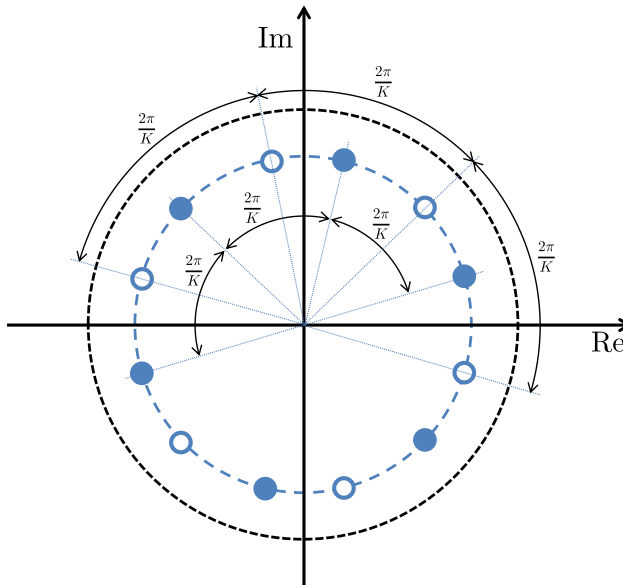


**Figure 7.2:** Representation of the eigenvalues characterizing the response of a periodic discrete-time system. A couple of complex conjugate poles is shown.

Following the same approach of the continuous-time case, the transition matrix can be written as

$$\Phi(t) = \sum_{j=1}^{N_s} \sum_{n=0}^{K-1} \mathbf{z}_{jn} \left( |\eta_j| e^{(i\angle(\eta_j) + n\frac{2\pi}{K})} \right)^k. \quad (7.35)$$

This shows that the  $j$ th mode is characterized by  $K$  exponents with the same modulus and different phases. Each exponent can be transformed into the continuous one using the following expression

$$\eta_{jc} = \frac{1}{\Delta t} \log(\eta_{jd}), \quad (7.36)$$

where  $\Delta t$  is the sampling time and subscripts  $(\cdot)_c$  and  $(\cdot)_d$  refer, respectively, to the continuous and discrete-time cases. Once the continuous-time exponents are computed, frequencies, damping and participation factors can be readily obtained as in the continuous-time case.

### 7.3 Illustration by a model problem

---

A simple model problem is used for illustrating the main characteristics of the classical periodic stability analysis described above. The problem represents the coupled side-side tower and edgewise blade response of a wind turbine in vacuo. In this simplified model, the side-side flexibility of the tower is rendered by an equivalent spring that connects the hub to the ground [86]. Similarly, the blade is represented by a rigid body connected to the hub by means of equivalent hinges, whose characteristics in terms of offset from the axis of rotation and stiffness are chosen so as to match the first edgewise natural frequency of the blade [68]. The model includes gravity because the blade stiffness varies periodically under the effects of its own weight, effects that depend on the blade azimuthal position in its travel around the rotor disk. Figure 7.3 shows a sketch of the system, whereas Table 7.1 reports a list of the main model parameters and their values.

The  $B + 1$  linearized periodic equations of motion of the system write

$$\mathbf{M}(\psi)\ddot{\mathbf{x}}(t) + \mathbf{C}(\psi)\dot{\mathbf{x}}(t) + \mathbf{K}(\psi)\mathbf{x}(t) = 0, \quad (7.37)$$

where the state vector is defined as

$$\mathbf{x}(t) = (\zeta_1(t), \zeta_2(t), \zeta_3(t), y_c(t))^T, \quad (7.38)$$

$\zeta_i$  being the lag angle of the  $i$ th blade and  $y_c$  the horizontal displacement of the hub,  $\psi = \psi_1 = \Omega(t)t$  and  $\psi_i = \psi_1 + (i - 1)2\pi/B$ ,  $i = 2, 3$ , the

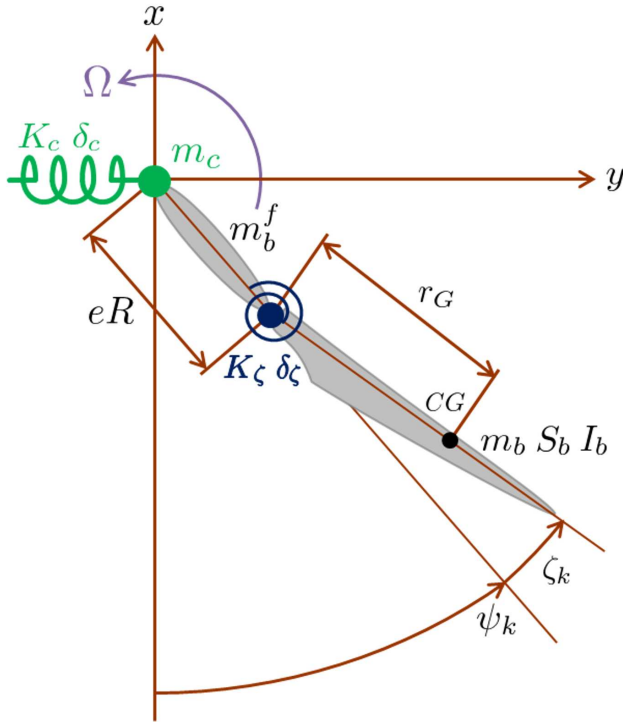


**Figure 7.3:** Schematic view of the rotor-tower model system. Only one blade is shown, for clarity.

**Table 7.1:** Rotor-tower model system: main parameters and their numerical values.

Parameter	Symbol	Value
Number of blades	$B$	3
Rotor radius	$R$	75 [m]
Rated rotor speed	$\Omega_r$	1.2 [rad s <sup>-1</sup> ]
Hinge offset	$e$	25.651 [%R]
Mass of hub	$m_h$	7.5000E+4 [kg]
Blade mass (movable part)	$m_b$	1.4482E+4 [kg]
Blade mass (fixed part)	$m_b^f$	1.0873E+4 [kg]
Blade static moment	$S_b$	2.7116E+5 [kg m]
Blade moment of inertia	$I_b$	7.4881E+6 [kg m <sup>2</sup> ]
Edgewise spring stiffness	$K_\zeta$	2.1192E+8 [N m]
Edgewise spring damper	$\delta_\zeta$	1.7555E+6 [N m s]
Tower spring stiffness	$K_c$	7.3116E+5 [N m <sup>-1</sup> ]
Tower spring damper	$\delta_c$	1.3294E+4 [N s m <sup>-1</sup> ]

azimuthal angle of rotor and individual blades, while

$$\mathbf{M}(\psi) = \begin{bmatrix} I_b & 0 & 0 & S_b s(\psi_1) \\ 0 & I_b & 0 & S_b s(\psi_2) \\ 0 & 0 & I_b & S_b s(\psi_3) \\ S_b s(\psi_1) & S_b s(\psi_2) & S_b s(\psi_3) & m_h + B(m_b + m_b^f) \end{bmatrix}, \quad (7.39a)$$

$$\mathbf{C}(\psi) = \begin{bmatrix} \delta_b & 0 & 0 & 0 \\ 0 & \delta_b & 0 & 0 \\ 0 & 0 & \delta_b & 0 \\ -2S_b \Omega s(\psi_1) & -2S_b \Omega s(\psi_2) & -2S_b \Omega s(\psi_3) & \delta_c \end{bmatrix}, \quad (7.39b)$$

$$\mathbf{K}(\psi) = \begin{bmatrix} K_{e\zeta} + g S_b c(\psi_1) & 0 & 0 & 0 \\ 0 & K_{e\zeta} + g S_b c(\psi_2) & 0 & 0 \\ 0 & 0 & K_{e\zeta} + g S_b c(\psi_3) & 0 \\ -S_b \Omega^2 c(\psi_1) & -S_b \Omega^2 c(\psi_2) & -S_b \Omega^2 c(\psi_3) & K_c \end{bmatrix}, \quad (7.39c)$$

where  $s(\psi)$  and  $c(\psi)$  indicate the sine and the cosine of angle  $\psi$ , and  $K_{e\zeta} = K_\zeta + eR\Omega^2$ .

A classical MBC-LTI analysis would lead to the identification of four modes, which include the tower side-side, backward in-plane whirling, blade edgewise and forward in-plane whirling modes, in the order from lower to higher. A time continuous periodic stability analysis was performed from varying rotor speeds, which, as previously discussed, reveals a much higher number of harmonics. To illustrate this fact, for the rated rotor speed case, the frequencies of the harmonics with the five highest participation factors are reported in Table 7.2; these frequencies were grouped according to the principal classical modes named above.

**Table 7.2:** Frequency of the harmonics with the five highest participation factors at rated rotor speed, grouped by classical modes.

	Tower	Backward whirl	Blade edgewise	Forward whirl
Super-harmonic ( $-j2\Omega$ )	0.0378	0.3036	0.4649	0.6823
Super-harmonic ( $-j\Omega$ )	0.1533	0.4940	0.6558	0.8731
Principal harmonic	0.3443	0.6847	0.8467	1.0640
Super-harmonic ( $+j\Omega$ )	0.5352	0.8756	1.0377	1.2549
Super-harmonic ( $+j2\Omega$ )	0.7262	1.0665	1.2286	1.4458

Figure 7.4 shows the response spectra of one of the blades, at left, and the hub, at right. By comparing these spectra with Table 7.2, one can eas-

## Chapter 7. Stability analysis of LTP systems

**Table 7.3:** Output-specific participation factor for the frequency of Table 7.2

	Tower		Backward whirl		Blade edgewise		Forward whirl	
	$\zeta_1$	$y_c$	$\zeta_1$	$y_c$	$\zeta_1$	$y_c$	$\zeta_1$	$y_c$
Harmonic ( $-i2\Omega$ )	0.002	0.000	0.001	0.000	0.000	0.001	0.014	0.001
Harmonic ( $-i\Omega$ )	0.376	0.000	0.098	0.000	0.011	0.003	0.919	0.000
Principal harmonic	0.002	0.999	0.017	0.994	0.973	0.968	0.010	0.934
Harmonic ( $+i\Omega$ )	0.606	0.000	0.872	0.000	0.016	0.001	0.056	0.000
Harmonic ( $+i2\Omega$ )	0.012	0.000	0.011	0.000	0.000	0.000	0.000	0.000

ily identify most frequencies. In particular, a part from the well known principal harmonics, one should notice the two tower super-harmonics that appear very prominently (and rather unexpectedly for the MBC-LTI view, for which these modes should not exist) in the blade response spectrum at 0.1533 and 0.5352 Hz.

Table 7.3 illustrates the fact that each fan of modes may exhibit a more or less periodic behavior when looking at specific outputs. For each frequency of Table 7.2, this new table reports the participation factors computed using output  $\zeta_1$  (at left) and output  $y_c$  (at right), using equation (7.27). For example, the tower fan of modes behaves as largely invariant when observed through the tower displacement  $y_c$  (cf. the principal harmonic participation at 0.9997), but has a strongly periodic character when observed through the blade lag response (cf. the principal harmonic participation at 0.0017, while the super-harmonics  $+i\Omega$  and  $-i\Omega$  are 0.6058 and 0.3763, respectively). A similar behavior is observed for the backward and forward in-plane whirls, while the opposite is true for the blade edgewise one. These non-classical effects stress further the difference between the LTI and LTP views of the problem, the latter being much more complex and richer than the former. This also highlights once more the arbitrariness of labeling a frequency as the principal harmonic: what appears prominently in one output (e.g. the “classical” tower frequency in the tower displacement), can almost disappear in comparison with the its super-harmonics in another output (e.g., again the “classical” tower frequency observed in the blade lag response). Nonetheless, we keep using this terminology in the following for its practical utility and to ease the exposition.

Figure 7.5 shows the computed frequencies, damping and participation factors, plotted for varying rotor speed. Each frequency plot represents a diverging fan, each fan labeled by the classical name of its principal harmonic. Looking at the participation factor plots, it appears that only the tower mode is largely invariant; on the other hand, both whirling modes are



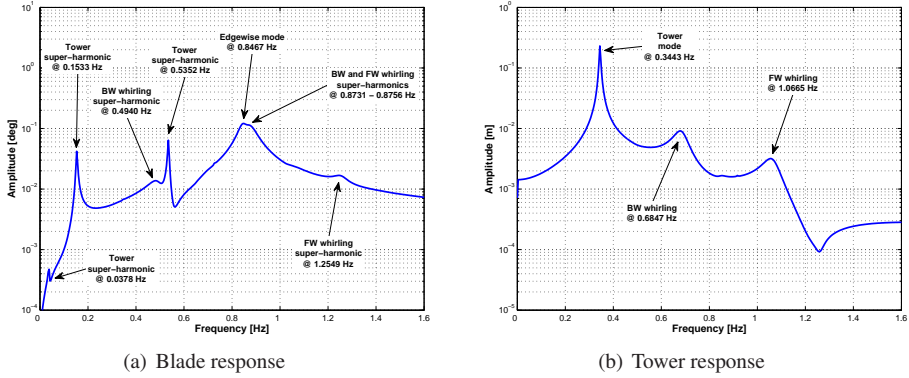


**Figure 7.4:** FFT of the transient response of the rotor-tower model problem.

characterized by a strongly periodic behavior, and their response is not well described by a single frequency.

Although the present model problem is quite simple, it still captures some interesting effects that help in clarifying the difference between a fully periodic and a MBC-LTI analysis. In fact, the presence of gravity renders the rotor anisotropic, due to a variation of lag stiffness that depends on the blade azimuthal position (cf. matrix  $\mathbf{K}(\psi)$  in equation (7.39c)). Hence, Coleman transforming the rotating lag degrees of freedom will not exactly remove periodicity from  $\mathbf{K}(\psi)$ , although it will do so for the mass and damping matrices. Given definition (7.38) of the state vector, the Coleman transformation matrix is [14]

$$\mathbf{B}(\psi) = \begin{bmatrix} 1 & c(\psi_1) & s(\psi_1) & 0 \\ 1 & c(\psi_2) & s(\psi_2) & 0 \\ 1 & c(\psi_3) & s(\psi_3) & 0 \\ 0 & 0 & 0 & 1 \end{bmatrix}, \quad (7.40)$$

and, upon transformation according to  $\mathbf{K}_{\text{MBC}}(\psi) = \mathbf{B}^{-1}(\psi)\mathbf{K}(\psi)\mathbf{B}(\psi)$ ,

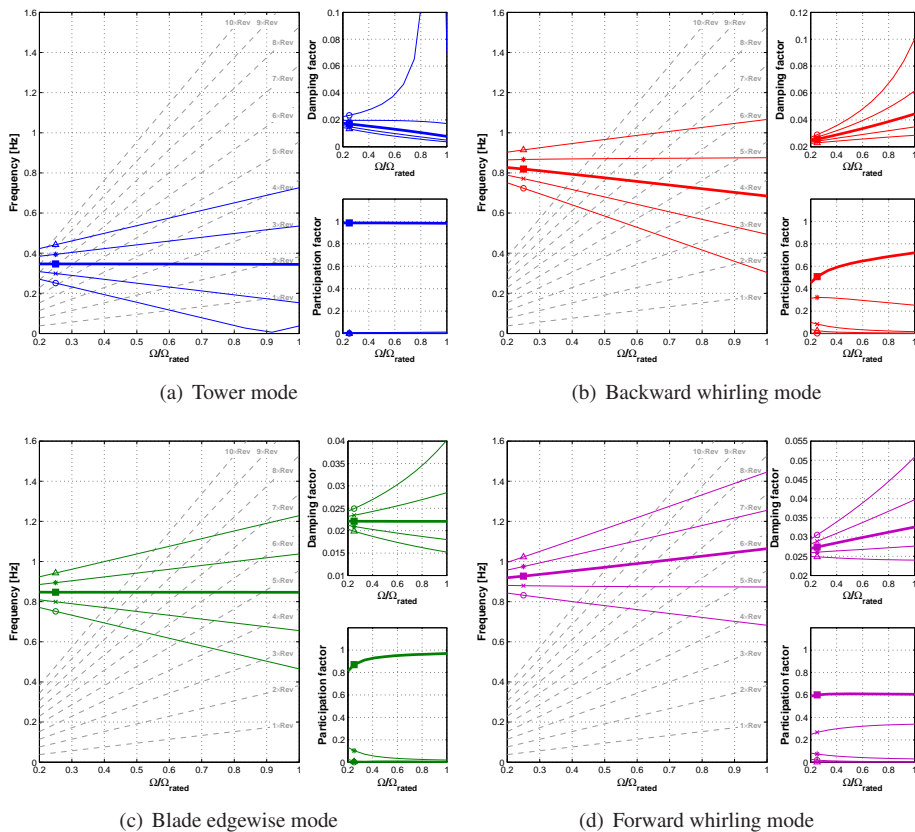
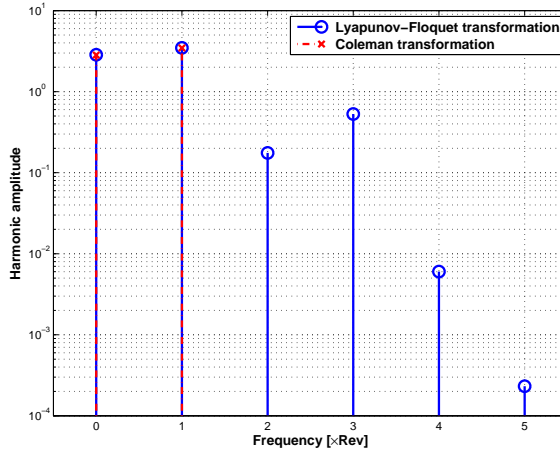


Figure 7.5: Frequencies, damping and participation factors for the rotor-tower model problem, computed at varying rotor speeds.

the resulting stiffness is

$$\mathbf{K}_{\text{MBC}}(\psi) = \begin{bmatrix} K_{e\zeta} & \frac{g S_b}{2} & 0 & 0 \\ g S_b & K_{e\zeta} + \frac{g S_b}{2} \mathbf{c}(3\psi_1) & \frac{g S_b}{2} \mathbf{s}(3\psi_1) & 0 \\ 0 & \frac{g S_b}{2} \mathbf{s}(3\psi_1) & K_{e\zeta} - \frac{g S_b}{2} \mathbf{c}(3\psi_1) & 0 \\ 0 & \frac{2}{3} \Omega^2 S_b & 0 & K_c \end{bmatrix}. \quad (7.41)$$

As expected, the transformed matrix exhibits a remaining periodicity at 3 per-rev due to the presence of gravity. Figure 7.6 shows the Frobenius norm of the amplitude of the first harmonics of the Lyapunov-Floquet and Coleman transformations. Among the infinite possible Lyapunov-Floquet transformations, we chose the one that is more similar to the Coleman one. To make this possible, one must set in Eq. 7.15 the initial condition of the periodic eigenvector equal to the initial condition of the Coleman transformation,  $\mathbf{P}(0) = \mathbf{B}(0)$ . The figure shows very clearly that the Coleman transformation approximates well the constant and the one per-rev content of the Lyapunov-Floquet transformation, while it completely neglects all higher frequencies.



**Figure 7.6:** Frobenius norm of the amplitude of the first harmonics of the Lyapunov-Floquet (circle marks) and of the Coleman (x marks) transformations.

The dependence of the Froude number, which measures the relative weight of the aerodynamic and gravitational forces, on the inverse of a characteristic length (e.g., the rotor radius), implies that gravitational effects are

## **Chapter 7. Stability analysis of LTP systems**

---

expected to play a prominent role in future very large wind turbines. In turn, this might soon emphasize the limits of the classical Coleman-based analysis.

---

## System identification of LTP systems from input-output data

---

**I**N the previous chapter it was shown how to conduct a rigorous stability analysis of LTP systems. In this section, we show how to build a discrete-time state-space LTP model from a sequence of  $N$  measurements, restricting the discussion to the single-input/single-output (SISO) case. This result is obtained in two steps: first a PARMAX input-output model is identified, which is then realized in state-space form to yield the final discrete-time model used for stability analysis.

Three different models are considered: the PARX model, (also noted as periodic equation-error model), the output-error and the PARMAX. Notice that equation-error and output-error can be viewed as two particular cases of the PARMAX model. The basic method for identifying such these models is the Prediction Error Method (PEM), [81].

Of course the identification and the analysis of periodic models is not new in literature. The study of several seasonal phenomena, as for example those related to hydrology, [87–90], electrical consumption, [91–93], climatology, [94], econometrics, [95], leads to the identification of periodic time series.

Moreover periodic models are largely used to the analysis and control of rotating systems, such that rotorcrafts and wind turbines, for example, the equation-error method was used in reference [96] for the identification of a PARX model of a helicopter rotor.

On the other hand, the output-error method [23, 80] was used in reference [74] to identify a PARX model from transient responses of a wind turbine. The output-error method has superior statistical characteristics since it allows to consider opportunely the presence of measurement noise, but necessitates of a non-linear iteration for its solution. To ease its convergence, the equation-error method is often used to generate a suitable initial guess for the non-linear solve. The equation and the output-error methods are briefly reviewed in the following in the context of the present PARX identification problem, Sections 8.1.1 and 8.1.2

Both these approaches could be able to characterize the response of a wind turbine, but their application must be restricted to systems subjected to deterministic inputs since their structure does not consider the presence of a process noise. This limitation could be restrictive if one tries to estimate a model from a turbine operating in a real environment, where the effects of wind turbulence can be important. To this reason, Section 8.1.3 is dedicated to the identification of PARMAX sequences, which is a model more adequate in describing the properties of the noise term.

## **8.1 Identification using the prediction error method (PEM)**

---

Consider a measure of a generic output of the system  $z$  and an input  $u$ , sampled at a constant rate  $\Delta t$  and note  $z(k)$  and  $u(k)$  respectively the measure the output and the input at a generic time instant  $k\Delta t$ , with  $k = 1, 2, \dots, N$  and  $N$  the number of samples.

Suppose then that the dynamics of  $z(k)$  is dictated by the Periodic Auto-Regressive Moving Average with eXogenous input sequence of period  $K$ ,

$$z(k) = \sum_{i=1}^{n_a} a_i(k)z(k-i) + \sum_{j=0}^{n_b} b_j(k)u(k-j) + \sum_{w=1}^{n_c} c_w(k)\eta(k-w) + \eta(k), \quad (8.1)$$

where  $a_i(k) = a_i(k + K)$ ,  $b_j(k) = b_j(k + K)$  and  $c_w(k) = c_w(k + K)$  are respectively the periodic coefficients of the Auto-Regressive (AR), of the eXogenous (X) and of the Moving Average (MA) part, and  $\eta(k)$  is the process noise supposed to be white, gaussian and with periodic variance  $\sigma(k)^2$ .

According to Ref. [97, 98], the optimal one-step ahead predictor of system (8.1) is

$$\begin{aligned} \hat{z}(k|k-1) = & - \sum_{i=1}^n (c_i(k)) \hat{z}(k-i|k-i-1) + \\ & + \sum_{i=1}^n (a_i(k) + c_i(k)) z(k-i) + \sum_{i=1}^n b_i(k) u(k-i), \end{aligned} \quad (8.2)$$

where  $\hat{z}(v|v-1)$  is the prediction of the measure at time  $v$ ,  $z(v)$ , from the knowledge of all data till time step  $v-1$ , and  $n = \max(n_a, n_b, n_c)$  is the order of the system. Since in this work, only one-step-ahead predictor are considered, to simplify the notation we drop the second time index when defining any predicted variables, thus  $\hat{z}(v) = \hat{z}(v|v-1)$ .

Now the estimation problem is simply formalized according to PEM: the identification problem is the one of finding the periodic coefficients  $a_i(k)$ ,  $b_i(k)$  and  $c_i(k)$  which minimize the cost function  $J$  defined as the mean value of the square of the prediction error

$$J = \frac{1}{N} \sum_{k=1}^N (\epsilon(k))^2 \quad (8.3)$$

where  $\epsilon(k)$  is the prediction error at time instant  $k$  defined as

$$\epsilon(k) = z(k) - \hat{z}(k). \quad (8.4)$$

The Equation (8.2) could be specialize on the basis of the particular model, leading to the different identification methods for equation error, output error and PARMAX.

### 8.1.1 Equation-error identification of LTP systems

In the equation-error approach, output measures  $z(k)$  are assumed to obey the PARX sequence,

$$z(k) = \sum_{i=1}^{n_a} a_i(k) z(k-i) + \sum_{j=0}^{n_b} b_j(k) u(k-j) + \eta(k), \quad (8.5)$$

which is obtained from (8.1) by fixing to the null value all the  $c_l$  coefficients, i.e. by neglecting the MA part. The unknowns to-be-estimated are then the periodic coefficients  $a_i(k)$  and  $b_j(k)$ . The lack of the MA part greatly

simplify the estimation because the predictor

$$\hat{z}(k) = \sum_{i=1}^n a_i(k)z(k-i) + \sum_{i=1}^n b_i(k)u(k-i), \quad (8.6)$$

becomes linear in the parameters and the identification problem involves the solution of a linear regression, as explained in detail in the following.

First, to reduce the number of unknowns, the periodic coefficients  $a_i(k)$  and  $b_j(k)$  can be approximated by using truncated Fourier expansions, i.e.

$$a_i(k) = a_{i0} + \sum_{l=1}^{N_{F_a}} (a_{il}^c \cos(l\psi(k)) + a_{il}^s \sin(l\psi(k))), \quad (8.7a)$$

$$b_j(k) = b_{j0} + \sum_{m=1}^{N_{F_b}} (b_{jm}^c \cos(m\psi(k)) + b_{jm}^s \sin(m\psi(k))). \quad (8.7b)$$

The unknown coefficients  $a_{i0}$ ,  $a_{il}^c$ ,  $a_{il}^s$ ,  $b_{j0}$ ,  $b_{jm}^c$  and  $b_{jm}^s$  are collected in a vector of parameters  $\mathbf{p}$  to be identified:

$$\mathbf{p} = (\dots, a_{i0}, a_{il}^c, a_{il}^s, \dots, b_{j0}, b_{jm}^c, b_{jm}^s, \dots)^T, \quad (8.8)$$

where  $i = (1, \dots, n_a)$ ,  $j = (1, \dots, n_b)$ ,  $l = (1, \dots, N_{F_a})$  and  $m = (1, \dots, N_{F_b})$ .

Define now the row vectors

$$\varphi_a(\psi(k)) = [1, \cos(\psi(k)), \dots, \cos(N_{F_a}\psi(k)), \sin(\psi(k)), \dots, \sin(N_{F_a}\psi(k))], \quad (8.9a)$$

$$\varphi_b(\psi(k)) = [1, \cos(\psi(k)), \dots, \cos(N_{F_b}\psi(k)), \sin(\psi(k)), \dots, \sin(N_{F_b}\psi(k))], \quad (8.9b)$$

and in turn

$$\mathbf{a}_{r,s} = z(r)\varphi_a(\psi(s)), \quad (8.10a)$$

$$\mathbf{b}_{r,s} = u(r)\varphi_b(\psi(s)). \quad (8.10b)$$

By writing equation (8.6) for all predicted output signals, one obtains the following overdetermined system

$$\hat{\mathbf{z}} = \mathbf{T}\mathbf{p}, \quad (8.11)$$



## 8.1. Identification using the prediction error method (PEM)

where  $\hat{z} = \{\hat{z}(q), \hat{z}(q+1), \dots, \hat{z}(N)\}^T$ ,

$$\mathbf{T} = \begin{bmatrix} \mathbf{a}_{q-1,q} & \cdots & \mathbf{a}_{q-n_a,q} & \mathbf{b}_{q,q} & \cdots & \mathbf{b}_{q-n_b,q} \\ \mathbf{a}_{q,q+1} & \cdots & \mathbf{a}_{q-n_a+1,q+1} & \mathbf{b}_{q+1,q+1} & \cdots & \mathbf{b}_{q-n_b+1,q+1} \\ \vdots & \vdots & \vdots & \vdots & \vdots & \vdots \\ \mathbf{a}_{N-1,N} & \cdots & \mathbf{a}_{N-n_a,N} & \mathbf{b}_{N,N} & \cdots & \mathbf{b}_{N-n_b,N} \end{bmatrix} \quad (8.12)$$

and  $q = \max(n_a, n_b) + 1$ .

Introducing the prediction error  $\boldsymbol{\epsilon} = \{\epsilon(q), \epsilon(q+1), \dots, \epsilon(N)\}^T$  and the measurement vector  $\mathbf{z} = \{z(q), z(q+1), \dots, z(N)\}^T$ , the following equation is derived

$$\boldsymbol{\epsilon} = \mathbf{z} - \mathbf{T}\mathbf{p} \quad (8.13)$$

The unknown vector of parameters is then readily minimizing the cost function  $J = \boldsymbol{\epsilon}^T \boldsymbol{\epsilon}$  through the pseudo-inversion of  $\mathbf{T}$  as

$$\mathbf{p} = (\mathbf{T}^T \mathbf{T})^{-1} \mathbf{T}^T \mathbf{z}. \quad (8.14)$$

### 8.1.2 Output-error identification of LTP systems

In the output-error approach, it is assumed that an error-free output signal  $y(k)$  obeys a PARX sequence

$$y(k) = \sum_{i=1}^{n_a} a_i(k)y(k-i) + \sum_{j=0}^{n_b} b_j(k)u(k-j), \quad (8.15)$$

whereas the error  $\eta(k)$  affects measures  $z(k)$ , i.e.

$$z(k) = y(k) + \eta(k). \quad (8.16)$$

The predictor of system (8.15–8.16) is

$$\hat{z}(k) = \sum_{i=1}^n a_i(k)y(k-i) + \sum_{i=1}^n b_i(k)u(k-i), \quad (8.17)$$

which is nonlinear in the parameters since the variable  $y$  depends in turn on the parameters  $\mathbf{p}$  as it is clear from Eq. (8.15).

As in the previous case, coefficients  $a_i(k)$  and  $b_i(k)$  are approximated with a suitable number of harmonics using (8.7). Then, the resulting unknown vector  $\mathbf{p}$  is computed by minimizing the sum of the square of the prediction error:

$$J = \sum_{k=1}^N (z(k) - \hat{z}(k))^2. \quad (8.18)$$

Minimization of  $J$  involves a non-linear iteration in which output  $y(k)$  is computed by solving (8.15) for  $k = \max(n_a, n_b) + 1, \dots, N$  starting from initial conditions chosen such that  $z(k) = y(k)$  for  $k = 1, \dots, \max(n_a, n_b)$ .

### 8.1.3 Identification of PARMAX model

The presence of the MA-part in the PARMAX model allows a more adequate characterization of the disturbance term with respect to that provided by the equation and output-error models, if the analyzed system is subject to a process noise. This freedom, unfortunately, reflects itself in a more complex estimation procedure.

According to the prediction error method, the predictor of the PARMAX model is

$$\hat{z}(k) = \sum_{w=1}^{n_c} c_w(k)(z(k-w) - \hat{z}(k-w)) + \sum_{i=1}^{n_a} (a_i(k))z(k-i) + \sum_{j=1}^{n_b} b_j(k)u(k-j), \quad (8.19)$$

which is non-linear in the parameters since any  $\hat{z}(k)$  is a function of its previous values  $\hat{z}(k-w)$  which in turn depend on the parameters.

Here again, the periodic unknowns  $c_w(k)$  are approximated in sine and cosine expansions as  $a_i(k)$ ,  $b_j(k)$ ,

$$c_w(k) = c_{w0} + \sum_{n=1}^{N_{Fc}} (c_{w_n}^c \cos(n\psi(k)) + c_{w_n}^s \sin(n\psi(k))), \quad (8.20)$$

and the parameter vector  $\mathbf{p}$  becomes

$$\mathbf{p} = (\dots, a_{i0}, a_{i_l}^c, a_{i_l}^s, \dots, b_{j0}, b_{j_m}^c, b_{j_m}^s, \dots, c_{w0}, c_{w_n}^c, c_{w_n}^s, \dots)^T, \quad (8.21)$$

where  $i = (1, \dots, n_a)$ ,  $j = (1, \dots, n_b)$ ,  $w = (1, \dots, n_c)$   $l = (1, \dots, N_{Fa})$ ,  $m = (1, \dots, N_{Fb})$ , and  $n = (1, \dots, N_{Fc})$ . Then,  $\mathbf{p}$  is estimated minimizing iteratively the sum of the square of the prediction error  $\epsilon(k) = z(k) - \hat{z}(k)$ .

Moreover, looking at the predictor (8.2), it is easy to verify that the predicted measure  $\hat{z}(k)$  obeys a PARX model, in which the unknowns  $c_w(k)$ , apart a change of sign, represent the coefficients of the periodic autoregressive part. Therefore it is possible that, during the optimization process, the coefficients  $c_w(k)$  involve an unstable predictor leading to the impossibility

---

## 8.2. Realization of the PARMAX sequence in state-space form

---

of performing effectively the identification. This happens if the parameters  $a_i(k)$  and  $c_w(k)$  describe a non-minimum phase PARMA model, i.e. a model with at least a zero which does not belong to the unit open disk, [77].

In literature there are basically three methods to overcome this problem. The first is an heuristic approach in which the coefficients  $c_w(k)$  are halved repeatedly till the achievement of a stable predictor. This method actually corresponds to a re-initialization of parameters  $c_w(k)$  with unknown effects on the convergence of the estimation. The second approach is based on the computation a new minimum phase representation of the non-minimum phase PARMA, such that the impulsive responses of both models, minimum and non-minimum, have the same autocorrelation function. This new canonical model is obtained by solving a suitable periodic Riccati equation, [97]. The third approach proposed in [98], is similar to the second but it is based on the multivariate Rissanen factorization algorithm, [99].

In the development of this work, an alternative and original method based on a constraint optimization is used: the stability of the predictor is enforced by a non-linear constraint within the estimation process and the resulting constraint optimization is performed by a Sequential Quadratic Programming (SQP) algorithm [35]. The estimation problem results then reformulated as

$$\min_{\mathbf{p}} J(z(k) - \hat{z}(k); \mathbf{p}), \quad (8.22a)$$

$$\text{s.t.: } |\mathcal{Z}(\mathbf{p})| \leq 1, \quad (8.22b)$$

where  $|\mathcal{Z}(\mathbf{p})|$  are the absolute values of the zeros of the PARMAX model defined by the unknown vector  $\mathbf{p}$ .

---

## 8.2 Realization of the PARMAX sequence in state-space form

---

For a given PARMAX coefficients a periodic realization in state-space form is necessary in order to perform the stability analysis as previously described, in Section 7.2.

In order to simplify the treatment, since the MA-part does not affect the stability of the system, only PARX models are here analyzed.

To this end, consider a discrete-time state-space system in observable canonical form

$$\mathbf{x}(k+1) = \mathbf{A}(k)\mathbf{x}(k) + \mathbf{B}(k)u(k), \quad (8.23a)$$

$$y(k) = \mathbf{C}(k)\mathbf{x}(k) + \mathbf{D}(k)u(k), \quad (8.23b)$$

where

$$\left[ \begin{array}{c|c} \mathbf{A}(k) & \mathbf{B}(k) \\ \mathbf{C}(k) & \mathbf{D}(k) \end{array} \right] = \left[ \begin{array}{cccc|cc} 0 & 0 & \dots & 0 & \alpha_n(k) & \beta_n(k) \\ 1 & 0 & \dots & 0 & \alpha_{n-1}(k) & \beta_{n-1}(k) \\ 0 & 1 & \dots & 0 & \alpha_{n-2}(k) & \beta_{n-2}(k) \\ \vdots & \ddots & \ddots & \vdots & \vdots & \vdots \\ 0 & 0 & \dots & 1 & \alpha_1(k) & \beta_1(k) \\ \hline 0 & 0 & \dots & 0 & 1 & \beta_0(k) \end{array} \right], \quad (8.24)$$

and  $\mathbf{x} = \{x_1 \ x_2 \ \dots \ x_n\}^T$

Through simple mathematical computations from (8.23a–8.24), the following sequence is derived

$$x_n(k) = x_{n-1} + \alpha_1(k-1)x_n(k-1) + \beta_1(k-1)u(k-1) \quad (8.25)$$

$$= x_{n-2}(k-2) + \alpha_2(k-2)x_n(k-2) + \alpha_1(k-1)x_n(k-1) + \beta_1(k-1)u(k-1) + \beta_2(k-2)u(k-2) \quad (8.26)$$

$$\beta_1(k-1)u(k-1) + \beta_2(k-2)u(k-2) \quad (8.27)$$

$$= \dots \quad (8.28)$$

$$x_n(k) = \sum_{i=1}^n \alpha_i(k-i)x_n(k-i) + \sum_{i=1}^n \beta_i(k-i)u(k-i). \quad (8.29)$$

From the output equation, (8.23b) and by the definition of matrix  $\mathbf{C}(k)$ , Eq. (8.30) is derived

$$y(k) = x_n(k) + \beta_0(k)u(k), \quad (8.30)$$

which leads, together with (8.25) to the input-output behaviour of system (8.23),

$$y(k) = \sum_{i=1}^n \alpha_i(k-i)y(k-i) + \sum_{i=1}^n [\beta_i(k-i) - \beta_0(k-i)\alpha_i(k-i)]u(k-i) + \beta_0(k)u(k). \quad (8.31)$$

Comparing (8.31) with (8.5), it can be easily shown that (8.23–8.24) is equivalent, i.e. it has the same impulsive response, to (8.5) if the system coefficients are chosen as follows

$$\alpha_j(k) = a_j(k+j), \quad \forall j = (1, \dots, n_a), \quad (8.32a)$$

$$\beta_0(k) = b_0(k), \quad (8.32b)$$

$$\beta_j(k) = b_j(k+j) + a_j(k+j)b_0(k), \quad \forall j = (1, \dots, n_b). \quad (8.32c)$$

---

# CHAPTER 9

---

## Results and conclusions

---

A detailed aero-elastic model of a direct-drive 6 MW wind turbine was used in this work for testing the proposed stability analysis formulation. The model, implemented with the wind turbine simulation code `Cp-Lambda` [16, 100], is based on a finite element multibody approach, using Cartesian coordinates and scaled Lagrange multipliers for the enforcement of constraints. Time marching is performed with an implicit non-linearly unconditionally stable energy decaying scheme. Blades and tower are modeled with geometrically exact beam elements, while aerodynamics is rendered by a classical blade-element momentum (BEM) model based on the annular stream-tube theory with wake swirl, including tip and hub loss models, including unsteady corrections and dynamic stall. While the implementation of a MBC-LTI approach in a code of similar complexity would be a major undertaking, we stress here again that the use of a different simulation tool other than `Cp-Lambda` would require no change to the software implementation of the proposed stability analysis procedures.

## 9.1 Rotor edgewise response

At first we consider the estimation of the level of damping of the edgewise rotor modes, which is typically quite light due to the small aerodynamic damping associated with such motions. In order to perturb the system, two edgewise force doublets were applied near the blade tip and at mid span. Amplitude and length of the doublets were tuned so as to excite a linear response of the modes of interest. The analysis was conducted in non-turbulent wind conditions, between rated rotor speed  $\Omega_r$  and  $1.33 \Omega_r$ , so as to investigate the behavior of the system in the over-speed regime.

The order of the to-be-identified reduced model was chosen according to some simple considerations. First, since the frequency content of the outputs shows three distinct peaks,  $n_a$  was set equal to 6. Second, the fact that the wind is constant allows one to identify only one coefficient,  $\beta_1(k)$ , of the exogenous part, so that  $n_b = 1$ . Furthermore, the periodicity of the coefficients was approximated with  $N_{F_a} = 1$  and  $N_{F_b} = 6$ . The number of time steps in a period and the number of periods used for the identification were chosen so as to achieve the best agreement between measures and predicted outputs.

Figure 9.1 shows a comparison between the normalized edgewise root bending moment that was measured on the simulation model (solid line) and the one predicted by the identified PARX one (dashed line), in the time (left) and frequency (right) domains, for a rotor speed equal to about  $1.13 \Omega_r$ . The plots show an excellent correlation between the quantities of the virtual plant and of the identified model. Notice that the third mode has a very short characteristic time, such that it vanishes very quickly in the first time instants after the perturbation; this is also the span of time used to compute the initial conditions. This implies that results related to the third mode do not have the same level of accuracy of the first and second modes. For this same operating condition, Table 9.1 reports the frequency, damping and participation factors of the lowest five harmonics for the first and second edgewise fans of modes.

Figure 9.2 shows, for lowest edgewise fan, the normalized frequencies (scaled by the rated rotor speed), damping and participation factors as a function of rotor speed. Note the rough behavior of the participation factors, due to the fact that uncertainties propagate more in these quantities than in frequencies or damping factors.

The periodic Campbell diagram of Figure 9.2 at left shows resonant conditions around a rotor speed of  $1.15 \Omega_r$ . In fact, not only the principal frequency with the highest participation intersects the 4 per rev, but also the

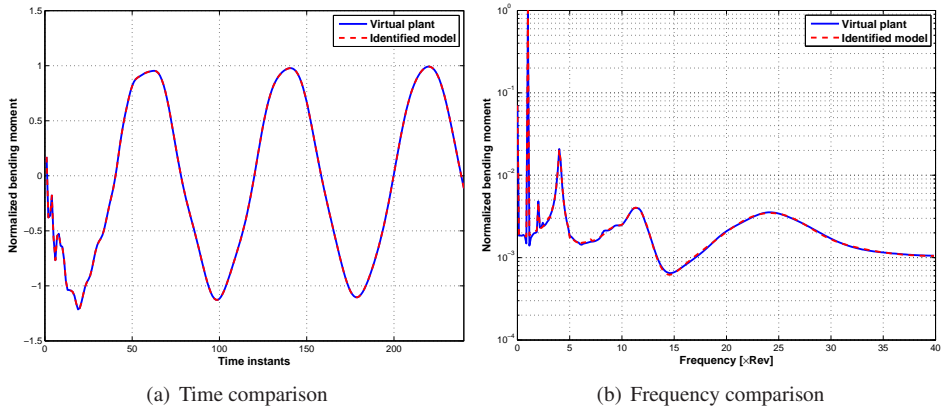


**Figure 9.1:** Comparison between measured (solid line) and predicted (dashed line) normalized blade root bending moment, in the time (left) and frequency (right) domains.

**Table 9.1:** First and second blade edgewise fans of modes.

(a) 1 <sup>st</sup> blade edgewise mode		
Frequency [ $\times$ Rev]	Damping	Participation
2.0321	0.0434	0.0114
3.0314	0.0291	0.1351
4.0311	0.0219	0.5807
5.0309	0.0175	0.1392
6.0308	0.0146	0.0013

(b) 2 <sup>nd</sup> blade edgewise mode		
Frequency [ $\times$ Rev]	Damping	Participation
9.2661	0.1137	0.0344
10.2602	0.1027	0.1839
11.2554	0.0936	0.4173
12.2514	0.0860	0.2112
13.2479	0.0796	0.0754

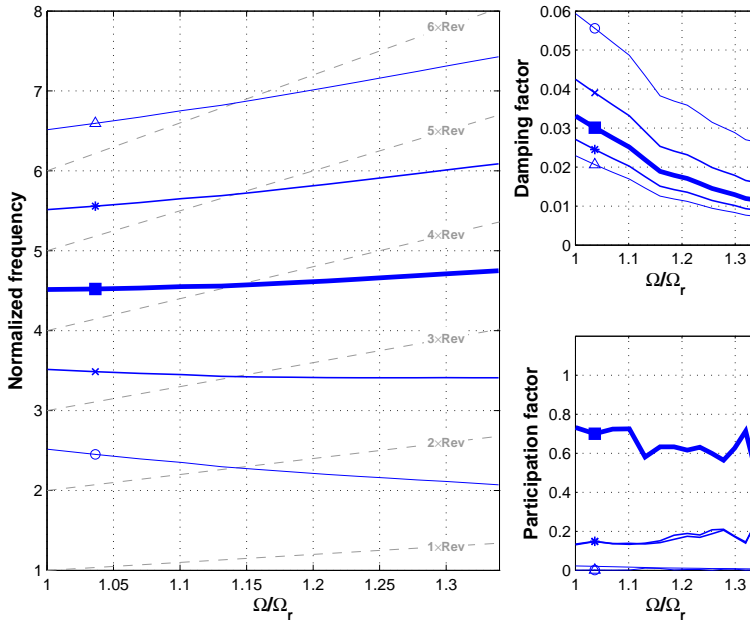


Figure 9.2: Frequencies, damping and participation factors of the first edgewise mode.

other super-harmonics intersect the per-rev excitation harmonics. These multiple resonances are in fact visible in the machine response. Figure 9.3 shows the amplitude of the harmonics of the blade root edgewise bending moment, computed in a stationary trimmed condition in constant wind, as a function of rotor speed. Notice, a part from the 4 per rev resonance, also the presence of other peaks at 2, 5 and 6 per rev, as predicted by the periodic Campbell diagram. Here again, the presence of these peaks could not be justified by a standard MBC-LTI analysis.

## 9.2 Tower side-side response

A zero-mean side-side force chirp applied at the tower top was used to perturb the machine operating in closed-loop under the effects of a steady mean wind. The time history of the blade root edgewise bending moment and tower root fore-aft and side-side bending moments were recorded from the end of the perturbing signal. In this case,  $n_a$  was set equal to 2 in order to model the presence of a single mode, and since the wind remains constant  $n_b$  equal to 1, while the Fourier truncation of the coefficients was performed with  $N_{F_a} = N_{F_b} = 5$ .

Figure 9.4 shows a comparison between the virtual plant measure and



## 9.2. Tower side-side response

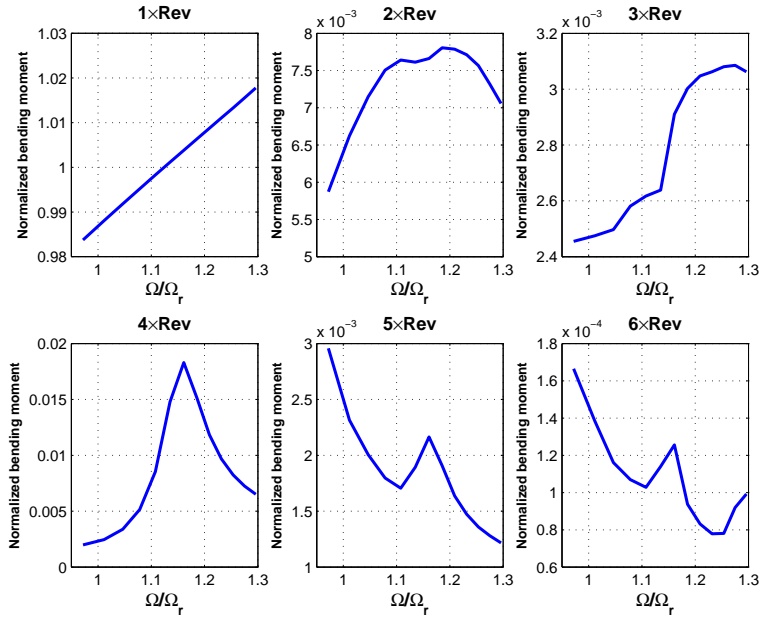


**Figure 9.3:** Amplitude of the 1 to 6 per rev edgewise blade root moment harmonics as a function of rotor speed. Values are scaled with the maximum edgewise moment at  $\Omega_r$ .

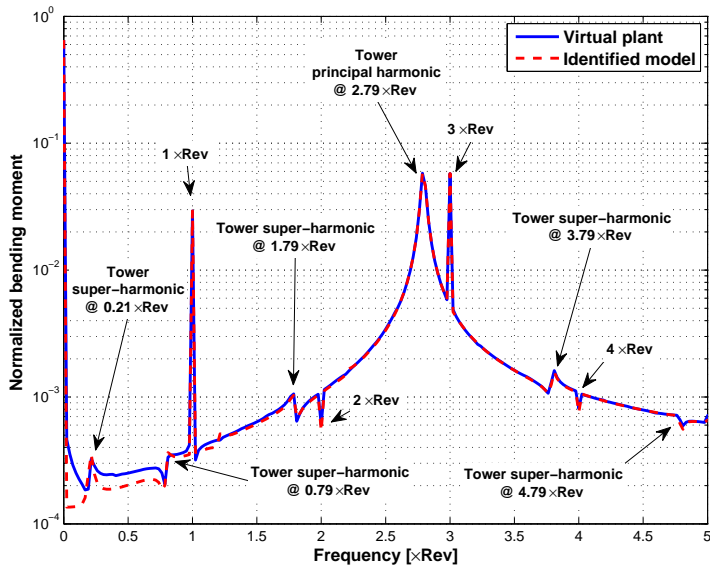


**Figure 9.4:** Comparison between measured (solid line) and predicted (dashed line) normalized tower root side-side bending moment in the frequency domain.

the identified output in the frequency domain, for the tower side-side bending moment at a wind speed of 5 m/s. Table 9.2 summarizes the results in terms of frequency, damping and participation factors for the first tower side-side fan of modes. Even if the principal tower frequency around 2.8 per rev has a participation that is close to 1, its associated super-harmonics are visible in the FFT of the response displayed in Figure 9.4.

**Table 9.2:** *First tower side-side fan of modes.*

Frequency [ $\times$ Rev]	Damping	Participation
0.2072	0.0783	0.007
0.7936	0.0204	0.004
1.7935	0.0090	0.006
2.7935	0.0058	0.964
3.7935	0.0043	0.009
4.7935	0.0034	0.002

The simplified model problem discussed previously showed that the tower super-harmonics may appear prominently in the blade response. To verify this fact with respect to the present more realistic case, we performed the identification of a new model using the blade root edgewise bending moment measurements. Figure 9.5 and Table 9.3 summarize the results. As expected from the model problem, even here the figure shows two prominent peaks related to the tower super-harmonics. Notice also, as a side note, the presence of a small peak at a frequency of about 10 per rev, which is one super-harmonic of the forward whirling in-plane fan, similarly to what can be observed for the simplified model problem in Figure 7.4(a).

Table 9.3(a) shows that, although the tower principal harmonic is not visible in the response (cf. Figure 9.5), its frequency is still correctly estimated (cf. the present value of 2.7955 with the one in Table 9.2 of 2.7935). The periodic identification is capable of assigning the two peaks related to the tower super-harmonics to a single mode fan, both having high participation factors approaching 50%, while a participation close to zero is assigned to the principal harmonic.

Comparing Tables 9.2 and 9.3(a), one can again observe the phenomenon previously illustrated with the help of the simplified model problem: the first tower side-side fan of modes has a markedly invariant character when observed through the tower response (the tower base bending in this case), while a strongly periodic one when observed through the blade response (the blade edgewise bending in this case). We further note that, due to the definition of the output in the realized state-space model of equa-

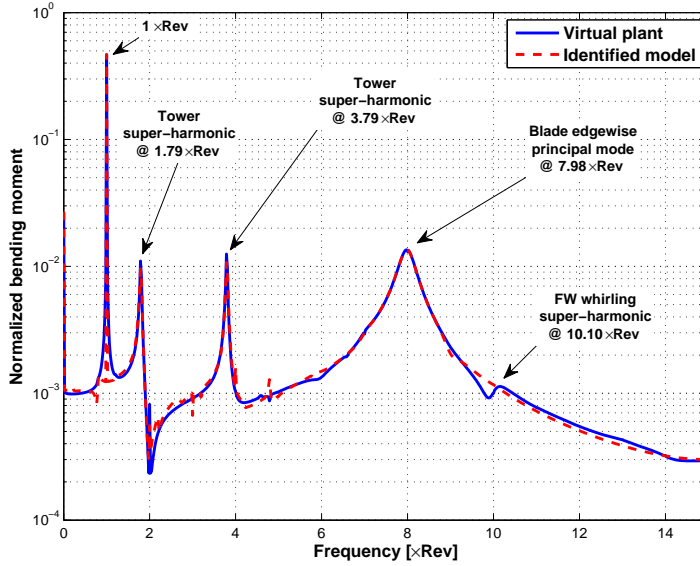


**Figure 9.5:** Comparison between measured (solid line) and predicted (dashed line) normalized blade root edgewise bending moment in the frequency domain.

**Table 9.3:** Side-side tower and blade edgewise fans of modes.

(a) 1 <sup>st</sup> tower side-side mode		
Frequency [ $\times$ Rev]	Damping	Participation
0.7957	0.0283	0.0243
1.7955	0.0125	0.3557
2.7955	0.0080	0.0901
3.7955	0.0059	0.4319
4.7954	0.0047	0.0685
(b) 1 <sup>st</sup> blade edgewise mode		
Frequency [ $\times$ Rev]	Damping	Participation
5.9900	0.0343	0.0015
6.9895	0.0294	0.0899
7.9891	0.0257	0.7872
8.9888	0.0229	0.0985
9.9885	0.0206	0.0021

tions (8.23–8.24), modal participation factors computed from the identification and realization of a PARX model are automatically output-specific.

### 9.3 Tower fore-aft and in-plane whirling response

---

Due to the coupling between fore-aft and side-side tower modes, the backward and forward in-plane whirling modes are visible in both the fore-aft and side-side tower root moments. In this work the in-plane whirling modes were identified from the fore-aft moment, since the response in the side-side direction is dominated by the very low damped side-side tower mode.

The two backward and forward whirling modes are separated in frequency by about  $2 \Omega$ . This fact may have an effect on the identification process, because different modes separated by multiples of the rotor frequency could be interpreted as different super-harmonics of the same fan of modes. To overcome this issue, an invariant model, obtained by simply setting  $N_{Fa} = 0$ , was fitted to the measures. The resulting model, which necessarily considers the backward and forward whirlings as two distinct modes since it is blind to the presence of fans, was then used as the initial guess for the identification of the periodic model.

Results of the identification conducted in this way are shown for a uniform wind condition at 5 m/s in Figure 9.6 and Table 9.4. The identified model matches well the response of the system, although there are minor spurious oscillations.

### 9.4 The periodic Campbell diagram

---

The previously identified fans of modes are collected in the partial periodic Campbell diagram shown in Figure 9.7. The figure shows the principal harmonic (thick solid line) and four super-harmonics (thin solid lines) for the first tower fore-aft, backward in-plane whirling, blade edgewise and forward in-plane whirling fans of modes. The per-rev excitation harmonics are reported as grey dashed lines emanating from the origin of the plot. For better readability, the plot is repeated four times, one for each fan of modes. Each plot reports in color solid lines the harmonics of one specific fan. A complete Campbell diagram should also report other relevant fans of modes, as the first tower side-side, blade flap, out-of-plane whirling modes, etc., which however were not reported here for the sake of simplicity.

This plot should highlight once again that the full picture of the possible resonant conditions emerging from a periodic analysis is much richer than the one obtained by classical means. This scenario is further complicated

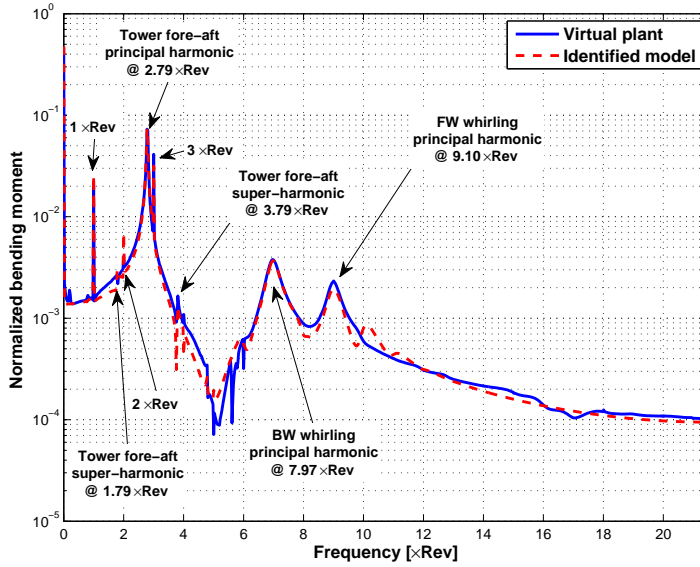


**Figure 9.6:** Comparison between measured (solid line) and predicted (dashed line) normalized tower root fore-aft bending moment in the frequency domain.

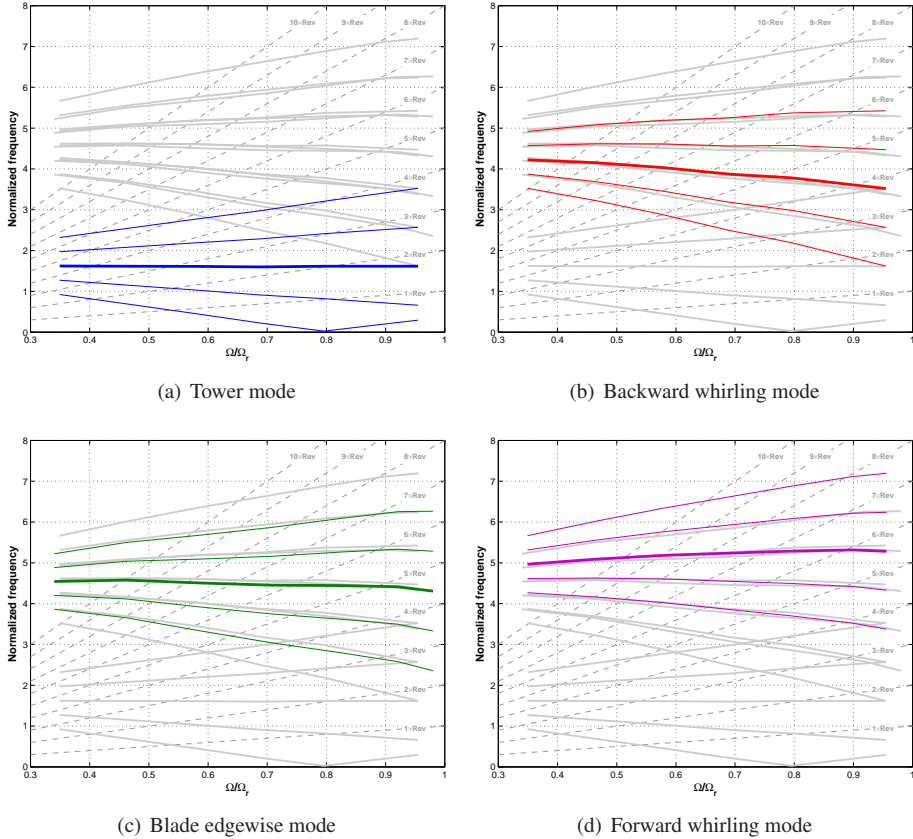
**Table 9.4:** First tower fore-aft and in-plane whirling fans of modes.

(a) 1 <sup>st</sup> tower fore-aft mode			(b) Backward in-plane whirling		
Freq [xRev]	Damping	Participation	Freq [xRev]	Damping	Participation
0.7858	0.0268	0.0008	4.9760	0.0394	0.0034
1.7856	0.0118	0.0675	5.9754	0.0328	0.0541
2.7856	0.0075	0.8691	6.9749	0.0281	0.5624
3.7855	0.0056	0.0607	7.9746	0.0246	0.1178
4.7855	0.0044	0.0014	8.9743	0.0218	0.1899

(c) Forward in-plane whirling		
Freq [xRev]	Damping	Participation
7.1021	0.0336	0.0583
8.1016	0.0295	0.1577
9.1012	0.0262	0.5758
10.1009	0.0236	0.1651
11.1007	0.0215	0.0306

by the fact that the same harmonic can have a high or low participation factor depending on the specific output considered, something that is difficult to synthesize in one single diagram as the one shown here.



**Figure 9.7:** Periodic Campbell diagram of the comprehensive multibody model of a 6 MW wind turbine.

## 9.5 Real wind turbines: the effect of turbulence

### 9.5.1 First blade edgewise mode

In order to identify the first blade edgewise mode from a more realistic scenario, the  $C_p$ - $\Lambda$  model of the 6MW wind turbine, in closed loop, was used also to perform simulations of the system in several different wind conditions from 3 to 9 m/s. All the simulations consider also an exponential model of the wind shear layer, with exponent equal to 0.2, as well as a wind

turbulence of category C, (about 10% of intensity).

To perturb the turbine in order to excite the edgewise modes, two edge-wise force doublets were applied near the blade tip and at mid span, as just described in 9.1.

The blade root bending moment edgewise was recorded from the end of the perturbation for a suitable number of rotor revolutions. To perform the identifications, the average values of wind speed and rotor speed are used.

The wind speed is considered as the sum of its mean value and the turbulence modeled as a process noise. The PARMAX models were chosen for identifying a model of the blade edgewise modes according to the PEM algorithm described in Section 8.1.3.

By means of a trial and error approach the complexity of the model was selected as  $N_a = 6$ ,  $N_b = 1$ ,  $N_c = 2$ ,  $N_{F_a} = 1$ ,  $N_{F_b} = 1$  and  $N_{F_c} = 0$ . Notice that the MA-part was considered not periodic ( $N_{F_c} = 0$ ) because actually there are no physical reasons to justify a periodic behavior (with the same period of the turbine) of the turbulence.

Figure 9.8 shows the comparison between the blade root bending moment edgewise measured and predicted with the identified PARMAX model in time domain (at left) and in frequency (at right), for a mean wind speed equal to 8 m/s. The goodness of the identification is proved by the excellent correlation achieved.

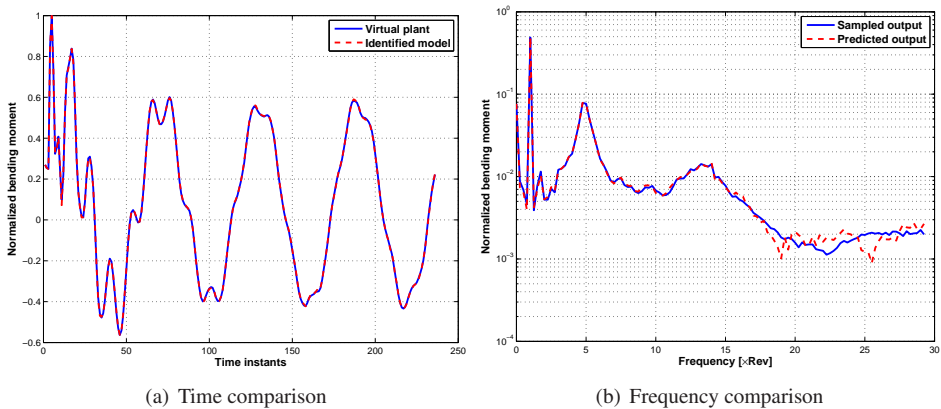


**Figure 9.8:** Comparison between measured (solid line) and predicted with PARMAX model (dashed line) normalized blade root bending moment, in the time (left) and frequency (right) domains.

The results of the stability analysis of the identified model, in term of frequencies, damping and participation factors of the first blade edgewise mode, are also reported in the Table 9.5.

Table 9.5: First blade edgewise fan of modes.

Frequency [ $\times$ Rev]	Damping	Participation
2.8770	0.0638	0.0110
3.8755	0.0474	0.2067
4.8746	0.0377	0.5442
5.8740	0.0313	0.2237
6.8736	0.0267	0.0087

Finally, the periodic Campbell diagram related to first blade edgewise fan of modes, obtained from transient responses of the turbines in turbulent wind by means of the PARMAX identification is shown in Figure 9.9.

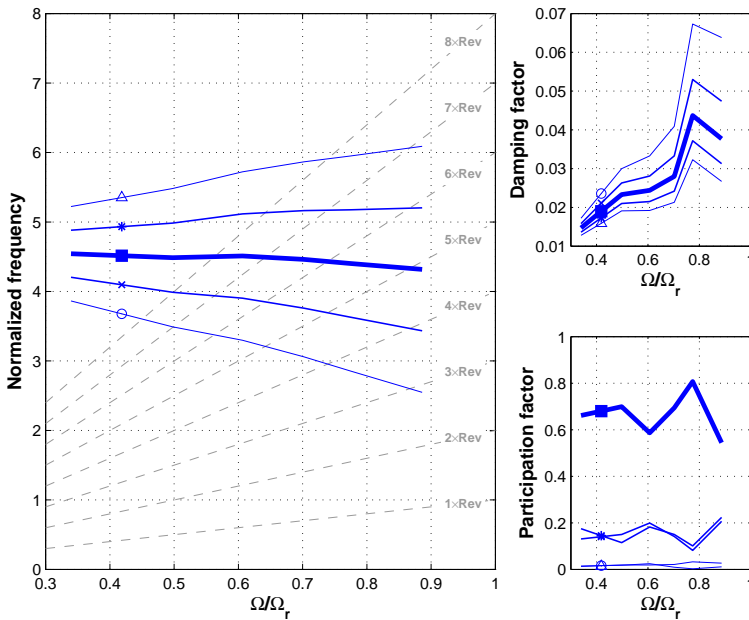


Figure 9.9: Frequencies, damping and participation factors of the first edgewise mode identified with PARMAX model.

## 9.6 Conclusions

In this work we have presented a new method for the stability analysis of wind turbines, that is based on the identification of a LTP reduced model that best fits a transient response of the system. Once the model has been identified, stability is assessed using the theory of Floquet for periodic systems.



Based on the results of this study, the following consideration can be drawn:

- The proposed method, since it operates on the bases of input-output sequences, is applicable to models of arbitrary complexity, as well as to arbitrary system (wind turbines, helicopters, etc.).
- Floquet theory shows that a single frequency is not sufficient to fully characterize a periodic mode, because in reality several multi-harmonics participate in the response of the system and each of them may resonate with the per rev excitations. The presence of these additional harmonics, that was shown to appear in the spectra of simplified model problems as well as more realistic wind turbine models, can not be explained by the widespread simplified approaches in current use.
- The use of the participation factor allows one to measure how periodically (or invariantly) a specific fan behaves. This concept also clarifies the issue of the apparent indetermination of characteristic exponents, which was a major source of confusion in the literature when it was tried to characterize a periodic mode with a single frequency.
- For the examples studied herein, it appears possible to identify reduced models of excellent quality, i.e. that produce outputs very close to the measured ones. For other common problems in system identification one has to guarantee the generality of the identified model, i.e. its ability to approximate also situations that are not in the identification data set. In the present application this is not necessary, and this greatly simplifies the problem of obtaining good quality reduced models, which in turn helps in obtaining good quality results from the stability analysis.
- The possibility of performing the proposed stability analysis of a real wind turbine was also explored, by simulating a real scenario in which the wind turbine operates in turbulent wind conditions. In such these conditions PARMAX models are identified instead of the simpler PARX, which are not adequate to consider turbulence as a process noise. The achieved results show a good quality of identified models and, consequently, accurate estimations of frequencies, damping and participation factors.
- An original procedure to estimate PARMAX model was also proposed: the minimization involved by the identification process is

viewed as a constraint optimization in which the stability of the PAR-MAX predictor is accounted as a nonlinear constraint. The optimization is then performed using a sequential quadratic programming (SQP) method. The proposed algorithm works as well as others proposed in literature, in which the stability of the predictor is guaranteed by projection methods based on the periodic Riccati equation or on the Rissanen factorization.

The present study can be improved and expanded in a few directions.

In terms of improvements, the most important might be the use of multiple outputs, as opposed to the single output used here. In fact, it was shown how super-harmonics could manifest themselves in different ways for different signals, as shown by the case of the tower super-harmonics that were inconspicuous in the tower loads but showed prominently in the blade ones. Furthermore, this means that one has to identify different models for different modes and has to pick the best signal for each, which complicates the process. The use of many outputs in the identification process could significantly simplify this aspect.

In terms of expansions of the proposed approach, the application to real wind turbines operating in the real environment must be studied more accurately, in order to understand if adequate estimations could be achieved also in presence of higher levels of turbulence with respect to those used in this work. According to the procedure described in this work, a suitable experimentation on real turbines requires at least the possibilities of perturbing the machines with an external impulsive forces, which can be reproduced in practice by a pyrotechnic loads, but of course it could be interesting to explore the possibility of performing the identification without external forces, using only the turbulence to excite the modes of interest of the turbine. Regarding the measurements, at the current state of the research, it seems that blade root and tower root loads as well as wind and rotor speed measurements be enough to perform the estimation of the most interesting modes.

---

# **Conclusions and outlook**



---

## System identification in the next future developments of wind turbine engineering

---

**F**UTURE improvements of wind turbines cannot be done without adequate developments of the supporting technologies. This is clearly visible looking at the fact that the current trend in wind turbine engineering is that of building bigger turbines for the off-shore environments.

The opportunities of the off-shore wind are great for two basic reasons. Off-shore wind first is a huge available resource and second, but not less important, it can relieve all the issues concerning the acceptability of large wind turbines, as precisely summarized in the acronym NIMBY (*Not In My Back Yard*). At least for the author's opinion, exploiting the off-shore resources appears to be mainly the way to go in order to make the wind energy can contribute more significantly to solve the energy problem in the global context.

On the other hand, the growth of dimensions of turbines leads irretrievably to an increasing of the cost of energy, if the up-scaling is performed without introducing innovative technologies, e.g. smart flexible blades, new control laws, new strategies in supervising the wind farms, *etc.* . . . , to significant technological problems (logistics and maintenance), and finally to the need of more sophisticated design methods, which could opportunely consider the hydro-aero-servo-elastic nature of the entire system.

These issues will surely stress even more the necessity of mathematical tools of analysis and validation, and consequently the importance of the system identification and of that rigorous theory on which this discipline is

based. Some interesting applications, in which this discipline can become essential in the next future, could be listed.

First, the possible use of blades with passive technology of loads alleviation, such that the bend-twist coupling, necessary to improve the performances and the life of the blades without increasing the duty cycle of the pitch actuators [101], will emphasize the need of an accurate characterization of the structural properties of blades in order to correctly capture the whole stiffness matrix. Currently, there are no works related to this important topic, which might be studied with the same tools and theory presented here. On the other hand the new advanced active control laws, such that the individual pitch control (IPC) proposed in [102], the Higher Harmonic Control (HHC) or the Receding Horizon Control (RHC) [103–105], need, in addition to an adequate structural model, also an accurate characterization of the rotor aerodynamic properties. The identification of blade aerodynamic properties can become a basic tool to use for obtaining a suitable rotor model and consequently for allowing the design of model-based control laws, which of course, without a validated aerodynamics, would have few possibilities of performing correctly in a real environment, as also notice in [103]. The identification of aerodynamic properties from wind tunnel data have performed very well, but the interesting and important extension to field data must be still studied accurately.

A second important application of the tools described in this work concerns again the advanced control of wind turbines. A periodic framework can be used to formulate many advanced controllers such that the Periodic Linear Quadratic Regulator [106] or the HHC and IPC [107, 108]. Currently there exist no studies related to the stability of the coupled systems wind turbine-HHC/IPC although the use of such controllers is extensively treated in literature. We can expect that in the next future this issue would surely emphasizes the importance of having rigorous tools for performing periodic stability analysis. Moreover, it's not so daring to foresee that the design of more complex machines, floating turbines or rotors which contemplate technologies of passive reduction of loads (e.g. the bend-twist coupling), will stress further the need of model-independent and rigorous stability analysis approach and possibly its introduction in automatic procedures of aero-structural turbine design.

All the tools developed in this thesis can be used for both the over mentioned applications, but of course many other possible uses of the system identification in wind turbine engineering could be found. Among the possible applications it is proper to mention the health monitoring [109] and the estimation of yaw misalignment [110] and the estimation of simple re-

duced model for tuning and optimizing the control laws [111, 112].





---

---

## Bibliography

---

- [1] L. Ljung. Perspectives on system identification. In *In Plenary talk at the Proceedings of the 17<sup>th</sup> IFAC World Congress*, Seoul, South Korea, 2008.
- [2] K. Christodoulou, E. Ntotsios, C. Papadimitriou, and P. Panetsos. Structural model updating and prediction variability using pareto optimal models. *Computer Methods in Applied Mechanics and Engineering*, 198:138–149, 2008.
- [3] Y. Haralampidis, C. Papadimitriou, and Pavlidou M. Multi-objective framework for structural model identification. *Earthquake Engineering and Structural Dynamics*, 34:665–685, 2005.
- [4] S.V. Modak, T.K. Kundra, and B.C. Nakra. Model updating using constrained optimization. *Mechanics Research Communications*, 27(5):543–555, 2000.
- [5] P.S. Veers, D.L. Laird, T.G. Carne, and M.J. Sagartz. Estimation of uncertain material parameters using modal test data. In *ASME/AIAA 1998 Wind Energy Symposium*, Reno, NV, USA., January 1998.
- [6] J.J. Corrigan and Shilling J.J. Empirical model for stall delay due to rotation. In *Proceedings of the American Helicopter Society Aeromechanics Specialists Conference*, San Francisco, CA, January 1994.
- [7] P.K. Chaviaropoulos and M.O.L Hansen. Investigating three-dimensional and rotational effects on wind turbine blades by means of a quasi-3d navier stokes solver. *Journal of Fluids Engineering*, 122(2):330–336, 2000.
- [8] C. Bak, J. Johansen, and P.B. Anderson. Three-dimensional corrections of airfoil characteristics based on pressure distributions. In *Proceedings of the European Wind Energy Conference*, Athens, Greece, February-March 2006.
- [9] J. Johansen and N.N. Sørensen. Airfoil characteristics from 3d cfd rotor computations. *Wind Energy*, 7(4):283–294, 2004.
- [10] F. Cadei. Analisi rans cfd di aerogeneratori in supporto al progetto ed alla sperimentazione in galleria del vento. Master's thesis, Politecnico di Milano, 2011. In Italian.
- [11] C. Bak, P. Fuglsang, N.N. Sørensen, H.A. Madsen, W.Z. Shen, and J.N. Sørensen. Airfoil characteristic for wind turbiens. Technical Report Risø-R-1065(EN), RisøNational Laboratory, Roskilde, Denmark, March 1999.

## Bibliography

---

- [12] M.O.L. Hansen, Sørensen J.N., Voutsinas S., N. Sørensen, and Madsen H.A. State of the art in wind turbine aerodynamics and aeroelasticity. *Progress in Aerospace Sciences*, 42(4):285–330, 2006.
- [13] R.P. Coleman and A.M. Feingold. Theory of self-excited mechanical oscillations of helicopter rotors with hinged blades. Technical report, NACA Report TN 1351, 1958.
- [14] P.F. Skjoldan and M.H. Hansen. Implicit floquet analysis of wind turbines using tangent matrices of a non-linear aeroelastic code. *Wind Energy*, 15(2):275–287, 2012.
- [15] P.F. Skjoldan and M.H. Hansen. On the similarity of the coleman and lyapunov-floquet transformation for modal analysis of blade rotor structures. *Journal of Sound and Vibration*, 327(3–5):424–439, 2009.
- [16] C.L. Bottasso and A. Croce. Cp-lambda: User’s manual. Technical report, Dipartimento di Ingegneria Aerospaziale, Politecnico di Milano, 2006–2012.
- [17] M.I. Friswell and J.E. Mottershead. *Finite Element Model Updating in Structural Dynamics*. Kluwer Academic Publishers, 1995.
- [18] R.V. Jategaonkar. *Flight Vehicle System Identification: a Time Domain Methodology*, volume 216. AIAA, Progress in Astronautics and Aeronautics, Reston, VA, USA, 2006.
- [19] G. Kerschen, K. Worden, A.F. Vakakis, and J.-C. Golinval. Past, present and future of nonlinear system identification in structural dynamics. *Mechanical Systems and Signal Processing*, 20:505–592, 2006.
- [20] A.D. Wright, N.D. Kelley, and R.M. Osgood. Validation of a model for a two-bladed flexible rotor system: Progress to date. Technical Report NREL/CP-500-25514, National Renewable Energy Wind Laboratory (NREL), 1617 Cole Boulevard, Golden, Colorado 80401-3393, November 1998. Presented also at AIAA/ASME Wind Energy Symposium. Reno, Nevada. January 11–14 1999.
- [21] C.L. Bottasso, A. Croce, B. Savini, W. Sirchi, and L. Trainelli. Aero-servo-elastic modeling and control of wind turbines using finite element multibody procedures. *Multibody Systems Dynamics*, 16:291–308, 2006.
- [22] D.A. Peters and C.J. He. Finite state induced flow models. part ii: Three-dimensional rotor disk. *Journal of Aircraft*, 32:323–333, 1995.
- [23] V. Klein and A. Morelli. *Aircraft System Identification, Theory and Practice*. AIAA, Reston, VA, USA,, 2006.
- [24] R. Waiboer. *Dynamic Modelling, Identification and Simulation of Industrial Robots— for off-line programming of robotised laser welding*. PhD thesis, Netherlands Institute for Metals Research in the Netherlands, 2007.
- [25] O. Bauchau. *Flexible Multibody Dynamics*, volume 176 of *Solid Mechanics and its Applications*. Springer Verlag, 2011.
- [26] M. Morandini, M. Chierichetti, and P. Mantegazza. Characteristic behavior of prismatic anisotropic beam via generalized eigenvectors. *International Journal of Solids and Structures*, 47:1327–1337, 2010.
- [27] G.L. Ghiringhelli and P. Mantegazza. Linear, straight and untwisted anisotropic beam section properties from solid finite elements. *Composites Engineering*, 4:1225–1239, 1994.
- [28] D.J. Malcolm and D. Laird. Modeling of blades as equivalent beams for aeroelastic analysis. In *ASME/AIAA Wind Energy Symposium*, Reno, NV, USA, January 2003.

- [29] M. Nielsen, F.M. Jensen, P.H. Nielsen, P. Berring, K. Martyniuk, A. Roczek, T. Sieradzan, V. Roudnitski, P. Kucio, R. Bitsche, P. Andreasen, T. Lukassen, Z. Andrlová, K. Branner, C. Bak, B. Kallesøe, M. McGugan, and C. Bak. Full scale test of ssp 34m blade, edgewise loading ltt. data report 1. Technical Report Risø-R-1718(EN), Risø National Laboratory, Denmark, 2010.
- [30] G.C. Larsen, M.H. Hansen, A. Baumgart, and I. Carlén. Modal analysis of wind turbine blades. Technical Report Risø-R-1181(EN), Risø National Laboratory, Denmark, 2002.
- [31] J. Paquette, J. van Dam, and S. Hughes. Structural testing of 9m carbon fiber wind turbine research blades. In *AIAA 2007 Wind Energy Symposium*, Reno, NV, USA, January 2007.
- [32] F.M. Jensen, B.G. Falzon, J. Ankersen, and H. Stang. Structural testing and numerical simulation of a 34m composite wind turbine blade. *Composite Structures*, 76:52–61, 2006.
- [33] G. Kerschen, K. Worden, A.F. Vakakis, and J.C. Golinval. Past, present and future of nonlinear system identification in structural dynamics. *Mechanical Systems and Signal Processing*, 20:505–592, 2006.
- [34] G.I. Schuëller and H.A. Jensen. Computational methods in optimization considering uncertainties. *Computer Methods in Applied Mechanics and Engineering*, 198:2–13, 2008.
- [35] A. Barclay, P.E. Gill, and J.B. Rosen. Sqp methods and their application to numerical optimal control. Technical Report Report NA 97–3, Department of Mathematics, University of California, San Diego, CA, USA, 1997.
- [36] G.C. Larsen and A. Kretz. Experimental determination of structural properties by non-destructive methods. In *European Wind Energy Conference 1994*, Thessaloniki, Greece, October 1994.
- [37] D.T. Griffith, J.A. Paquette, , and T.G. Carne. Development of validated blade structural models. In *46th AIAA Aerospace Sciences Meeting and Exhibit*, Reno, NV, USA, January 2008.
- [38] D.T. Griffith. Structural dynamics analysis and model validation of wind turbine structures. In *50th AIAA Structures, Structural Dynamics, and Materials Conference*, Palm Springs, CA, USA, May 2009.
- [39] D.T. Griffith and T.G. Carne. Experimental modal analysis of 9-meter research-sized wind turbine blades. In *28th International Modal Analysis Conference*, Jacksonville, FL, USA, February 2010.
- [40] C.L. Bottasso, S. Cacciola, and A. Croce. Estimation of blade structural properties from experimental data. *Wind Energy*, 2012. In press. Available online.
- [41] J. Renegar. *A Mathematical View of Interior Point Methods in Convex Optimization*. SIAM, 2001.
- [42] R.B. Nelson. Simplified calculation of eigenvector derivatives. *AIAA Journal*, 14:1201–1205, 1976.
- [43] J. Jonkman, S. Butterfield, W. Musial, and G. Scott. Definition of a 5-mw reference wind turbine for offshore system development. Technical Report NREL/TP-500-38060, National Renewable Energy Laboratory, Golden, CO, USA, 2007.
- [44] Leica Geosystems AG. Heinrich Wild Strasse, CH-9435 Heerbrugg, St. Gallen, Switzerland. <http://www.leica-geosystems.com>.
- [45] D.T. Griffith, P.S. Hunter, D.W. Kelton, T.G. Carne, and J.A. Paquette. Boundary condition considerations for validation of wind turbine blade structural models. In *Society for Experimental Mechanics Annual Conference*, Albuquerque, NM, USA, June 2009.

## Bibliography

---

- [46] O.A. Bauchau, C.L. Bottasso, and Y.G. Nikishkov. Modeling rotorcraft dynamics with finite element multibody procedures. *Mathematics and Computer Modeling*, 33:1113–1137, 2001.
- [47] C.L. Bottasso, A. Croce, B. Savini, W. Sirchi, and L. Trainelli. Aero-servo-elastic modeling and control of wind turbines using finite element multibody procedures. *Multibody System Dynamics*, 16(3):291–308, 2006.
- [48] P. Schito. *Large Eddy Simulation of Wind Turbines: interaction with turbulent flow*. PhD thesis, Politecnico di Milano, 2011.
- [49] D. Althaus. *ProfilPolaren für den Modellflug, Band 1*. Necktar-Verlag, Vs-Villingen, 1988.
- [50] I.H. Abbott and A.E. von Doenhoff. *Theory of Wing Sections: Including a Summary of Airfoil Data*. Dover Publication, Inc., 31 East 2nd Street, Mineola, N.Y. 11501, 1959.
- [51] M. Drela and M.B. Giles. Viscous-inviscid analysis of transonic and low reynolds number airfoils. *AIAA Journal*, 25(10):1347–1355, October 1987.
- [52] E. Lindenburg. Modeling of rotational augmentation based on engineering consideration and measurements. In *European Wind Energy Conference (EWEC)*, London, GB, November 2004.
- [53] C.L. Bottasso, F. Campagnolo, and A. Croce. Multi-disciplinary constrained optimization of wind turbines. *Multibody System Dynamics*, --, 2012. To appear 2012, in press.
- [54] C. L. Bottasso, F. Campagnolo, Croce A., S. Dilli, M.B. Nielsen, and C. Tibaldi. Optimization of wind turbine rotor blades by integrated sectional/multibody/3dfem analysis. *Multibody System Dynamics*, 2012. Under review.
- [55] S.Y. Sheu and M.W. Walker. Identifying the independent inertial parameter space of robot manipulators. *The International Journal of Robotics Research*, 10(6):668–680, 1991.
- [56] S.S. Shome, D.G. Beale, and D. Wang. A general method for estimating dynamic parameters of spatial mechanism. *Nonlinear Dynamics*, 16:349–368, 1998.
- [57] W. Khalil and E. Dombre. *Modeling, Identification and Control of Robots*. Hermes Pelton Science, London, 2002.
- [58] F. Campagnolo. *Wind turbine wind tunnel testing: aerodynamics and beyond*. PhD thesis, Politecnico di Milano, 2013.
- [59] N.A. Olesen. Personal communication. vestas wind systems a/s. aarhus, denmark, 2009.
- [60] R. Mikkelsen and J.N. Sørensen. Modelling of wind tunnel blockage. In *Proceeding of the 2002 Global Windpower Conference and Exhibition*, 2002.
- [61] A.S. Bahaj, A.F. Molland, J.R. Chaplin, and W.M.J. Batten. Power and thrust measurements of marine current turbines under various hydrodynamic flow conditions in a cavitation tunnel and a towing tank. *Renewable Energy*, 32:407–426, 2007.
- [62] J.B. Barlow, W.H. Rae, and A. Pope. *Low-speed wind tunnel testing*. John Wiley & Sons, third edition, 1999.
- [63] M. Biava. *RANS computations of rotor/fuselage unsteady interactional aerodynamics*. PhD thesis, Politecnico di Milano, 2007.
- [64] J.T. Bialasiewicz and M.O. Richard. Advanced system identification techniques for wind turbine structures. Technical report, NREL/TP-442-6930, 1995.
- [65] M.H. Hansen, K. Thomsen, and P. Fuglsang. Two methods for estimating aeroelastic damping of operational wind turbine modes from experiments. *Wind Energy*, 9(1-2):179–191, 2006.
- [66] S. Chauhan, M.H. Hansen, and D. Tcherniak. Application of operational modal analysis and blind source separation / independent component analysis techniques to wind turbines. In *Proceedings of 27th IMAC Conference*, Orlando, Florida,, February 9–12 2009.

- [67] I. Balaguer, S. Kanev, D. Tcherniak, and M. Rossetti. System identification methods on alstom eco 100 wind turbine. In *Proceedings of 3rd Torque Conference*, Heraklion, Crete, Greece, June 28–30 2010.
- [68] D.M. Eggleston and F.S. Stoddard. *Wind Turbine Engineering Design*. Van Nostrand Reinhold Company, New York, 1987.
- [69] A.M. Lyapunov. Sur une série relative à la théorie des équations différentielles lineaires à coefficients périodiques. *Comptes Rendus de l'Académie des Sciences*, 123(26):1248–1252, 1896. In French.
- [70] G. Floquet. Sur les équations différentielles linéaires à coefficients périodiques. *Annales Scientifiques de l'E.N.S.*, 2(12):47–88, 1883. In French.
- [71] M.H. Hansen. Aeroelastic stability analysis of wind turbines using an eigenvalue approach. *Wind Energy*, 7(2):133–143, 2004.
- [72] W. Johnson. *Helicopter Theory*. Princeton University Press, Princeton, NJ, 1981.
- [73] G. Bir. Multi-blade coordinate transformation and its application to wind turbine analysis. In *Proceedings of the AIAA Wind Energy symposium*, Reno, Nevada, January 7–10 2008.
- [74] C.L. Bottasso and S. Cacciola. Periodic stability analysis of wind turbines. In *EWEA 2012 Annual Event*, EWEA 2012 Annual Event, April 16–19 2012.
- [75] C.L. Bottasso and S. Cacciola. Model-independent periodic stability analysis of wind turbines from input-output data using a periodic arx reduced model, (poster). In *The science of Making Torque from Wind (TORQUE)*, 2012.
- [76] C.L. Bottasso and S. Cacciola. Model-independent periodic stability analysis of wind turbines. *Wind Energy*. Under Review.
- [77] S. Bittanti and P. Colaneri. *Periodic systems. Filtering and control*. Springer, 2009.
- [78] D.A. Peters, Lieb S.M., and L.A. Ahasus. Interpretation of floquet eigenvalues and eigenvectors for periodic systems. *Journal of the American Helicopter Society*, 56(3):032001–1–11, 2010.
- [79] W.A. Gardner. *Cyclostationarity in Communications and Signal Processing*. IEEE press, Piscataway, NJ, 1994.
- [80] L. Ljung. *System Identification — Theory for the User*. Prentice Hall, Englewood Cliffs, NJ, USA, 1999.
- [81] S. Bittanti, P. Bolzern, L. De Nicolao, and L. Piroddi. Representation, prediction and identification of cyclostationary processes—a state space approach. In W.A. Gardner, editor, *Cyclostationarity in Communications and Signal Processing*, pages 267–294. IEEE press, Piscataway, NJ, 1994.
- [82] J.F. Hauer, C.J. Demeure, and L.L. Scharf. Initial results in prony analysis of power system response signals. *IEEE Transaction on Power System*, 5(1):80–89, 1990.
- [83] M.S. Allen, M.W. Sracic, S. Chauhan, and M.H. Hansen. Output-only modal analysis of linear time periodic systems with application to wind turbine simulation data. *Mechanical Systems and Signal Processing*, 25(4):1174–1191, 2011.
- [84] M. Borri. Helicopter rotor dynamics by finite element time approximation. *Computers & Mathematics with Applications*, 12A(1):149–160, 1986.
- [85] P. Van Dooren and J. Sreedhar. When is a periodic discrete-time system equivalent to a time-invariant one? *Linear Algebra and its Applications*, 212–213:131–151, 1994.
- [86] C.E. Hammond. An application of floquet theory to prediction of mechanical instability. *Journal of the American Helicopter Society*, 14(4):14–23, 1976.

## Bibliography

---

- [87] V.A. Vecchia. Periodic autoregressive-moving average (PARMA) modeling with application to water resources. *JAWRA Journal of the American Water Resources Association*, 21(5):721–730, 1985.
- [88] D.J. Noakes, A. McLeod, and K.W. Hipel. Forecasting monthly riverflow time series. *International Journal of Forecasting*, 1(2):179–190, 1985.
- [89] Y.G. Tesfaye, M.M. Meerschaert, and P.L. Anderson. Identification of periodic autoregressive moving average models and their application to the modeling of river flows. *Water resources research*, 42(1):No. W01419, 2006.
- [90] L. Benyahya, A. St-Hilaire, T.B.M.J. Quarda, B. Bobée, and B. Ahmadi-Nedushan. Modeling of water temperatures based on stochastic approaches: case study of the deschutes river. *Journal of Environmental Engineering and Science*, 6(4):437–448, 2007.
- [91] M. Espinoza, C. Joye, R. Belmans, and B. DeMoor. Short-term load forecasting, profile identification, and customer segmentation: A methodology based on periodic time series. *IEEE Transactions on Power Systems*, 20(3):1622–1630, 2005.
- [92] D.R. Osborn and J.P. Smith. The performance of periodic autoregressive models in forecasting seasonal u.k. consumption. *Journal of Business & Economic Statistics*, 7(1):117–127, 1989.
- [93] M. Borgosz-Koczvara, A. Weron, and A. Wyłomańska. Stochastic models for bidding strategies on oligopoly electricity market. *Mathematical Methods of Operational Research*, 69(3):579–592, 2012.
- [94] R. Lund, H. Hurd, P. Bloomfield, and R. Smith. Climatological time series with periodic correlation. *Journal of Climate*, 8(11):2787–2809, 1995.
- [95] E. Broszkiewicz-Suwaja, A. Makagon, R. Weron, and A. Wyłomańska. On detecting and modeling periodic correlation in financial data. *Physica A: Statistical Mechanics and its Applications*, 336(1–2):196–205, 2004.
- [96] V. Bertogalli, S. Bittanti, and M. Lovera. Simulation and identification of helicopter rotor dynamics using a general-purpose multibody code. *Journal of the Franklin Institute*, 366(5):783–797, 1999.
- [97] S. Bittanti and L. De Nicolao. Spectral factorization of linear periodic systems with application to the optimal prediction of periodic ARMA models. *Automatica*, 29(2):517–522, 1993.
- [98] S. Bittanti, P. Bolzern, G. De Nicolao, L. Piroddi, and D. Purassanta. A minimum prediction error algorithm for estimation of periodic ARMA models. In *European Control Conference ECC 1991*, pages 1200–1203, Grenoble, France, 1991.
- [99] J. Rissanen. Algorithms for triangular decomposition of block hankel and toeplitz matrices with applications to factoring positive matrix polynomials. *Mathematics of Computation*, 27(121):147–154, 1973.
- [100] O.A. Bauchau, C.L. Bottasso, and L. Trainelli. Robust integration schemes for flexible multi-body systems. *Computer Methods in Applied Mechanics and Engineering*, 192:395–420, 2003.
- [101] C.L. Bottasso, F. Campagnolo, A. Croce, and C. Tibaldi. Optimization-based study of bend-twist coupled rotor blades for passive and integrated passive/active load alleviation. *Wind Energy*, 2012. available online.
- [102] E. Bossanyi. Individual blade pitch control for load reduction. *Wind Energy*, 6(2):119–128, 2003.
- [103] C.E.D. Riboldi. *Advanced control laws for variable-speed wind turbines and supporting enabling technologies*. PhD thesis, Politecnico di Milano, 2012.

- [104] C.L. Bottasso, A. Croce, C.E.D. Riboldi, and Y. Nam. Multi-layer control architecture for the reduction of deterministic and non-deterministic loads on wind turbines. *Renewable Energy*, 51(0):159 – 169, 2013.
- [105] M. Soltani, R. Wisniewski, P. Brath, and S. Boyd. Load reduction of wind turbines using receding horizon control. Technical report, Department of Electronics Systems, Aalborg University, Aalborg, Denmark and Vestas Technology R&D, Aarhus, Denmark and Department of Electrical Engineering, Stanford University, Palo Alto, CA, 2010.
- [106] K. Stol. *Dynamics modeling and periodic control of horizontal axis wind turbines*. PhD thesis, University of Colorado, 2001.
- [107] M. Lovera, P. Colaneri, C. Malpica, and R. Celi. Closed-loop aeromechanical stability of hingeless rotor helicopters with higher harmonic control. *Journal of Guidance, Control and Dynamics*, 29(1):179–189, 2006.
- [108] M. Lovera, P. Colaneri, C. Malpica, and R. Celi. Discrete-time, closed-loop aeromechanical stability analysis of helicopters with higher harmonic control. *Journal of Guidance, Control and Dynamics*, 30(5):1249–1260, 2007.
- [109] N. Perisic, P.L. Green, K. Worden, and P.H. Kirkegaard. Identification of time-varying non-linear systems using differential evolution algorithm. In *IMAC-XXXI – Conference & Exposition on Structural Dynamics*. Society for Experimental Mechanics, Garden Grove, CA, USA, February 2013.
- [110] C.L. Bottasso and C.E.D. Riboldi. Observation of wind misalignment from blade loads. In *The Science of Making Torque from Wind*, Oldenburg, Germany, October 2012.
- [111] M. Iribas-Latour and I.-D Landau. Identification of wind turbines in closed-loop operation in the presence of three-dimensional turbulence wind speed: torque demand to measured generator speed loop. *Wind Energy*, 12(7):660–675, 2009.
- [112] M. Iribas-Latour and Landau I.-D. Closed loop identification of wind turbines model for pitch control. In *17th Mediterranean Conference on Control & Automation*, Thessaloniki, Greece, June 2009.